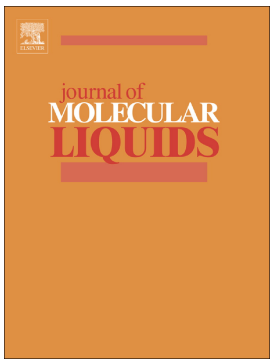

A Review on Graphene based Nanofluids: Preparation, Characterization and Applications

Adeel Arshad, Mark Jabbal, Yuying Yan, David Reay

PII: S0167-7322(18)35020-7
DOI: https://doi.org/10.1016/j.molliq.2019.01.153
Reference: MOLLIQ 10384

To appear in: *Journal of Molecular Liquids*

Received date: 28 September 2018
Revised date: 14 January 2019
Accepted date: 28 January 2019

Please cite this article as: A. Arshad, M. Jabbal, Y. Yan, et al., A Review on Graphene based Nanofluids: Preparation, Characterization and Applications, Journal of Molecular Liquids, https://doi.org/10.1016/j.molliq.2019.01.153

A Review on Graphene based Nanofluids: Preparation, Characterization and Applications

Adeel Arshad[a,*], Mark Jabbal[a], Yuying Yan[a,b,*], David Reay[c]

[a] *Fluids & Thermal Engineering (FLUTE) Research Group, Faculty of Engineering, University of Nottingham, Nottingham NG7 2RD, United Kingdom*
[b] *Research Centre for Fluids and Thermal Engineering, University of Nottingham Ningbo China, Ningbo 315100, China*
[c] *David Reay & Associates, PO Box 25, Whitley Bay, Tyne & Wear NE26 1QT, UK.*

Abstract

A wide range of heat transfer systems require efficient heat transfer management from source to sink and vice versa. Over the last decade, graphene nanoparticles, matrix nanofluids have been one of the most investigated nanoparticles for a wide range of engineering applications. Graphene–based nanoparticles have several advantages over other nanoparticles: high stability, high thermal conductivity, low erosion and corrosion, and higher carrier mobility. Graphene–based nanofluids have found applications such as heat transfer, defect sensor, anti–infection therapy, energy harvesting systems, biomedical and cosmetics. With advancement of technology, more compact and efficient cooling media are needed to ensure efficiency and reliability of engineering systems and devices. This research study reports an overview of experimental and numerical investigations of graphene nanometer–sized particles with different base host fluids for major engineering applications of energy transfer systems and further thermophysical properties of graphene nanofluids.

Keywords: Graphene Nanoparticles, Graphene Nanofluids, Heat Transfer Management, Cooling medium, Base fluids

*Correspondence authors
Email addresses: adeel.arshad@nottingham.ac.uk, adeel_kirmani@hotmail.com (Adeel Arshad), yuying.yan@nottingham.ac.uk (Yuying Yan)

Contents

Nomenclature

GE	Graphene
GO	Graphene Oxide
RGO	Reduced Graphene Oxide
GQD	Graphene Quantum Dot
NDG	Nitrogen-doped Graphene
HEG	Hydrogen induced Exfoliated Graphene
f-HEG	Functionalized Graphene
CNDG	Crumpled nitrogen-doped graphene nanosheet
GONs	Graphene oxide nanosheets
GNPs	Graphene nanoplatelets
HU	Hummers and Offeman method
NPs	Nanoparticles
BF	Base fluid
CONC	Concentration
SFTs	Surfactants
Charac. Tech.	Characteristics Techniques
PS	Particle size
SM	Synthesis method
PM	Preparation method
DW	Distilled water
DI	Deionized
EG	Ethylene glycol
PG	Propyl glycol
LP	Liquid paraffin
CLD	Chemical Liquid deposition
CVD	Chemical Vapor deposition

1. Introduction

Graphene oxide (GO), also called graphitic acid [1], was first discovered in 1859 and its reduced form, reduced graphene oxide (RGO), is intensively used due to its ease for large scale production than graphene. It also has the potential for a wider range of applications. GO, a 2D material, is the oxidized form of graphene having carbon/oxygen ratio (C/O) atomic ratio of 2.0 to 2.9. It has a larger and more irregular chemical structure layer than graphene with the range of 0.6 to $1.1nm$, depending on the preparation method of GO [2]. Graphene is a single atom thick layer sheet of highly densed carbon atoms of sp^2-bonded in hexagonal (honey–comb) pattern, which is the basic pattern for other nano-structured materials [3] such as carbon nanotubes [4] and fullerene [5]. With the removal of O functional groups from the surface layer of GO, all the physical properties can be adapted to those of graphene by which it converts into semi–metal from insulating material. Graphene, which is hydrophobic, but with the presence of O functional groups making it GO, can be dispersed into water due to its hydrophilic nature [6]. The flake size of GO can also be tuned from nm to mm [7]. The characteristic of varying flake sizes and chemical composition have made GO appealing for many engineering and medical sciences applications such as sensors, heat pipes, micro–mini channels, heat sinks, clean energy devices, composite materials, medicine, auto–mobiles, cosmetic, refrigeration and air conditioning, solar energy devices, lubricants and coolants, as shown in Figure 1 [8]. With favourable characteristics, graphene has become the emerging material in spectroscopic and microscopic measurement techniques [9, 10]. In the previous decade, Novoselov et al. [11] suggested the graphene an attractive material in engineering science after reporting the unusual electronic characteristics as the best carrier mobility. From the last decade, numerous engineering applications studies of graphene have been reported due to its exceptional electronic, thermal, optical and mechanical properties. Graphene nanoparticles have the following advantages over other nanoparticles [12, 13, 14]:

1. High thermal conductivity
2. Easily synthesized and more stable
3. Require less pumping power and energy saver
4. Reduced need of heat transfer fluid
5. Reduced corrosion, clogging and erosion
6. Larger surface area to volume ratio–enhanced the heat transfer ability

In the review article, details of synthesis and preparation methods of graphene based nanofluids, their thermophysical properties and use of graphene nanofluids in various engineering applications have been critically summarized.

2. Graphene–based materials

Graphene, "the mother of all graphitic forms of carbon", is a single layer of carbon atoms that are held together by a backbone of overlapping sp^2–bonded carbon atoms [15]. The extraordinary and significant characteristics of graphene initiate from the $2p$ orbitals which form the $\pi-$bonds. These $\pi-$bonds are

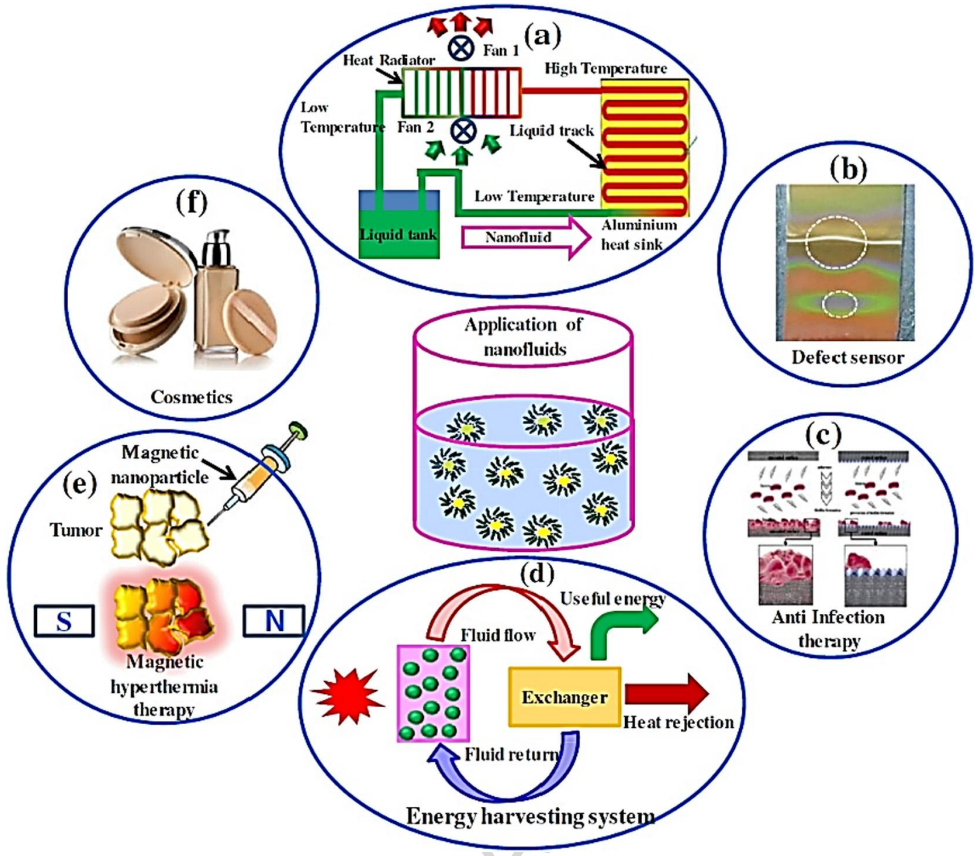

Figure 1: Some common engineering applications of graphene nanofluids, from Ref. [9], reused with permission from Elsevier license number 4456431386352.

further hybridized together to form the $\pi - \pi$bands that are delocalized over the sheet of carbon that form the graphene. As a consequence of this, graphene pretends highly stiffness with exhibiting higher thermal conductivity, high mobility of charge carriers, zero effective mass, impermeable to gases and optically transparent [16]. Figure 2 illustrates the major type of graphene–based materials which are being used to prepare nanofluids for various engineering applications. The structure of pristine graphene is characterized as a 2D array and sp^2-hybridization of pure carbon atoms are arranged in a hexagonal lattice with covalent bonds. Moreover, the functionalized graphenes are produced by synthesis and preparation such as the carbon core structure can be oxidized forming GO, the reduced structure with vacancy defects is RGO, and structures a few nanometres in size with quantum phenomena are GQDs [17]. The classification of graphene–based materials on the basis of three fundamental attributes (number of graphene layers, the atomic C/O ratio, and average lateral dimensions) is shown in Figure 3.

Several preparation techniques have been proposed for high quality graphene in bulk quantities, to fulfil the need of industry and academia. The list of preparation strategies of graphene, which have been proposed in literature with a few them adopted by graphene supplying industries, are as follows [13]:

- Mechanical exfoliation
- Chemical vapor deposition (CVD)
- Liquid phase exfoliation

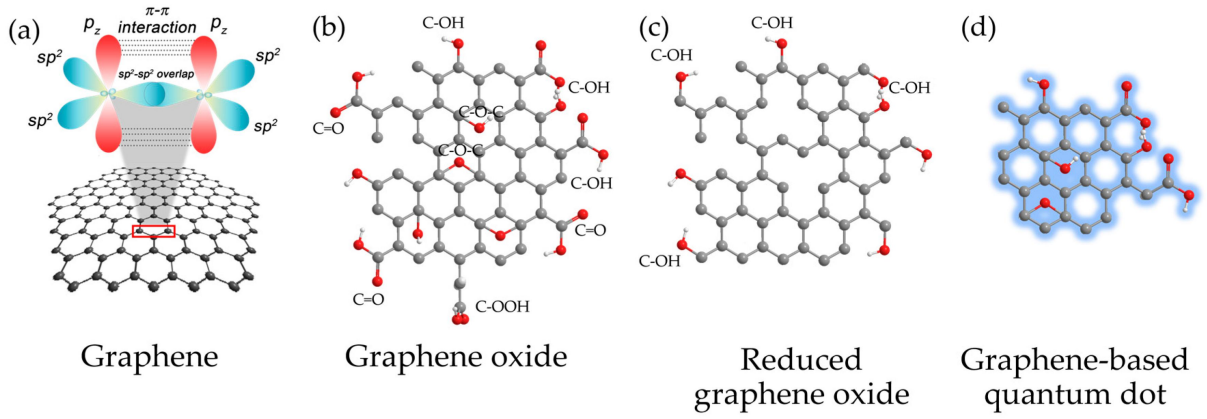

Figure 2: Structures of graphene-based materials show (a) the pristine graphene (pure-arranged carbon atoms) with sp^2-hybridized carbon atoms, and the chemically modified graphene, including (b) GO; (c) RGO and (d) GQD [18].

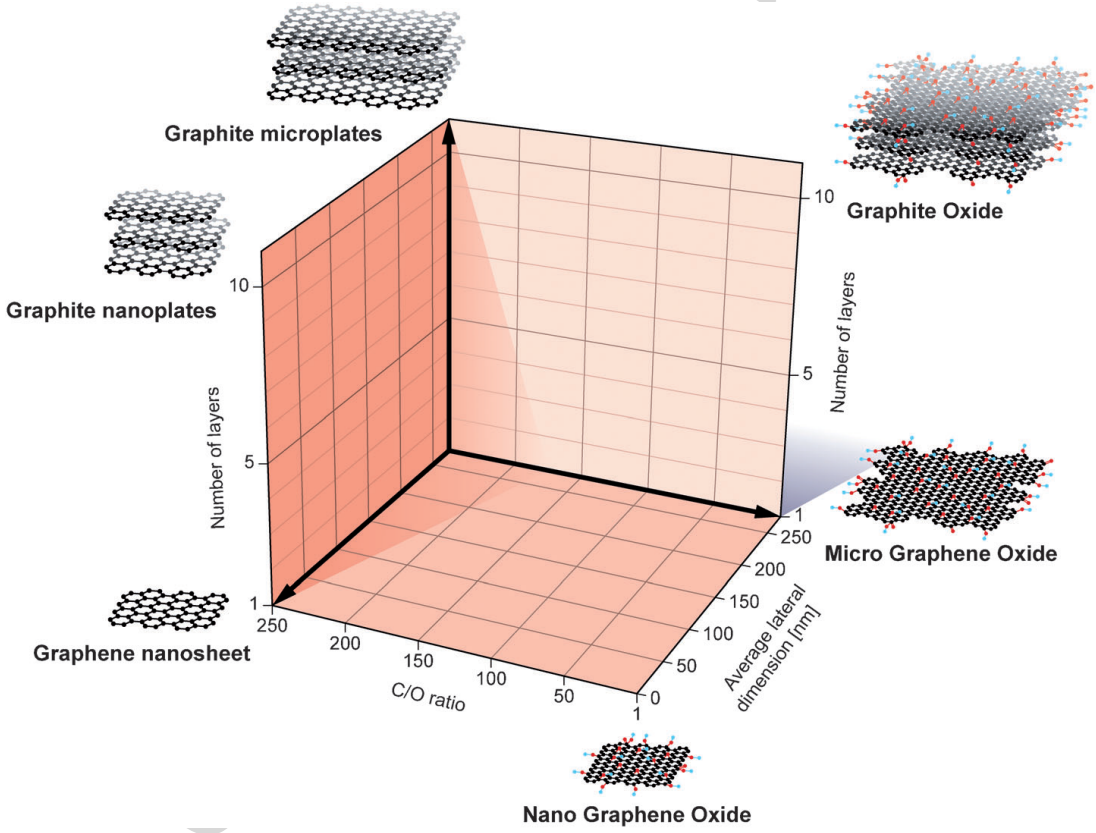

Figure 3: Classification for different graphene-type materials based on the number of layers, the C/O ratio and the lateral dimensions, from Ref. [19], reused with permission from John Wiley and Sons license number 4456461364577.

- Electrochemical exfoliation
- Chemical reduction of of GO
- Bottom-up synthesis

3. Preparation methods of Graphene Oxide

The first synthesis of GO was described by Baronet Benjamin Collins Brodie (in 1859) which was known as the "*Brodie method–the reaction of bulk graphite with potassium chlorate and fuming nitric acid*". Before that, Brodie presented a short technical note in 1855 in Annales de Chimie in French [20]. The complete formation of GO, composition and chemical reactions, was published in the Philosophical Transactions of the Royal Society of London [21] and after that this paper was translated in French and German languages [22, 23]. The interesting thing to note was that Brodie did not give any name to this new compound in all of his first four publications [20, 21, 22, 23] and the title of his publication in English version was as follows: *On the atomic weight of graphite*. In his first publication, he defined the name of new compound as *Oxyde de graphite* and *graphitic acid* in later articles. A detailed history of invention of GO with different reagents fuming nitric acid, concentrated sulphuric acid and potassium chlorate with $KMnO_4$, $HCrO_4$, gaseous ClO_2, Mn_2O_7 is reported in a book titled *Graphene oxide: Fundamentals and applications* [10].

GO is derived from graphene by using various oxygen functionalities. In GE, the oxygen atoms are covalently bonded to carbon atoms, are converted from the sp^2–hybridized state into the sp^3–hybridized state to form the GO. In a typical GO, the number of carbon atoms bonded to oxygen atoms, exceeds the number of intact sp^2–hybridized carbon atoms which changes characteristics of GO from parent graphene. One of the most prominent characteristic is the hydrophilicity that is the ability to be dissolved and to form the stable colloid aqueous and non–aqueous solutions. The final product from the oxidation process is known as graphite oxide, which is multi–layered and appears brown in colour. GO is synthesized from graphite by oxidation with strong oxidants such as potassium chlorate $KClO_3$, potassium permanganate ($KMnO_4$), and solid sodium nitrate ($NaNO_3$) in concentrated acid media such as nitric acid ((HNO_3) and sulphuric acid (H_2SO_4). On the basis of oxidant and acidic media, there are three major methods to prepare GO: Brodie method [20], Staudenmaier method (ST) [24], and Hummers and Offeman method (HU) [1].

In the Brodie method, $KClO_3$ was used as an oxidant agent in fuming nitric acid (HNO_3+NO_2) media. This method was not so effective, because it was not completed in a single step and in a one vessel. The partially oxidized product obtained from the first reaction further needed to be isolated, purified and subjected to a new oxidation cycle several times until sufficiently oxidized product was obtained.

The Staudenmaier method (ST) [24] used exfoliated graphite and added it in a mixture of fuming nitric acid (HNO_3+NO_2) and H_2SO_4 at room temperature conditions using $KClO_3$ as an oxidant. In this research it was reported that the oxidation reaction got faster with faster addition of $KClO_3$ and used 25g of graphite for one procedure. In continuation of the ST method, Kohlschutter and Haenni [25], Hofmann and Frenzel [26] and Hamdi [27] used powered graphite instead of exfoliated graphite and found longer reaction times compared with ST method; further, their methods were hazardous. Hofmann method [28] involved the concentrated nitric acid (HNO_3) instead of fuming nitric.

A successful attempt of GO formation was presented by HU method [1]. Concentrated H_2SO_4 was used instead of HNO_3, and $NaNO_3$ and $KMnO_4$ were used as an oxidant. The process was completed in two hours at a temperature less than 45°Cm which is safe to carry it out. A schematic representation

is shown in Figure 4. The HU method is indeed far better and safer than Brodie's and Staudenmaier's methods, however it is faster only with the small particle size of powdered graphite, which was employed by Hummers and Offeman. For the larger particle size graphite oxidation using HU method, an incomplete oxidized graphite–GO is achieved. Figures 5 presents the existence of GO flakes in two different environments–the aqueous solution of GO flakes in its 2D single–layer form (Fig. 5a) and being placed on a substrate (Si/SiO_2) surface (Fig. 5b) [10]. In solution, GO flakes are totally surrounded by the solvent molecules whereas on a substrate surface, the GO flakes are in contact with the surface of Si/SiO_2 from one side and with air from the other side.

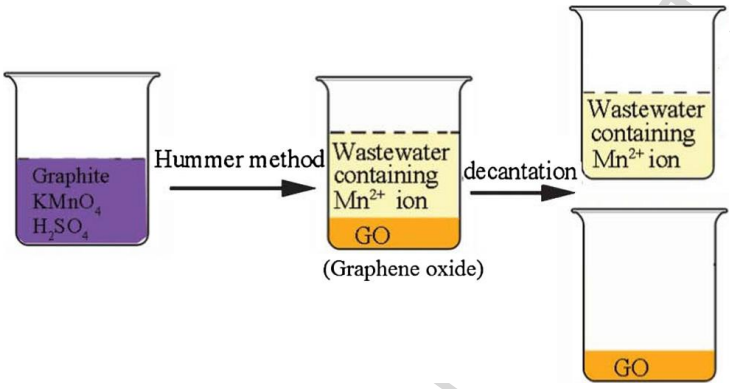

Figure 4: Schematic procedure of HU method, from Ref. [29], reused with permission from Elsevier license number 4384840187548.

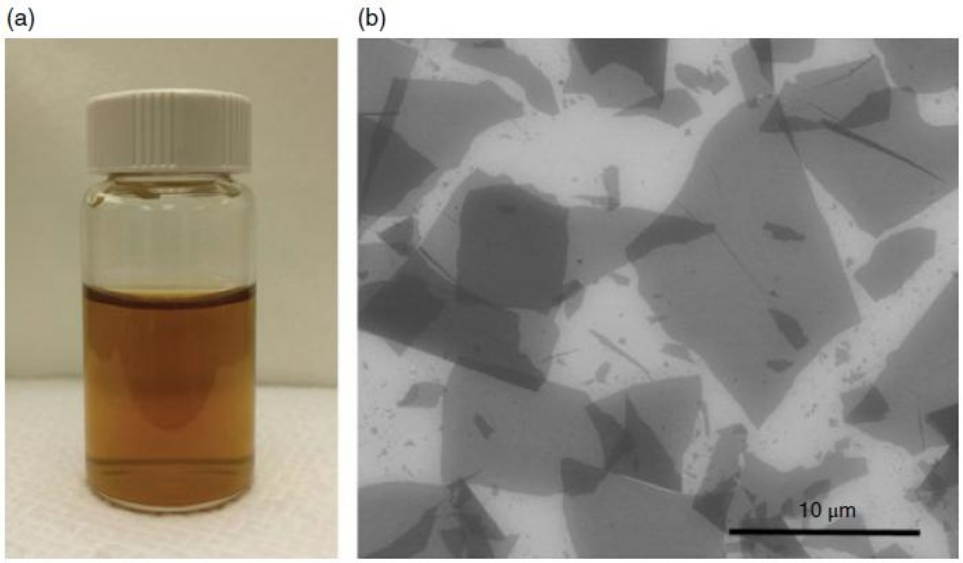

Figure 5: GO in its true 2D single-layer form. (a) Photograph of GO aqueous solution; the solution colour may vary from yellow to brown. (b) Scanning electron microscope image of GO flakes on a Si/SiO_2 wafer. The number of layers can be distinguished by their opacity. All the flakes on this image are single–layered. The image is darker where the flakes are folded or overlapped, making double–layered structures, from Ref. [10], reused with permission from John Wiley and Sons license number 4384850712781.

4. Preparation and stability of graphene nanofluids

A comprehensive summary of graphene based nanofluids is given in Table 2 with summarized information of use of base fluids, type of surfactants, methods to study the morphological and thermal properties, used size of graphene nanoparticle, the synthesis and preparation methods, their findings and conclusions.

4.1. Potential features of graphene nanofluids

- Increased thermal conductivity and specific heat capacity.
- Enhanced heat transfer rate.
- Reduced erosion, corrosion and collaging in micro minichannels, heat pipes and other micro systems.
- Reduced friction coefficient resulting in superior lubrication.
- More stability (i.e. thermal and chemical) over other nanoparticle–based fluids.
- Reduced pumping power and pressure drop.

4.2. Preparation methods of graphene nanofluids

Conventionally, there are two methods of preparation of nanofluids (1) *one–step method* and (2) *two–step method*.

4.2.1. One–step method

In one–step method, the nanofluid is prepared simultaneously, making and dispersing of nanoparticle in base fluids [30] which includes the liquid and vapour chemical deposition methods [31, 32, 33, 34]. In one–step method, drying, storage, transportation, and dispersion of nanoparticles are avoided to enhance the stability and to minimize the agglomeration of nanoparticles. Uniformly dispersed nanoparticles can be prepared resulting in improved stable suspension in the based fluids and reduced production cost. Some advanced techniques have been introduced to prepare the nanofluid via the one–step method due to the difficulty of preparing a stable nanofluid via the two–step method. The direct condensation and evaporation, laser ablation and SANSS (submerged–arc nanoparticles synthesis system) methods [35, 36] are adopted for one–step nanofluids preparation, in which the metals are vaporized using mechanical technology and cooled into liquid to obtain the desired nanofluid. The physical methods control the size of particles very well, producing the stable nanofluid. The vacuum-SANSS is another efficient method to produce nanofluids using different dielectric liquids [35, 37]. Through dielectric liquids of various thermal conductivity properties, different morphologies of nanoparticles are obtained such as needle-like, polygonal, circular and square shapes. By adopting this method, various undesired particle aggregation can be avoided. However the residual reactants still remain in the nanofluid due to incomplete chemical reaction and stabilization, which is a key disadvantage of this method. A recently developed one–step method is chemical solution method (CSM), which can successfully produce nine different kinds of nanofluids of various synthetizations microstructures [38, 39]. The nanofluid prepared by CSM has higher thermal

conductivity and stability. Despite this, the synthetization of nanofluid via on–step method is difficult on a large scale.

4.2.2. Two–step method

The most widely used method to synthesize nanofluids is the two–step method, which utilizes the nanoparticles, nanofibers, nanorods, nanowires, nanosheets, nanotubes, droplets, and other nanomaterials. Initially, the dry powder is prepared through mechanical and chemical methods such as milling, grinding, sol–gel, and vapour phase. This nanosized powder is then mixed with the host fluid (water, ethylene glycol, oil) with ultrasonic vibrators, magnetic force agitation, high–shear mixing, homogenizing and ball milling. Constant stirring reduces the agglomeration of nanofluids, which is a major issue of synthesizing of nanofluids [40]. The two–step method is quite an economic way to produce nanofluids at commercial scale. From previous investigations, it has been explored that due to high surface area and surface activity, nanoparticles have the tendency to aggregate. Also to prepare the nanofluids via two–step method using oxide nanoparticles than metallic nanoparticles are more stable because the nanosized powder aggregate easily because of Van der Waals forces among the particles. The most effective solution to enhance the stability of nanofluids is the use of surfactants. Figure 6 represents the two–step method to prepare the nanofluids [41]. Although this method is economical to produce the nanofluids, there are some issues of drying, storage and transportation. The thermal conductivity of nanofluids is decreased due to agglomeration and clogging. However, the microstructure of nanoparticles can be varied and enhanced by the altering the synthesis parameters such as temperature, acidity (pH), ultrasonic and microwave irradiation, reactant and additive types, concentrations and order. The following techniques are mostly widely adopted to prepare the nanofluids [9]:

- Direct evaporation technique
- Direct condensation technique
- Chemical reduction
- SANSS (submerged–arc nanoparticles synthesis system)
- Laser ablation
- Polyol process
- Microwave irradiation
- Phase–transfer method

4.3. Stability of graphene nanofluids

Even in the advancement of technological methods to prepare nanofluids, there is still difficulty to make an ideal nanofluid without the formation of agglomerates, which causes the settlement and clogging in micro heat transfer devices. The aggregation of nanoparticles in host fluids mostly occurs due to the strong Van der Waal forces and high surface areas among the nanosized powder, and sedimentation

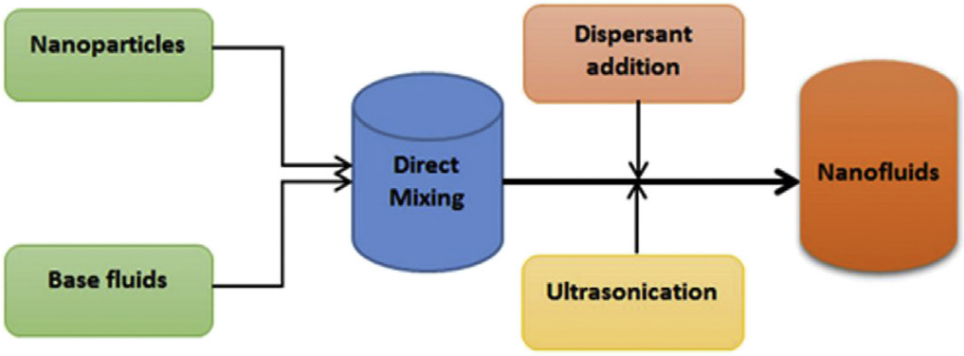

Figure 6: The two–step preparation method of nanofluids, from Ref. [41], reused with permission from Elsevier license number 4384851312147.

resulting in the density difference between the nanoparticles and base fluid. It is reported [42] that clustering and clogging features of nanofluids increase the thermal conductivity of nanofluids. Therefore, while preparing nanofluids, their stability and thermal conductivity should be under consideration at a balance level [43, 44]. The stability of nanofluids depends on the characteristic of depressed nanoparticles and base fluids. According to Stokes's law, the sedimentation velocity (V_{sed}) as formulated from Eq. 1:

$$V_{sed} = \frac{r^2(\rho_{np} - \rho_{bf})g}{9\mu} \tag{1}$$

Here, r^2 is the radius of dispersed particle, ρ_{np} and ρ_{bf} are the densities of nanoparticle and base fluid respectively, g is the gravitational acceleration, and μ is the dynamic viscosity of the nanofluid. From the Eq. 1, it can be seen that V_{sed} decreases with decreasing size of nanoparticle and the density difference of nanoparticle and base fluid and increasing viscosity of the base fluid.

4.3.1. Methods of stability evaluation

The following are some methods to evaluate the stability of nanofluids [29, 45, 46]:

1. Zeta potential measurements
2. UV-Vis spectrophotometer
3. Sedimentation photograph capturing
4. Transmission Electron Microscopy (TEM)
5. Scanning Electron Microscopy (SEM)
6. Sedimentation balance method
7. 3ω method
8. Dispersion analyser centrifuge
9. Thermal conductivity measurement

4.3.2. Methods to enhance the stability

The following are three solutions to enhance the stability of graphene based nanofluids:

Use of surfactant in Nanofluids The surfactants (also called dispersant) that are used in nanofluids, is an easy, popular and economic method to enhance the stability of two-phase nanofluids by affecting the surface characteristics of the mixture. The dispersant normally consists of two portions; one is the hydrophobic tail portion, usually long chain hydrocarbon, and second is hydrophilic polar head portion. The use of surfactant in two–phase mixture increases the interface conjunction of two materials, which introduces a degree of continuity between the two–phase systems, also known as wettability. The dispersant reduces the surface tension at the interface of nanoparticles and base fluid thus increasing the suspension time of nanoparticles. Surfactants are selected as per requirement, which convert the hydrophobic surfaces of nanoparticles to hydrophilic and vice versa to increase the solubility of aqueous and non–aqueous solutions. According to composition of the head; surfactants are categorized into four classes;

- Nonionic surfactants–without charge head groups (include polyethylene oxide, alcohols, and other polar groups). Typical examples are Triton X-100, Polyvinyl Pyrrolidone (PVP), and Tannic Acid (TA) [47, 48, 49, 50, 51, 52].
- Anionic surfactants: With negatively charged head groups (include long–chain fatty acids, sulfosuccinates, alkyl sulfates, phosphates, and sulfonates). Typical examples are Sodium Dodecyl Sulfate (SDS), Sodium Dodecylbenzene Sulfonate (SDBS), Sodium Octanoate (SOCT), Sodium Cholate (SC), Sodium Taurodeoxy Cholate (STC), Gum Arabic (GA), and Oleic acid [51, 52, 53, 54, 55, 56, 57].
- Cationic surfactants: With positively charged head groups (include protonated long-chain amines and long-chain quaternary ammonium compounds). Typical examples are Cetyl Trimethyl Ammonium Bromide (CTAB), Hexadecyl Trimethyl Ammonium Bromide (HCTAB), and Dodecyl Trimethyl Ammonium Bromide (DTAB) [52, 54].
- Amphoteric surfactants: With zwitterionic head groups (depend on pH and include betaines and amine oxides).

The selection of a suitable surfactant has significant importance such as for polar solvent base fluids, the water–soluble surfactant is suitable; otherwise, oil–soluble surfactant is suitable. The term hydrophilic/lipophilic balance (HLB) value can be used to evaluate the solubility of nonionic surfactant either in aqueous and non–aqueous nanofluid solutions. For higher value of HLB, nonionic surfactants are more soluble in water while for lower value of HLB, oil–soluble surfactant is suitable. Choosing an unsuitable surfactant can cause sedimentation, clogging, and aggregation which affects the thermal properties of nanofluids such as viscosity, thermal conductivity, specific heat. Zhu et al. [48] studied graphite nanofluids and obtained a stable nanofluids using PVP using steric effect. Sarsam et al. [54] used the SDBS, SDS, CTAB, GA as a surfactant and concluded that the highest stability was obtained by SDS–GNP/water nanofluid at $60min$ ultrasonication time. Zubir, et al. [49, 50] used Tannic Acid (TA) , Mehrali et al. [47] used Triton $X-100$, Sun et al. [51] used PVP, STC, SC as surfactants. The detailed description of used different surfactants are reported in Table 2.

Surface modification techniques: surfactant–free method. The use of surfactants, although quite an effective and promising technique to increase the dispersibility of nanoparticles with base fluids, may cause several problems [58]. For instance, heat transfer contamination medium, formation of foam while heating, creating thermal resistance between the nanoparticles and host fluid, because of the interaction of the surfactant molecules with surfaces of nanoparticles. The proper selection of functionalized nanoparticles has the tendency to improve the long–term stability of nanofluids which represents the surfactant–free technique.

4.3.3. Stability mechanism

The stability mechanism of nanofluids is defined as the rate of aggregation of nanoparticle dispersed in base fluid, which is generally explained by the frequency of collisions and probability of cohesion during collision. Nanoparticles start to adhere together to form aggregates at larger scale or size, when in dispersion, resulting in sedimentation or phase transition between the base fluid and nanoparticles. According to the theory of Derjaguin, Verway, Landau, and Overbeek (DVLO) [59, 60], which is based on colloidal stability, the stability of a particle in any solution is determined by the sum of Van der Waals attractive forces and the electrical double layer repulsive forces that exist between the nanoparticles as they approach each other due to the Brownian motion they are undergoing. If the attractive Van der Waals forces are larger than the repulsive forces between the particles then the particles will collide or aggregate and will settle at the base of the fluid resulting in a non-stable suspension. Contrarily, if the net electrical repulsive forces are high between the particles, then the suspension will remain stable and nanoparticles will not aggregate. According to the type of repulsion forces, by the colloidal stability may affect, the suspended nanoparticles can be stabilized by steric repulsive and electrostatic (charge) or electro–steric repulsive forces, as shown in Figure 7 [46].

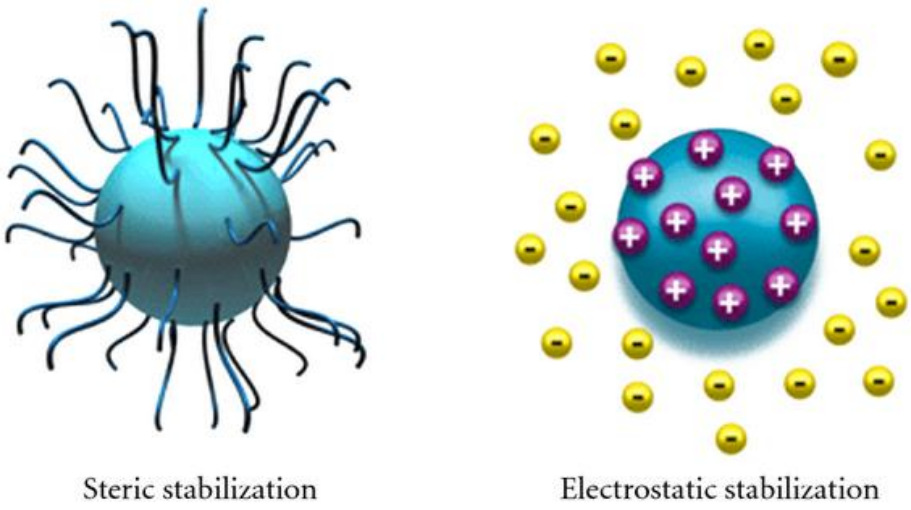

Figure 7: Types of colloidal stabilization. [46]

In steric stabilization, the polymers are directly involved into the suspension system and absorbed on the surface of the nanoparticles producing an additional steric repulsive force. And in case of elec-

trostatic stabilization, the surface charge, on the surface of nanoparticle, will be developed by following mechanisms:

- Preferential adsorption of ions
- Dissociation of surface changed species
- Isomorphic substitution of ions
- Accumulation or depletion of electrons at the surface
- Physical adsorption of charged species onto the surface

Table 2: The detailed summary of particle size, based fluids, synthesis methods, preparation methods, surfactants, characteristics techniques, and thermal properties enhancement of graphene based nanofluids.

Ref.	NPs	SM	PS	CONC.	BF	SFTs	PM	pH	Charac. Tech.	Findings
[61]	GNPs	Supplied by manufacturer	N/A	0.05%	Gallic acid, DW	N/A	Two–step method	Neutral	Zeta potential analyser, Ultrasonic Vibration-vis absorption spectroscopy	The enhancement in thermal conductivity was obtained of 24.18% at 45°C and viscosity was closer to the distilled water viscosity at low concentrations.
[62]	GNPs	Supplied by manufacturer	$\approx 4\mu m$	0.10–0.50wt.%	Water+EG	NH4OH solution	Two–step method	2–10	SEM, UV-vis spectrometer, TEM, Zeta potential test, DLS	The thermal conductivity, viscosity and density were increased with mass concentration of GNPs up to 5%, 12.6%, and 0.3%, respectively.
[63]	Graphite	Supplied by manufacturer	$\sim 10nm$	N/A	DI water	N/A	Two–step method	N/A	SEM, EDS, UV-vis spectrometer, TEM, HRTEM, XRD, XPS	The authors performed the experimental study to determine the contribution of cations and anions in exfoliation of graphite into graphene.
[64]	GE-COOH, MGE	Supplied by manufacturer	t=0.8–1.2nm	0.01% 0.03% 0.05%	$[HMIM]BF_4$	N/A	Two–step method	N/A	XPS, FT-IR, TEM, Zeta potential test, UV-vis-NIR Spectrometer, transient hot plane method	The results showed that MGE/[HMIM]BF_4 had the higher receiver efficiency than GE-COOH/[HMIM]BF_4 at higher temperature.
[65]	Graphite flakes	Modified Hummers method	10nm	1–4%	Red wine	N/A	Two–step method	N/A	XRD, Raman spectra, X-ray photoemission, FTIR, UV-vis spectrometer, Zeta potential test, FESEM	The enhancement in thermal conductivity was between 3.8% and 45.1%. The red wine reduced GO nanofluid exhibited the Newtonian behaviour and viscosity was decreased from 86.2% to 87.9%.
[54]	GNPs	Supplied by manufacturer	t=2nm d=2μm	0.1 wt.%	DW	SDBS, SDS, CTAB, GA	Two–step method	N/A	UV-vis spectrometer, TEM, Zeta potential test, Average particle size	The authors evaluated the stability of GNP/water nanofluid using three different surfactants for ultrasonication times of 15, 30, 60, 90 and 120mins. The finding concluded that highest stability was obtained by SDS-GNP/water nanofluid at 60mins ultrasonication time.

[53]	GE	Supplied by manufacturer	t=1–5nm	0.05% 0.1% 0.15%	DW	SDBS	Two–step method	N/A	SEM, Zeta potential test	The viscosity showed an average increment of 47.12%, while the surface tension showed an average decrement of 18.7% for the measured range of the temperature when the volume concentration was at 0.15%.
[49]	RGO	Chemical exfoliation	t=2nm d=2μm	0.05wt.%	DI water	Tannic Acid (TA)	Two–step method	8–9	XRD, Raman spectra, UV-vis spectrometer, Zeta potential test, XRD	The result showed the 25% and 4% enhancement in thermal conductivity and viscosity, respectively.
[66]	GNPs, Ag	Chemical reaction method	d=2μm	0–0.1%	DW	Not Used	Two–step method	N/A	XRD, Raman spectra, FESEM	The results showed the improvement in thermal conductivity and heat transfer. Further, the 32.7% enhancement was found in Nu number depending on the enhancement in temperature function and weight concentration.
[67]	GNPs	Supplied by manufacturer	t=2nm d=2μm	0.025% 0.05% 0.075% 0.1%	DW	Not used	Two–step method	N/A	N/A	The authors reported the convective heat transfer coefficient enhancement from 83-200% also heat transfer coefficient increased with the increase of flow rate and specific area.
[68]	GNPs	Supplied by manufacturer	t=2nm d=2μm	0.025% 0.05% 0.075% 0.1%	DW	Not used	Two–step method	N/A	N/A	The findings revealed that thermal conductivity was enhanced between 12%–28%, convective heat transfer coefficient was found 15%, and frictional entropy generation was increased whereas thermal entropy generation was decreased with the increase of concentration.
[47]	NDGs	Hummers method	t=1.8nm	0.01% 0.02% 0.04% 0.06%	Water	Triton X-100	Two–step method	N/A	UV-vis spectrometer, Zeta potential test, XRD, TEM, FESEM, Raman spectra, FT-IR, BET method	The results reported that the electrical conductivity increased linearly up to 1814.96% with the increase of concentration NDG nanoparticles.
[69]	GNPs	Supplied by manufacturer	N/A	0.0125wt.% 0.025wt.% 0.05wt.% 0.075wt.%	DI water	GO	Two–step method	8	UV-vis spectrometer, Zeta potential test, XRD, TEM, FESEM, Raman spectra, FT-IR	They explored the increase in viscosity at lower shear rate and achieved optimum level of mixing of GO and GNPs.

[55]	GE, MWCNT	Supplied by manufacturer	(MWCNT: d=20nm, t=5μm), GE: t=8nm	0.3-3.0%	DW	SDBS, SDS	Two–step method	N/A	FESEM	The authors found that GN nanofluid using SDBS and SDS showed longer stability, SDBS was better for MWCNTs and SDS for GN. The positive enhancements in thermal conductivity were 4.202%, 5.546% and 4.706% for varying mass concentrations. Further authors found the decreasing trend of thermal conductivity due to sedimentation of nanoparticles.
[50]	RGO	Chemical exfoliation	t=2nm d=2μm	0.05wt.%	DI water	Tannic Acid	Two–step method	8–9	XRD, Raman spectra, UV-vis spectrometer, Zeta potential test, XRD	The authors found the enhancement in convective heat transfer coefficient as well as in thermal conductivity and the enhancement of 144% was found in Nu.
[70]	GE	Supplied by manufacturer	t=6–8nm	0.05% 0.07% 0.09%	Acetone	Not used	Two–step method	N/A	SEM	The authors found the 70.3% reduction in thermal resistance and 61.25% enhancement in evaporator heat transfer coefficient.
[71]	GNPs	Supplied by manufacturer	t=0.55–3.74nm d=0.5–3μm	0.025wt.% 0.05wt.% 0.1 wt.%	DI water	COOH SDBS	Two–step method	N/A	TEM, FTIR	The findings concluded that thermal conductivity was higher by GNP-COOH/water than the GNP-SDBS/water nanofluid. The maximum thermal conductivity was achieved of $\approx 0.83 W/mK$ at 50°C for GNP-COOH (0.1%). The maximum percent increase in viscosity was 29.4% for GNP-COOH (0.1%) at 80°C.
[72]	GE	Supplied by manufacturer	t=6–8nm, d=5–15μm	0.001-0.01%	DW	Not used	Two–step method	N/A	Transient hot wire method, SEM, Rotational digital viscometer	They found that thermal conductivity was increased of 5.47% and 4.45%, further the rate of viscosity was increased of 15.65%.
[73]	Al_2O_3, GO	CVD	t=45nm d=5–15μm	N/A	DI water	Not Used	Two-step method	N/A	Raman spectroscopy	The wetting and evaporative aggregation of a hydrophobic graphene-coated (GC) along with a hydrophilic cover glass (CG) substrate. It was found that ratio of migration and evaporation time levels were low for both GC and CG substrates.
[52]	NDG, GO	Hummers method	d=45μm	0.01wt.% 0.02wt.% 0.04wt.% 0.06wt.%	DI water	Trition X-100, GA, CTAB, SDS	Two–step method	11	Zeta potential test, UV-vis spectrometer, TEM, XPS, XRD	The authors found the enhancement of thermal and electrical conductivities of 26.78% and 1814.94%, respectively.

[42]	GNPs	Supplied by manufacturer	t=2nm d=45μm	0.025wt.% 0.05wt.% 0.07wt.% 0.1wt.%	DW	Not used	Two–step method	10	Zeta potential test, UV-vis spectrometer, TEM, XPS, XRD	The authors found thermal conductivity enhancement of 27.64% and significant improvement of electrical conductivity was observed.
[74]	GE	Supplied by manufacturer	N/A	0.03wt.%, 0.06 wt.%	[HMIM]BF_4	Not used	Two–step method	N/A	DSC, viscometer, TGA	The result reported that the density decreases with the increase of the weight percentage of graphene nanoparticles.
[75]	GE/SiO_2	CLD	d=40nm	0.1wt.%	DI water	SDBS	Two–step method	8–9	TEM, XRD, HR-TEM, EDS, UV-vis spectrometer	The authors found that SiO_2-coated GE coating improved the hydrophilicity, stability and thermal conductivity of GE/SiO_2/water nanofluid. The maximum thermal conductivity was found $\approx 0.88 W/mK$ at 65°C.
[76]	GNPs	Supplied by manufacturer	N/A	0.5vol.% 1vol.% 2vol.% 3vol.% 4vol.%	EG	No used	Two–step method	N/A	UV-vis spectrometer, XRD, Raman spectroscopy, HRTEM, FTIR	The authors found the thermal conductivity ratio was increased 1.030–1.332 from 0.5–4% concentration at 90°C.
[77]	GO	Modified Hummers method	d=1–3μm	0.05wt.% 0.10wt.% 0.15wt.% 0.20wt.% 0.25wt.%	DI water	Not used	Two–step method	N/A	UV-vis spectrometer, XRD, SEM	They found that thermal conductivity was depended on concentration of GO and temperature. They found the 33.9% at 20°C and 47.5% at 40°C enhancement of 0.25wt.%.
[78]	GO	Modified Hummers method	t=20.11nm	0.001wt.% 0.002wt.% 0.003wt.% 0.004wt.% 0.005wt.% 0.006wt.%	DW, EG	Not used	Two–step method	3–10	XRD, TEM, FE-SEM, FTIR, Raman spectroscopy, UV-vis spectrometer, Zeta potential test	The 25.678% enhancement of electrical conductivity of GO/water nanofluid at 0.006 wt% and thermal conductivity enhancement of 30% were obtained for GO/EG nanofluid.
[79]	GE	CVD	N/A	0.100wt.% 0.125wt.% 0.150wt.%	EG	Not used	Two–step method	N/A	XRD, TEM	For maximum concentration of graphene (0.15 wt%), the density and viscosity of base fluid increased by 15.76% and 39.28%, respectively, and the heat capacity decreased by 18.9%.
[80]	MWCNT, GO, HEG, Ag	Hummers method	20–100nm	0.005% 0.01% 0.02% 0.03% 0.04%	EG, DI water	Not used	Two–step method	Neutral	XRD, FESEM, HRTEM, Raman spectroscopy	The reported enhancement of thermal conductivity and convective heat transfer coefficient were 8% and 570% at 0.04 vol.% and 0.005 vol.%, respectively.

[51]	GE	Polymer exfoliation	10μm	N/A	Polymer P19 and P20	PVP, STC, SC	Two–step method	N/A	SEM, UV-vis spectrometer, TEM, EDX	The findings concluded that the enhancement of thermal conductivity of 25% was obtained with 0.055% volume dispersion of GE.
[81]	GNS	CVD	t=500nm	0.01–0.05wt.%	DI water	N/A	Two–step method	7	SEM, TEM, Raman spectroscopy, FT-IR	The authors obtained the enhancement of thermal conductivity of 13.5% and 12.5% at 0.05% and 0.03%, respectively, at 25°C.
[82]	GE	N/A	N/A	0.05% 0.1% 0.15% 0.2%	Water	N/A	N/A	N/A	N/A	The transport phenomena of GE/water nanofluid was examined and claimed that enhancement in thermal conductivity was due to the dual behaviour of sheet percolation and Brownian motion.
[57]	GNSs	Modified Hummers method	t=0.7–1.3nm	0.01–0.05wt.%	EG	SDBS	Two–step method	N/A	TEM, AFM, FT-IR, Transient hot wire method	The authors determined the thermal conductivity enhancement of 86% at 5.0vol.% of GNS.
[83]	GNSs	Hummers method	t=100nm d=2μm	0.01–0.05%	DW, PG, LP	Oleylamine	Two–step method	N/A	TEM, FT-IR, AFM, UV-vis spectrum, XPS, Transient hot wire method	It was observed that enhancement ratios of thermal conductivity had constant trend with varying temperatures. Further, with increase of GNSs loading, thermal conductivity was increased but it was decreased with the increase of thermal conductivity of base fluid.
[84]	GNSs	Modified Hummers method	t=1–3μm	0.01–0.05%	EG	N/A	Two–step method	N/A	TEM, FT-IR	Thermal conductivity was constant of 07 days and enhancement ratio of 61% was obtained at 5.0 vol.%.
[56]	GNSs	Modified Hummers method	t=1–2μm	0.01–0.05%	EG	SDS	Two–step method	N/A	AFM, TEM, FT-IR, UV-vis absorption spectrum, Transient hot wire	The authors obtained the thermal conductivity of 61% at 0.05 vol.% and concluded that heat transport was the effective phenomenon to increase the thermal conductivity.
[85]	Ag/HEG	Hummers method	t=100nm	0.01–0.07%	DI water, EG	Not used	Two–step method	N/A	XRD, FT-IR, FE-SEM, TEM, Raman spectroscopy, UV-vis absorption spectrum	At volume fraction of 0.05%, the enhancement in thermal conductivity was ∼25% at 25°C and 86% at 70°C with DI water nanofluid. At 0.07% volume fraction, the enhancement in thermal conductivity is ∼6% at 25°C and ∼14% at 70°C with EG nanofluid.
[86]	GO, HEG, f-HEG	Hummers method, Exfoliating graphite oxide	100nm	0.005%, 0.009%, 0.02–0.08%	DI water, EG	Not used	Two–step method	N/A	XRD, FT-IR, FE-SEM, TEM, Raman spectroscopy, UV-vis absorption spectrum	The f-HEG/DI water nanofluid showed the enhancement in thermal conductivity of 16% and 75% for 25°C and 50°C, respectively of 0.05% volume fraction.

[87]	GO	Hummers method	t=100nm	0.005% 0.007% 0.009% 0.02% 0.03% 0.05%	DI Water, EG	Not used	Two–step method	6–7	FT-IR, Raman spectroscopy, UV-vis absorption spectrum, FESEM, TEM	The GO/DI-water and EG nanofluid showed the thermal conductivity of 14% and 64% at 25°C and 50°C, respectively at volume concentration 0.056%.
[88]	CuO/HEG	Hydrogen induced exfoliated graphene	t=20nm	0.01–0.07%	DI water, EG	Not used	Two–step method	N/A	XRD, FT-IR, FE-SEM, TEM	For 0.05% volume fraction of CuO/HEG dispersed in DI water, the enhancement in thermal conductivity was obtained of ∼28% at 25°C and almost 90% enhancement was observed for the same volume fraction at 50°C. At 0.07% volume fraction of CuO/HEG dispersed in EG, the enhancement in thermal conductivity was ∼17% at 25°C and it was ∼23% at 50°C for same volume fraction.
[89]	GNSs, GO	CVD, Hummers method	t=5nm	0.05–0.2vol.%	Water	Not used	Two–step method	N/A	TEM, DLS, UV-vis absorption spectrum	It was found that the thermal conductivity was enhanced of 27% at 0.2% concentration.
[14]	GNPs	Supplied by manufacturer	N/A	0.25wt.% 0.50wt.% 0.75wt.% 1.00wt.%	Water	N/A	Two–step method	N/A	EDS, SEM, DSC	The 12% enhancement was achieved in thermal conductivity for 1.00wt.% concentration of GNPs.
[90]	GNSs	Hummers method	N/A	0.008% 0.055% 0.083% 0.11% 0.138%	EG, DI water	Not used	Two–step method	10	TEM, EDX, FT-IR	The enhancement of 6.5% and 13.6% in thermal conductivity was obtained at 25°C for GNSs/EG and GNSs/DI water nanofluid, respectively.
[91]	GN	N/A	N/A	0.1% 0.2% 0.3%	Water, EG, Water+EG	N/A	N/A	N/A	N/A	The results revealed that with increasing concentration of GN increased the thermal conductivity of flow.
[92]	TiO_2, Al_2O_3, CuO, Fe_3O_4, GO	N/A	N/A	0.01% 0.02% 0.03%	Water, Kerosene, Engine oil	N/A	N/A	N/A	N/A	The findings concluded that GO-water had the higher temperature in comparison of other nanofluids.

[93]	GNSs	N/A	t=5.65–5.67nm	N/A	Water, EG (1:1)	N/A	N/A	N/A	N/A	The authors performed the molecular dynamics simulation, firstly, to investigate the effect of types of functional group and number, secondly, to evaluate the particle-size of graphene nanosheets. They found that the floating of larger nanoparticles were more stable than to smaller nanoparticles.

5. Thermal Properties of graphene nanofluids

Thermal transport is the key objective of understanding the phase change heat transfer phenomenon of two–phase flow system. Many researchers have done experimental as well as theoretical studies to investigate the thermophysical properties of nanofluids. The fundamental properties are highly of interest and include thermal conductivity, specific heat, viscosity and density.

5.1. Thermal conductivity measurements techniques

The following techniques can be adopted to measure the thermal conductivity of nanofluids. The transient hot–wire method is extensively used among researchers [9, 94, 95].

1. Transient hot–wire method
2. Thermal constant analyser techniques
3. Steady–state parallel plate method
4. 3ω method
5. Cylindrical cell method
6. Thermal comparator method
7. Temperature oscillation method
8. Laser flash technique (Flash method)

A brief summary and procedure of the above methods can be obtained [9].

5.2. Thermal conductivity of graphene nanofluids

Thermal conductivity is the ability of a material to transport energy in the form of heat (energetic vibrations). In solids, this energy exchange directly at atomic level, lattice vibrations and free electron diffusion. Whereas, in liquids and gases, this energy exchange is because of direct molecular contact and molecular diffusion. Thermal conductivity is inherent/intrinsic property of physical materials which is defined as the amount of energetic power per unit length and temperature gradient [96].

Thermal conductivity of suspension fluid has key importance while investigating the convection heat transfer phenomenon. Obviously, the emergence of nanoparticles in different base materials such as ethylene glycol, propylene glycol, methanol, glycerol, gear oil, engine oil, water, organic and inorganic materials, increase the thermal conductivity of composite suspension. There are two significant reasons for the increase in thermal conductivity of nanofluids: Brownian motion and liquid layering at liquid-particle interface. In Brownian motion nanoparticles move through the liquid and possibly collide, thus enabling direct solid–solid transport of heat from one particle to another which results in increases of the thermal conductivity of nanofluids [82, 97]. The Brownian motion is characterized by the particle diffusion constant D, given by the Stokes–Einstein formula:

$$D = \frac{k_B T}{3\pi\mu d} \tag{2}$$

where k_B is the Boltzmann Constant, T and μ are the temperature and viscosity, respectively, of the nanofluid, and d is the diameter of nanoparticle. As the temperature of the nanofluid increases in response

of this, the viscosity of the host fluid decreases, the Brownian motion of nanoparticles is increased and in consequence of this convection–like effects are remarkably increased, resulting in increased thermal conductivity [98]. Secondly, the interfacial liquid layer between the liquid molecules in conjunction with nanoparticle surface form a nano–layer structure, as shown in Figure 8. The liquid molecules closed to the solid nanoparticles form a nano–layered structures by which the atomic structure of the liquid layer is significantly more ordered than that of the bulk liquid. These nano–layered structures act as a thermal path between the solid nanoparticles and bulk liquid molecules and present in an intermediate physical state which increase the thermal conductivity of nanofluids greater than the bulk single-phase fluid [99]. The first successful effort to measure the thermal conductivity of graphene was accomplished by Alexander Balandi's team at University of California-Riverside using an opto–thermal Raman technique, shown in Figure 9 [100].

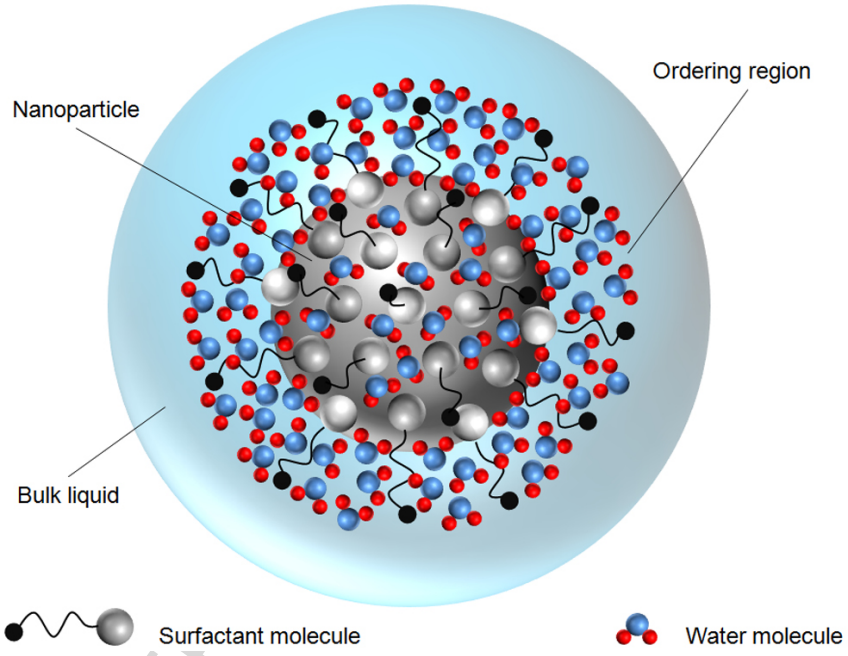

Figure 8: Nanoparticle–fluid structure with bulk liquid and nanolayers at solid–liquid interface [101].

5.2.1. Effective parameters on thermal conductivity

From the literature [102], it has been noted that the thermal conductivity of nanofluids depends on several factors such as concentration, particle size and shape, material, purity level, motion, and temperature as represented in Figure 10.

1. Effect of particle size:

   The size of nanoparticle is a significant physical parameter which affects the thermal conductivity and the stability of nanofluids. From the review of previous studies on nanoparticle formation, researchers have strongly declared that the size of nanoparticle has a significant role in increase and decrease of thermal conductivity of nanofluid. As the size of nanoparticles varies within nanoscale range $1 - 100nm$ at least in one dimension on the basis of their dimensionality classification. The

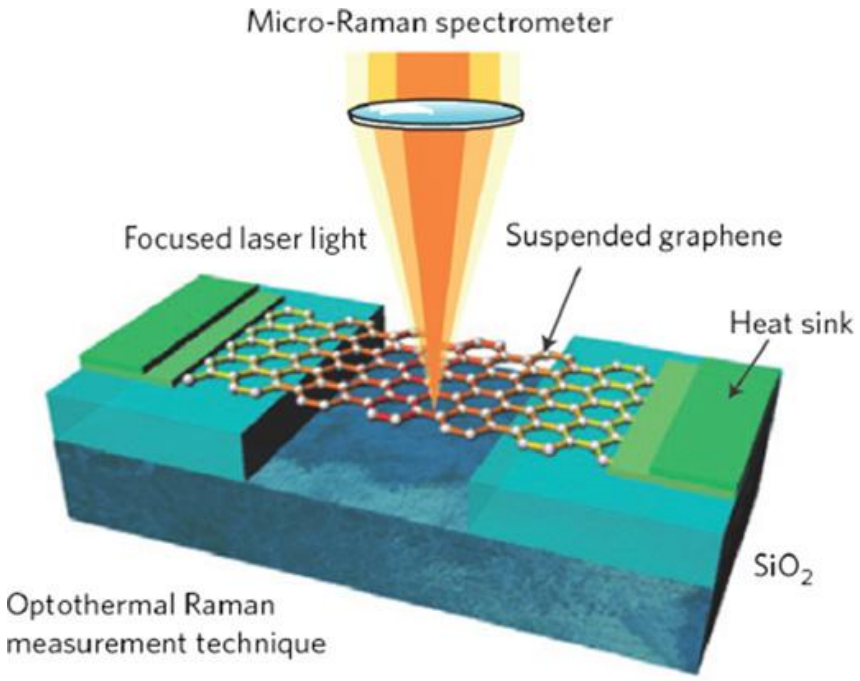

Figure 9: Thermal conductivity measurement of graphene using an opto-thermal Raman technique, from Ref. [100], reused with permission from Elsevier license number 4384861240443.

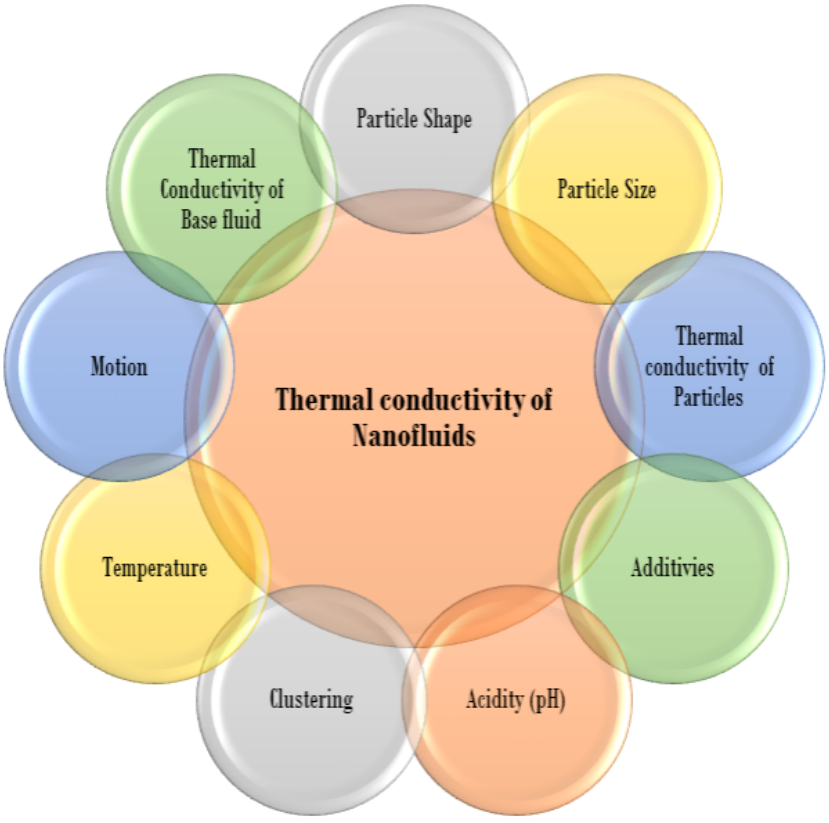

Figure 10: Factors affecting the thermal conductivity of nanofluids.

experimental studies showed that there is an inverse relation between the particle size and thermal conductivity [91].

2. Effect of particle Shape:

   It has been shown that generally two particle shapes, cylindrical and spherical, have been proved to have the highest thermal conductivity [103]. The effect of particle shape is generally expressed by the aspect ratio; length–to–diameter ratio. Experiments showed that the higher the aspect ratio (AR) of cylindrical or rod shape nanoparticles had the higher enhancement in thermal conductivity of nanofluids than the spherical shape nanoparticles due to more surface area along the length of the particle [9].

3. Temperature:

   From the recent experimental investigation [104], it has been found that temperature has a significant role on thermal conductivity of nanofluid and has a direct relation, that is, with increase of temperature increases the thermal conductivity of the nanofluid. Two fundamental aspects, Brownian motion and clustering, are affected by the change of temperature.

4. Motion:

   There are three types of motion which have an influence on the thermal conductivity of nanofluids [29]:

   - Thermo–phoretic motion (due to temperature gradient)
   - Brownian motion (force)
   - Osmophoretic motion (due to concentration gradient)

   The previous studies claimed that Brownian motion has the most significant role in the increase of thermal conductivity of nanofluids. However, the Osmophoretic motion, which is caused by concentration difference, has the least impact on increase in thermal conductivity because it varies with percent of concentration.

5. Thermal conductivity of particles:

   Obviously, the thermal conductivity of the nanoparticle itself has a major role in enhancement of thermal conductivity for specific base fluid nanofluid. Experiments have proven that [105], for a specific base fluids e.g. water, the suspension of nanoparticles of different materials show the different behaviour on the overall thermal conductivity of a nanofluid. A nanoparticle with higher thermal conductivity results in higher thermal conductivity of nanofluid.

6. Thermal conductivity of base fluid:

   One of the major influencing parameter in nanofluids, viscosity, has an effect on the thermal conductivity of nanofluid. As it is studied that Brownian motion plays a significant role in particle motion, the viscosity of base fluid has the direct relation with flow motion of nanoparticles [106]. The effect of interfacial layer around the nanoparticle suspended in base fluid, also called electrical double layer, is considered a dominant factor in thermal conductivity of the nanofluid.

7. Clustering:

   Another feature which can be the consequence on thermal conductivity of nanofluids is clustering. With increasing concentration level of nanoparticles and preparation higher time, nanoparticles tend to cluster resulting in a reduction of the effective interaction area with base fluid and ultimately

reduction in the thermal conductivity of nanofluids. Zhu et al. [107] claimed that clustering and particle alignment had significantly role in increasing the thermal conductivity of nanofluid.

8. Additives:

   Additives are added to keep the nanoparticles in suspension and prevent them from agglomeration. Actually, additives form an insulting layer around the nanoparticle to be dispersed in base fluid which ultimately help to make uniform suspended solution. Hence, it is expected that additives have some role in the enhancement of thermal conductivity of nanofluids [12].

9. Acidity (pH):

   From the previous investigations, it is revealed that there?s not much research on the effect of pH of base fluid on the thermal conductivity of nanofluids.

5.2.2. Thermal conductivity models

Until now there are different types of models to predict the thermal conductivity of nanofluids. These models are categorized into five sub–group based on k models, as follows [108, 109]:

1. Classical effective medium theory (EMT)
2. Nanoscale layer
3. Brownian motion
4. Agglomeration
5. Other mechanisms

The further sub–categories of these models are shown in Figure 11. Table 3 summarises the various conventional theoretical models from previous studies to evaluate the thermal conductivity of nanofluids.

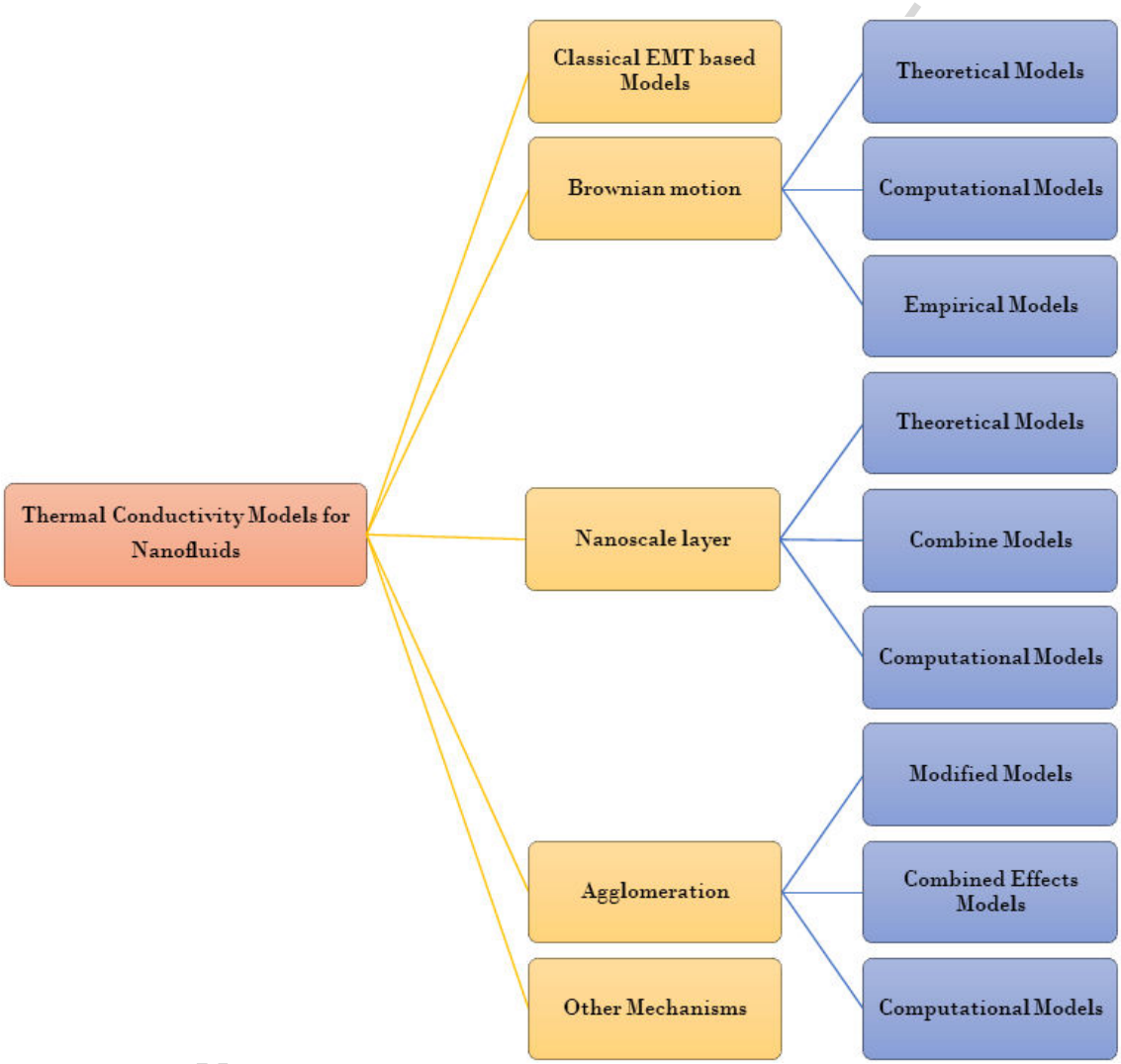

Figure 11: Thermal conductivity models for nanofluids.

Table 3: A few conventional thermal conductivity measurement models for nanofluids.

Authors	**Mathematical formulation**	**Key parameters**	**Remarks**
Maxwell [110]	$\frac{\kappa_{eff}}{\kappa_{bf}} = \frac{\kappa_{np}+2\kappa_{bf}+2(\kappa_{np}-\kappa_{bf})\varphi}{\kappa_{np}+2\kappa_{bf}-(\kappa_{np}-\kappa_{bf})\varphi}$	κ_{np}, κ_{bf}, φ	To determine the effective thermal conductivity of dilute solid-liquid mixture of spherical shaped particles, based fluid and volume concentration of solid particles.
Bruggeman et al. [111]	$\frac{\kappa_{eff}}{\kappa_{bf}} = \frac{1}{4}\left[(3\varphi-1)\frac{\kappa_{np}}{\kappa_{bf}}+(2-3\varphi)\right] + \frac{\sqrt{\Delta}}{4}$ $\Delta = \left[(3\varphi-1)^2\left(\frac{\kappa_{np}}{\kappa_{bf}}\right)^2+(2-3\varphi)^2+2(2+9\varphi-9\varphi^2)\left(\frac{\kappa_{np}}{\kappa_{bf}}\right)\right]$	κ_{np}, κ_{bf}, φ	To determine the effective thermal conductivity at particle interaction of spherical particles. Identical to Maxwell relation at low volume concentrations but discrepancy increased as the volume concentration and thermal conductivity ratio increases.
Hamilton and Crosser [112]	$\frac{\kappa_{eff}}{\kappa_{bf}} = \frac{\kappa_{np}+(n-1)\kappa_{bf}-(n-1)(\kappa_{bf}-\kappa_{np})\varphi}{\kappa_{np}+(n-1)\kappa_{bf}-(\kappa_{bf}-\kappa_{np})\varphi}$	κ_{np}, κ_{bf}, φ	To determine the effective thermal conductivity of two heterogeneous components systems with different particle shapes, composition and sizes. The empirical shape factor, $n = 3/\psi$, ψ is the particle sphericity.
Hashin and Shtrikman [113]	$\frac{\kappa_{np}+2\kappa_{bf}+2(\kappa_{np}-\kappa_{bf})\varphi}{\kappa_{np}+2\kappa_{bf}-(\kappa_{np}-\kappa_{bf})\varphi} \leq \frac{\kappa_{eff}}{\kappa_{bf}} \leq \frac{3\kappa_{bf}+2(\kappa_{np}-\kappa_{bf})\varphi\kappa_{np}}{3\kappa_{np}-(\kappa_{np}-\kappa_{bf})\varphi\kappa_{bf}}$	κ_{np}, κ_{bf}, φ	To determine the effective thermal conductivity of multiphase materials in series and parallel mode of thermal conduction in terms of phase permeabilities and volume concentrations.
Jeffrey [114]	$\frac{\kappa_{eff}}{\kappa_{bf}} = 1+3\varphi\beta+\varphi^2\left(3\beta^2+\frac{3\beta^3}{4}+\frac{3\beta^3}{16}\frac{\chi+2}{3\chi+3}+\frac{3\beta^4}{64}+...\right)$ where, $\beta = \frac{\kappa_{nf}-\kappa_{bf}}{\kappa_{nf}-2\kappa_{bf}} = \frac{\chi-1}{\chi+2}$ and $\chi = \frac{\kappa_{nf}}{\kappa_{bf}}$	κ_{np}, κ_{bf}, φ	To determine the effective thermal conductivity of stationary random homogenous suspension of spherical particles with small volume concentration assuming heat conduction mode.
Wasp [115]	$\frac{\kappa_{eff}}{\kappa_{bf}} = \frac{\kappa_{np}+2\kappa_{bf}+2(\kappa_{np}-\kappa_{bf})\varphi}{\kappa_{np}-2\kappa_{bf}+(\kappa_{np}-\kappa_{bf})\varphi}$	κ_{np}, κ_{bf}, φ	To determine the effective thermal conductivity of spherical particles as the Maxwell and Hamilton and Crosser models with $\psi = 1$.
Davis [102]	$\frac{\kappa_{eff}}{\kappa_{bf}} = 1+\frac{3(\alpha-1)}{\{\alpha+2-(\alpha-1)\varphi\}}\left\{\varphi+f(\alpha)\varphi^2+O(\varphi^3)\right\}$ with, $\alpha = \frac{\kappa_{np}}{\kappa_{bf}}$	κ_{np}, κ_{bf}, φ	To determine the effective thermal conductivity of composite materials of spherical inclusions.

Hasselman and Johnson [116]	$\frac{\kappa_{eff}}{\kappa_{bf}} = \frac{\kappa_{np}(1+2\gamma)+2\kappa_{bf}+2(\kappa_{np}(1+\gamma)-\kappa_{bf})\varphi}{\kappa_{np}(1+2\gamma)+2\kappa_{bf}-(\kappa_{np}(1+\gamma)-\kappa_{bf})\varphi}$ where γ is dimensionless parameter defined as; $\gamma = \frac{r_K}{r_{np}}$ here r_K is the Kapitza radius,as fellow; $r_K = R_K\kappa_{bf}$,here R_K is the Kapitza or thermal boundary resistance.	κ_{np}, κ_{bf}, φ	To determine effective thermal conductivity of composite introducing thermal barrier resistance at the interface of materials with dilute concentrations of spherical, cylindrical, and flat plate configurations dispersed components.
Nan et al. [117]	$\frac{\kappa_{eff,11}}{\kappa_{bf}} = \kappa_{eff,22}\left[\frac{2+\varphi\{\beta_{11}(1-L_{11})(1-\langle\cos^2\theta\rangle)+\beta_{33}(1-L_{33})(1-\langle\cos^2\theta\rangle)\}}{2-\varphi\{\beta_{11}L_{11}(1+\langle\cos^2\theta\rangle)+\beta_{33}L_{33}(1-\langle\cos^2\theta\rangle)\}}\right]$ and $\frac{\kappa_{eff,33}}{\kappa_{bf}} = \left[\frac{1+\varphi\{\beta_{11}(1-L_{11})(1-\langle\cos^2\theta\rangle)+\beta_{33}(1-L_{33})(1-\langle\cos^2\theta\rangle)\}}{1-\varphi\{\beta_{11}L_{11}(1-\langle\cos^2\theta\rangle)+\beta_{33}L_{33}\langle\cos^2\theta\rangle\}}\right]$ with, $\beta_{ii} = \frac{\kappa_{ii}^c-\kappa_{bf}}{\kappa_{bf}+L_{ii}(\kappa_{ii}^c-\kappa_{bf})}$ and $\langle\cos^2\theta\rangle = \frac{\int\rho(\theta)\cos^2\theta,\sin\theta d\theta}{\rho(\theta)\sin\theta d\theta}$	κ_{np}, κ_{bf}, φ	To determine the effective thermal conductivity of particulate composites of arbitrary shapes (i.e. continuous fibers, flat plates, spheres and misoriented ellipsoidal) using effective medium approach based on Kapitza resistance.
Aberoumand et al. [118]	$\kappa_{nf} = (3.9\times10^{-5}T - 0.0305)\varphi^2 + (0.086 - 1.6\times10^{-4}T)\varphi + 3.1\times10^{-4}T + 0.129 - 5.77\times10^{-6}\kappa_{np} - 40\times10^{-4}$	κ_{np}, T, φ	To determine the thermal conductivity of nanofluids knowing the bulk temperature in °C, volume fraction (0-2%), and thermal conductivity of nanoparticles.
Afrand et al. [119]	$\frac{\kappa_{eff}}{\kappa_{bf}} = 0.7575 + 0.3\varphi^{0.323}T^{0.245}$	T, κ_{bf}, φ	To determine the thermal conductivity of magnetic nanofluids using curve-fitting.
Khdher et al. [120]	$\frac{\kappa_{eff}}{\kappa_{bf}} = 1.268\times\left(\frac{T}{80}\right)^{-0.074}\times\left(\frac{\varphi}{100}\right)^{0.036}$	T, κ_{bf}, φ	To determine thermal conductivity of nanofluids based on the function of concentration, temperature and thermal conductivity of base fluid.
Yang et al. [121]	$\kappa_{eff} = \frac{(H+2t)\kappa_{eff,x}+(R+t)\kappa_{eff,z}}{H+R+3t}$	H, R, $\kappa_{eff,x}$, $\kappa_{eff,z}$	To determine thermal conductivity of nanorod-based nanofluid knowing radius and height of nanorods, thickness of interfacial layer and effective thermal conductivity in x and z directions.
Yang and Xu [122]	$\frac{\kappa_{eff}}{\kappa_{bf}} = \frac{\bar{\kappa}_{pe}+\kappa_{bf}(n-1)+(n-1)(\bar{\kappa}_{pe}-\kappa_{bf})\varphi_e}{\bar{\kappa}_{pe}+\kappa_{bf}(n-1)-(\bar{\kappa}_{pe}-\kappa_{bf})\varphi_e}$	$\bar{\kappa}_{pe}$, κ_{bf}, φ_e	To determine the effective thermal conductivity of CNT based nanofluid by renovating Hamilton and Crosser model.
Ahmadi Nadooshan [123]	$Enhancement = \frac{1.8454-5.2302\varphi^{0.29216}}{T^{0.29216}-3.457}$	T, φ	To achieve the enhancement in thermal conductivity of ZnO/EG-water nanofluid as function of volume fraction and temperature.
Parsian and Akbari [124]	$\frac{\kappa_{eff}}{\kappa_{bf}} = \frac{(9.6128+\varphi)}{9.3885-0.00010759T^2} - \frac{0.0041099}{\varphi}$	T, κ_{bf}, φ	To determine thermal conductivity of $Al_2O_3 - Cu/EG$ nanofluid based on volume fraction and temperature.
Wang et al. [125]	$\frac{\kappa_{nf}}{\kappa_{bf}} = 1 + 21.487\varphi - 91.30\varphi^2$	T, κ_{bf}, φ	To determine thermal conductivity of $GNPs/W + EG$ nanofluid based on volume fraction and temperature.

5.3. Viscosity of graphene nanofluids

Viscosity of the nanofluids is key a parameter on heat transfer performance between the medium because the pressure drop and pumping power depend on it. The effective viscosity of nanofluids depends on the viscosity of the base fluid and volume fraction of the nanoparticles suspended in the fluid. In like manner, other physical parameters like particle size and types of nanoparticles contribute to the effects on viscosity. However the key parameter, temperature, has the significance influence on the viscosity of the nanofluids. Generally, the piston-type rheometer, rotational rheometer, and the capillary viscometer instruments are employed to measure the viscosity of nanofluids [126].

5.3.1. Effective parameters on viscosity of nanofluids

Several factors influence the viscosity of graphene nanofluids, as shown in Figure 12, such as viscosity of base fluid, volume concentration, morphology, clustering, shear rate and temperature.

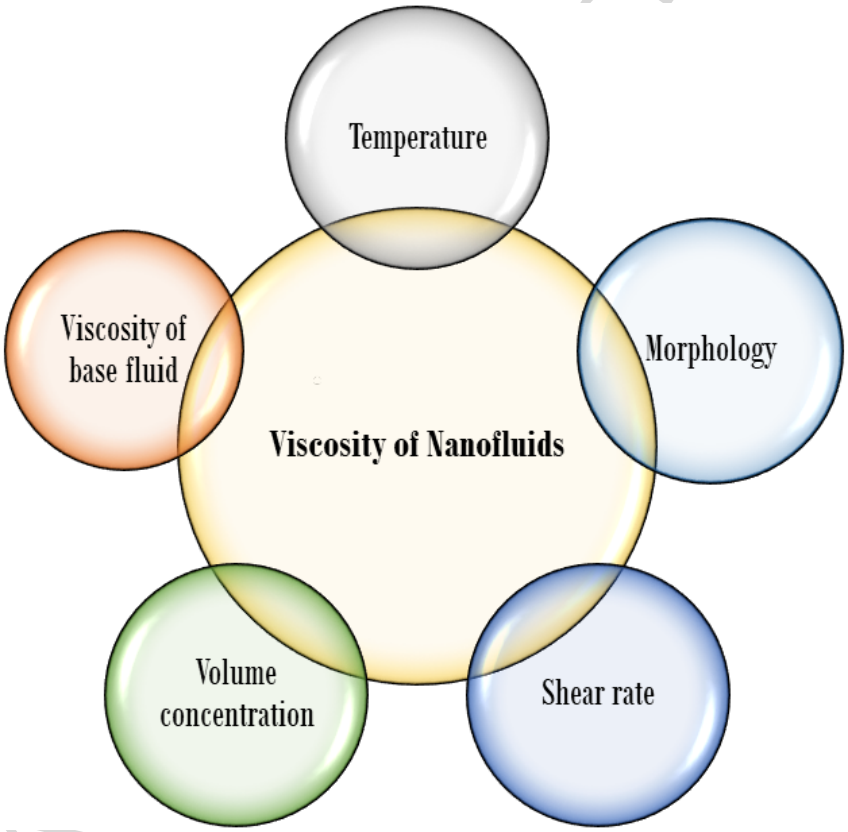

Figure 12: Factors affecting the viscosity of nanofluid.

1. Viscosity of base fluid:

   The inherent viscosity of base fluid has a significant role in increasing and decreasing trend of nanofluids either for both aqueous and non-aqueous solutions. As the pressure drop and pumping power are closely related to each other while using the nanofluids as the cooling medium. Higher the viscous fluid experiences the higher viscosity and pressure drop as well as need more pumping power [127]. Apart from these, high viscosity base fluid needs more critical preparation and stabilize criteria as per the need of application. In contrast of less viscous base fluid experience pressure

drop and pumping power. Additionally, more homogeneous and rheological behaviour are expected while using for heat transfer systems.

2. Clustering:

   The formation of clustering also possesses a significant impact on the viscosity of the nanofluids. The effect of clustering in nanofluid varies gradually with the increase of the concentration of nanoparticles. Initially, at low concentration after sonication, the particles are well dispersed and exhibit low viscosity. But with time and higher concentration, the particles start to form both stable (small and well dispersed cluster) and unstable (big clusters) which lead to increase of viscosity. This stable and unstable clusters come closer after time and form thick agglomerates, which eventually sediment due to gravitational force, resulting in increased viscosity [127]. As a consequence of this, the settling of nanoparticles not only decreased the overall heat transfer rate, but also led to abrasion of surfaces, clogging in micro heat transfer systems, and a decrease in pressure which resulting in an increase of pumping power [106].

3. Effect of volume concentration:

   The volume concentration of nanofluids has the significant influence on the viscosity of nanofluids and generally it is effected by the weight percentage of nanoparticles [128]. From the previous experimental literature survey, it is concluded that the viscosity of nanofluids increases with the increase of particle concentration in the base fluid [53].

4. Effect of temperature:

   The temperature is another the most important and significant parameter which affects the viscosity of the nanofluids. Many studies have been conducted regarding different types of nanoparticle and concluded that temperature has inverse relation with viscosity of nanofluids [129, 130, 131, 132]. With increase of the particle volume fraction the dynamic viscosity increases however with rise of temperature it clearly decreases.

5. Effect of morphology:

   The morphology (size and shape) of the nanoparticles influences the viscosity of the nanofluids along with the pumping power of the heat transfer system [106]. The physical parameters such as particle shape, size, texture and phase distribution of nanoparticles are expressed by the specific surface area (SSA) of nanoparticle, defined in Eq. 3 [29].

$$SSA = \frac{A_{np}}{V_{np}} \tag{3}$$

   Here, A_{np} and V_{np} are the surface area and volume, respectively, of the nanoparticle. From experimental studies of Refs. [129, 133], it was shown that increasing the size of nanoparticle resulted in increases in the viscosity of nanofluid.

6. Effect of shear rate:

   Nanofluids behave as shear-thinning materials at concentration loading range of $0.35 - 5.2\%$ with different temperature of $20 - 80°C$ [134]. Research revealed that at lower volume concentration of particles the nanofluids has Newtonian behaviour whereas at higher volume concentration it represents the non-Newtonian behaviour [135, 136]. Additionally, at higher loading of nanoparticles,

the nanofluids performed as a shear-thinning fluid. At higher shear rate the relative viscosity of nanofluids is slightly decreased and does not fluctuate with temperature.

5.4. Density of graphene nanofluids

Normally, the density of nanofluids directly relates with the Reynolds number, friction factor, pressure loss, and Nusselt number. From a researcher point of view, the density of phase-change mediums is measured either in terms of volume fraction or weight fraction. Generally, the density of the nanofluids increases with increasing concentration of nanoparticles at constant temperature. Few studies have been reported on the density of graphene nanofluid. Liu et al. [74] carried out an experiment to determine the density of graphene nanofluid of graphene weight percentage (wt.%) of 0.03% and 0.06%. The result reported that the density decreases with the increase of the weight percentage of graphene nanoparticles, is shown in Figure 13. Moreover, the density of nanofluid can be calculated by using following relation Eq. 4.

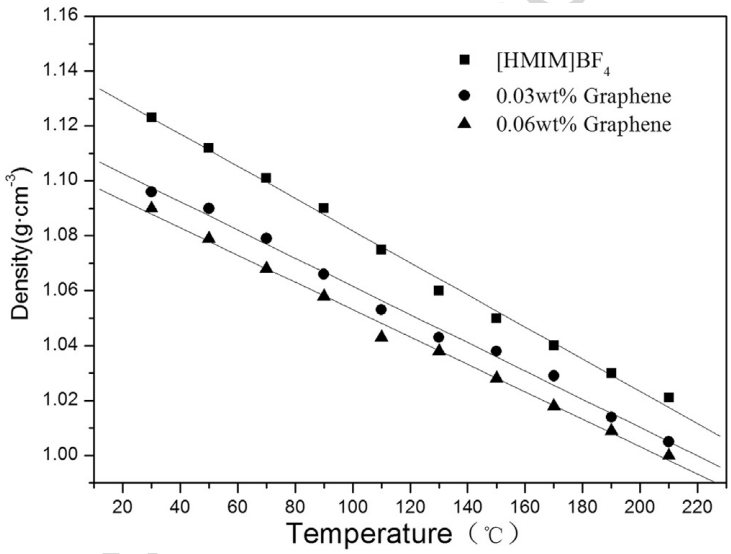

Figure 13: Density variation of at different weight percentage of graphene nanoparticles, from Ref. [74], reused with permission from Elsevier license number 4384870183116.

$$\rho_{nf} = \varphi\rho_{np} + (1-\varphi)\rho_{bf} \tag{4}$$

Here, ρ_{nf}, ρ_{np}, and ρ_{bf} , respectively, are the density of nanofluid, nanoparticles and base fluids and φ is the volume fraction of nanoparticles.

5.5. Specific heat of graphene nanofluids

The specific heat, which is defined as the amount of heat energy transferred from a one unit mass or substance by a unit degree temperature to change the system temperature. There are two specific heat models to determine the specific heat of nanofluids. Model I is based on the volume concentration of nanoparticles, which was presented by Pak and Cho [137], by considering the liquid–particle mixture formula. The specific heat of nanofluids $(C_p)_nf$ defined by Model I by Eq. 5.

$$(C_p)_{nf} = \varphi(C_p)_{np} + (1-\varphi)(C_p)_{bf} \tag{5}$$

Model II, which is based on the assumption of thermal equilibrium between the nanoparticles and surrounding fluid, was presented by Xuan and Roetzel [138]. Model II can be expressed by Eq. 6.

$$(C_p)_{nf} = \frac{\varphi(\rho C_p)_{np} + (1-\varphi)(\rho C_p)_{bf}}{\varphi\rho_{np} + (1-\varphi)\rho_{bf}} \tag{6}$$

Here, $(C_p)_{np}$ and $(C_p)_{bf}$ are the specific heat of nanoparticles and base fluids, respectively. Eq. 6 is more conveniently used to determine the specific heat because specific heat is a specific mass based quantity which have the effects of density of the system component and mixture.

6. Applications of graphene nanofluids

Nanotechnology has been used for many energy applications for efficient and cleaner uses and supplies. However, the efficient heat transfer distribution through an energy system is a key point that is required to reduce the cost of maintenance or reinstalling. Effective thermal performance requires efficient transport phenomenon of thermal properties including thermal conductivity as well as specific heat, viscosity, and density. Along with this, there are several other parameters such as surface condition (rough or smooth), type of surfactants, base fluid properties (i.e. thermal, chemical, and rheological), system configuration (i.e. size, geometry, orientation) and material that affect the performance of heat transfer (i.e. conduction and convective heat transfer coefficients, critical heat flux, diffusion coefficient.) [139]. Additionally, the flow regimes (i.e. laminar, transitional and turbulent) of nanofluids through the thermal energy systems are of key importance to enhance the heat transfer rate. Figure 14 shows the different technologies areas of nanofluids applications [94, 140, 141].

6.1. Electronics cooling

The two increasing ranges of heat flux; high–heat–flux ($10^2 - 10^3$) and ultra–high-heat–flux ($10^3 - 10^5$) [142] are less explored relative to dissipate the magnitude of heat from various electronics such as supercomputers, power devices, battery operated electric vehicles and advanced avionics using suitable type of coolant. The utilization of graphene based nanofluid with pin–fin heat sinks was examined by Ali and Arshad [143, 144]. The experimental study examined the effect of channel angles of 22.5°, 45° and 90° of pin–fin heat sink using graphene nanoplatelets (GNPs)/distilled water (DW) nanofluid. The authors found the optimum angle of 22.5° pin–fin heat sink with the lowest thermal resistance of 0.011 K/W which had the 22.17% reduction using GNPs nanofluid with respect to conventional DW [143]. The enhancement ratio in convective heat transfer coefficient of 23.86% was obtained using GNPs/DW nanofluid, shown in Figure 15. Additionally, the authors reported that decreasing the pin angle provided the better heat transfer coefficient, as the pin angles of 22.5° and 45° heat sink showed 84.30% and 38.48% higher convective heat transfer coefficient than the 90° of pin–fin heat sink. The effect of varying input heat fluxes of 47.96 kW/m^2, 59.95 kW/m^2, and 71.94 kW/m^2 using GNPs/DW as coolant through integral fin heat sink was further studied by Arshad and Ali [144]. The heat transfer and fluid flow

Figure 14: General applications of nanofluids.

parameters were investigated by changing the Reynolds number and pumping power. The lowest base temperature of 36.81°C, lowest thermal resistance of 0.049 K/W and maximum pumping power of 0.041 W were achieved with integral fin heat sink at heat flux of 47.96 kW/m^2 and a Reynolds number of 972 using GNPs/DW nanofluid. Additionally, the average enhancement in convective heat coefficient was achieved of 21.52%, 15.38%, and 13.76% at heat flux of 47.96 kW/m^2, 59.95 kW/m^2, and 71.94 kW/m^2, respectively, using GNPs/DW nanofluid.

6.1.1. Discussion

The thermal management of electronics through active cooling media has always been a great challenge for electronic industries especially for high heat generating electronic devices. Research [143, 144] contributed a remarkable advancement in active cooling technology introducing two different arrangement of fin heat sinks with GNPs/DW nanofluid. It can be seen that heat transfer and pumping power are significantly dependent on the provided heat flux. At low input heat flux, the GNP/DW nanofluid has the better heat transfer performance than at high heat flux, however, higher pumping power is needed at low heat flux [144]. Comparing the lowest thermal resistances of 0.011 K/W and 0.049 K/W found in investigations [143, 144], it can be suggested that a pin–fin heat sink of 22.5° fin angle is more effective than integral fin heat sink using GNPs/DW nanofluid. Moreover, it can also be suggested that integral fin heat sink with GNPs nanofluid is highly suitable for electronic devices dissipating the maximum heat flux around ≈ 50 kW/m^2. The detail summary of these studies is reported in Table 4.

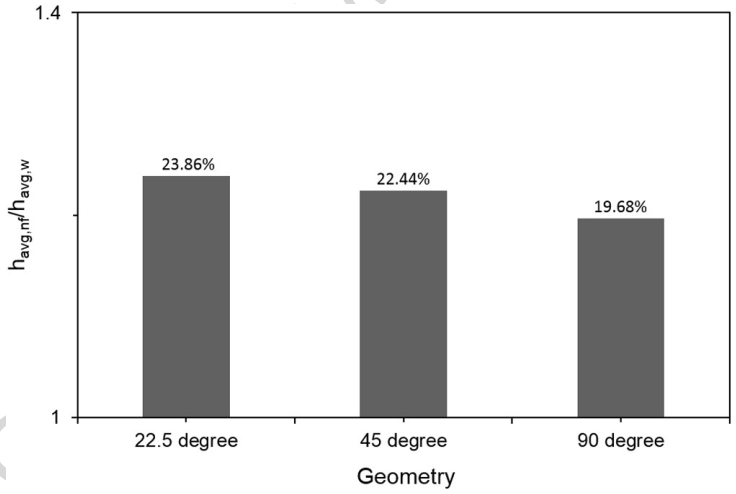

Figure 15: Comparison of convective heat transfer coefficient enhancement ratio GNPs water based nanofluid, from Ref. [143], reused with permission from Elsevier license number 4503690637201.

Table 4: Graphene based nanofluids for electronics cooling

Ref.	NPs	SM	PS	CONC.	BF	SFTs	PM	pH	Charac. Tech.	Findings
[143]	GNPs	Supplied by manufacturer	d=5–10μm	10 wt.%	DI water	PVP	Two–step method	N/A	N/A	They experimental examined the effect of channel angle of heat sink of 22.5°, 45° and 90° angles, water as a base fluid and GNPs. The results showed that, using GNPs, the 22.5° pin–fin heat sink had the lowest thermal resistance of 0.011 K/W with percentage reduction of 22.17% with GNPs with respect to distilled water. Furthermore, the enhancement ratio of 23.86% was obtained of convective heat transfer coefficients using GNPs with respect to distilled water.
[144]	GNPs	Supplied by manufacturer	d=5–10μm	10 wt.%	DI water	PVP	Two–step method	N/A	N/A	The lowest base temperature of 36.81°C, lowest thermal resistance of 0.049 K/W and maximum pumping power of 0.041 W were achieved with integral fin heat sink at heat flux of 47.96 kW/m^2 and Reynolds of 972 using GNPs/DW nanofluid. Additionally, the average enhancement in convective heat coefficient was achieved of 21.52%, 15.38%, and 13.76% at heat flux of 47.96 kW/m^2, 59.95 kW/m^2, and 71.94 kW/m^2, respectively.

6.2. Heat pipe

The heat pipe, which is a two–phase heat transfer device, is investigated with various coolant mediums as an advance active and passive cooling technology. So far, various graphene based nanomaterials such as GNSs, NDG, GNPs, and GO in miniature loop heat pipe (mLHP), wick and grooved heat pipe, and oscillating heat pipe (OHP) [145, 146, 147, 148, 149].

The effect of thermal performance and entropy generation analysis were conducted using GNSs/DW [145, 146] nanofluids of volume concentration range of $0.003 - 0.009$ vol.%. Authors reported significant enhancement in thermal conductivity, heat transfer coefficient; and reduction in thermal resistance and entropy generation. The enhancement in thermal conductivity, heat transfer coefficient, and thermal efficiency with GNSs/DW nanofluids of 27.6%, 62.3%, and 93% are obtained respectively, and lowest thermal resistance of 0.083 K/W at optimum volume concentration of 0.006 vol.% than which is 21.6% than DW [145]. The increase in second law efficiency predicted 19.4% and 37.5% efficiencies for 0.003 vol.% and 0.006 vol.%, respectively, and average reduction in entropy generation of 23.9% and 34.6% was obtained for the same concentration [146], shown in Figure 16.

The thermal performance of nitrogen–doped graphene (NDG) nanosheets dispersed in DI–water nanofluid was investigated in grooved heat pipe at varying concentrations and inclination angles by Mehrali et al. [147]. An optimum inclination angle of 90° was predicted at which the heat pipe showed the best heat transfer performance. At 90° inclination angle and concentration of 0.06 wt.%, the maximum reduction in thermal resistance and enhancement in heat transfer coefficient of 58.6% and 99% were obtained respectively. Additionally, at low input heat rates NDG nanofluid had better thermal conductivity and deposition of nanosheets helped to increases the heat transfer performance. In another experimental investigation on sintered wick heat pipe, Sadeghinezhad et al. [148] examined the inclination angles $0 - 90°$ and weight concentrations $0.025 - 0.1$ wt.% of GNP/DW nanofluid. They found the optimum inclination angle of 60° and 0.1 wt.% concentration at which maximum reduction in thermal resistance of 48.4% was achieved. Additionally, maximum effective thermal conductivity enhancements of 23.4%, 29.8%, 37.2%, and 28.3% were obtained at input powers of 20, 40, 60, and 80 W, respectively, at 60° and 0.1 wt.%. The results of thermal efficiency is shown in Figure 17, and it can be seen the maximum thermal efficiency of $\sim 80\%$ is obtained at highest input power and weight concentration because at high input load the thermal resistance is lower. Yarmand et al. [150] examined the thermal conductivity, density, viscosity, specific heat capacity, overall heat transfer coefficient and friction factor under turbulent flow regime using f-GNPs/water nanofluid as a coolant in a square heat pipe. The results revealed the enhancement of thermal conductivity, viscosity and density with the increase of weight concentrations. Further improvement in Nusselt number and overall heat transfer coefficient 26.5% and 19.68% at 0.1 wt.%, were obtained respectively, and 9.22% increased in friction factor at Reynolds number of $17,500$.

The effect of GO/water based nanofluid in a screen mesh wick heat pipe was investigated by Kim and Bang [151] and showed that evaporator side had lower thermal resistance of 25% at 0.01 vol.%. The reason for the lower thermal resistance on the evaporator side of heat pipe is because of the GO nanoparticles–coated layer formed a hydrophobic layer on the wick structure resulting in higher liquid flow through the screen mesh wick heat pipe. Su et al. [149] measured the effect of mass fraction, thermal conductivity

and surface tension of OHP using self–rewetting nanofluid based on GO with n-butanol alcohol aqueous solution. The findings revealed that maximum heat transfer performance was 16% with self–rewetting nanofluid at 0.07 wt.% of GO and 0.07 wt.% of n–butanol concentration, whereas it was 12% with GO aqueous nanofluid.

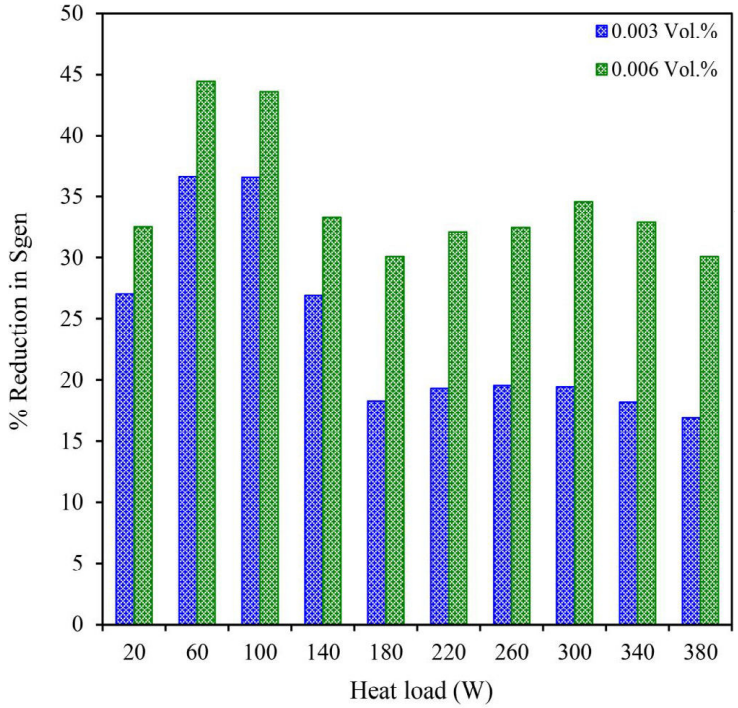

Figure 16: Reduction in entropy generation with GNS/water nanofluids, from Ref. [146], reused with permission from Elsevier license number 4384870973598.

6.2.1. Discussion

So far, it can been observed that the utilization of GE based nanofluids with various types of heat pipes have been under investigation and have achieved remarkable enhancement in heat transfer performance. The GNSs based nanofluids with mLHP proves that at 0.006 vol.% concentration GNSs has the best thermal performance by achieving 62.3%, 93% and 37.5% enhancement in heat transfer coefficient and thermal efficiency and second law efficiency, respectively. Additionally, lowest thermal resistance and reduction in entropy generation are obtained of 0.083 K/W and 34.6%, respectively, at 0.006 vol.% concentration GNSs based nanofluid [145, 146]. The findings on inclined heat pipes with GE based nanofluids provided the two different optimum angles i.e 90° [147] and 60° [148] but these results are with two different types of GE nanomaterials i.e. NDG and GNPs, respectively. Thus, the authors suggest further exploration of the optimum inclination angle adopting various optimization techniques by keeping or varying same types of GE nanomaterials, concentrations and host fluids. The optimum concentration of GNPs of 0.1 wt.% obtained by [148, 150] which shows the maximum heat transfer performance in terms of achieving maximum reduction in thermal resistance of 48.4% [148] and highest Nu number of 26.5% [150]. Here it is noted that the functionalization of GNPs may exhibit the different effects in thermal performance of heat pipes. So, it is suggested to compare the thermophysical and heat transfer

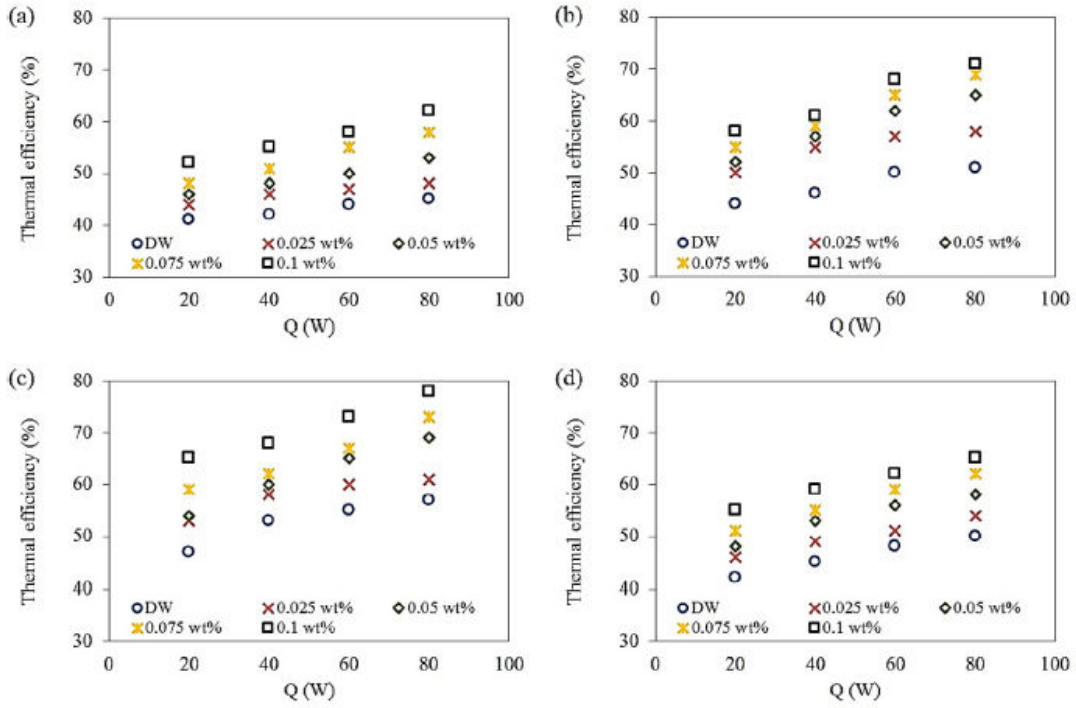

Figure 17: Thermal efficiency of heat pipe as a function of power at various titled angles; (a) 0° (b) 30°(c) 60° (d)90°, from Ref. [148], reused with permission from Elsevier license number 4384880309615.

performance results of functionalized and non-functionalized GE based nanomaterials by varying base fluids. Table 5 gives a detailed summary of graphene based nanofluids with heat pipe application.

Table 5: Graphene based nanofluids with heat pipe.

Ref.	NPs	SM	PS	CONC.	BF	SFTs	PM	pH	Charac. Tech.	Findings
[145]	GNSs	Supplied by manufacturer	t=1–5nm	0.003% 0.006% 0.009%	DW	N/A	Two–step method	N/A	Zeta potential test, Particle size test	The authors found the 0.006% the optimum concentration and found thermal resistance of 0.083 K/W and thermal conductivity of 27.6% of heat pipe using GE water nanofluid.
[146]	GNSs	Supplied by manufacturer	t=1–5nm	0.003 vol.% 0.006 vol.%	DW	Not used	Two–step method	N/A	Zeta potential test, TEM	It was found that entropy generation was reduced of 23.9% and 34.6% for 0.003 vol.% and 0.006 vol.% respectively. Further, the second law of efficiency was increased by 19.4% and 37.5%.
[147]	NDG	Modified Hummers method	d< 45μm	0.01% 0.02% 0.04% 0.06%	DI water	Triton X-100	Two–step method	11	UV–vis spectrometer, Zeta potential test, FESEM, TEM, XPS	At 90° inclination angle and concentration of 0.06 wt.%, the maximum reduction in thermal resistance and enhancement in heat transfer coefficient were obtained of 58.6% and 99%, respectively.
[150]	f-GNPs	Supplied by manufacturer	d=5–10μm	0.02–0.1 wt.%	water	Not used	Facile method	N/A	Dynamic light scattering (DLS), UV-vis spectrometer, TEM, FTIR, FESEM, XRD	The results revealed the enhancement of thermal conductivity, viscosity and density with the increase of weight concentrations. Nusselt number and overall heat transfer coefficient were obtained 26.5% and 19.68% at 0.1 wt.%, respectively, and 9.22% increased in friction factor at Reynolds number of 17,500.
[148]	GNPs	Supplied by manufacturer	t=2nm d=2μm	0.025% 0.05% 0.075% 0.1%	DW	N/A	Two–step method	N/A	FESEM, TEM,	The results found the optimum inclination angle of 60° and 0.1 wt.% concentration at which maximum reduction in thermal resistance was achieved of 48.4%. Additionally, the maximum effective thermal conductivity enhancements were obtained of 23.4%, 29.8%, 37.2%, 28.3% at input powers of 20, 40, 60, and 80W, respectively, at 60° and 0.1 wt.%.

[151]	GO	chemical oxidation and exfoliation	t=1nm	0.01% 0.03%	DW	N/A	Two–step method	N/A	Zeta potential test	They found that wall temperature was lower than water heat pipe, further evaporator side had lower thermal resistance of 25% using GO/water nanofluid.
[149]	GO	Supplied by manufacturer	t=50–200nm d=0.8–1.2μm	0-0.12%	n-butanol alcohol	N/A	Two–step method	N/A	N/A	The findings revealed that maximum heat transfer performance was 16% with self–rewetting nanofluid at 0.07 wt.% of GO and 0.07 wt.% of n-butanol concentration, whereas it was 12% with GO aqueous nanofluid.

6.3. Automotive engine cooling

Thermal management of automotive engines strongly influences the performance of vehicles directly and indirectly as it affects engine performance, fuel consumption, human comfort, emissions, maintenance, component life and vehicles reliability. For the efficient cooling of automotive engines using GE nanofluid has been under investigation by various researchers. Amiri et al. [152] used CNDG with DI water–EG mixture and Selvam et al. [153, 154] used GNPs dispersed in EG–water mixture, as a coolant flowing through an automobile radiator. The excellent cooling performance of CNDG/DI water+EG based nanofluid was obtained exhibiting excellent Mouromtseff number, convective heat transfer coefficient and Nusselt number for all temperatures and weight concentrations. The results showed that the ratios of Mouromtseff and Nusselt number of CNDG/water+EG nanofluid to the base fluid were higher than 1 which showed potential enhancement in heat transfer. Enhancement in heat transfer coefficient and thermal conductivity of 83% and 19.4%, respectively, was achieved at weight concentration of 0.01 wt.% which revealed that the enhancement in convective heat transfer was better than the thermal conductivity [152]. Selvam et al. [153] reported enhancement in convective heat transfer of 20% and 51% at inlet temperatures of 35°C and 45°C, respectively, at highest concentration (0.5 vol.%) and mass flow rate (100 g/s). Increasing trend of pressure drop was observed with increasing volume concentration of $0-0.5$ vol.% from 3.07 to 4.88 kPa at 35°C while it increased from 3.02 to 4.04 kPa at 45°C for 100 g/s. Figure 18 shows that with increasing *Re* number and nanoparticles loading, highest convective heat transfer coefficient was achieved. Moreover, the higher enhancement in thermal conductivity of GNP/water+EG nanofluid was achieved with increase of temperature as well as GNPs loading. The enhancement in overall heat transfer coefficient using GNP/water-EG nanofluid, is shown in Figure 19, with different *Re* numbers at constant air velocity of 5 m/s for two inlet temperatures of $T = 35^{\circ}$ and $T = 45^{\circ}$ [154]. The maximum enhancement in overall heat transfer coefficient obtained was about $\sim 108\%$ and $\sim 81\%$ at 35°C and 45°C, respectively, for $0.5vol\%$, 62.5 g/s and 5 m/s. From figure 19, it can be seen the the OHTC has the increasing trend with the increase of *Re* number and loading of GNPs.

6.3.1. Discussion

There has been research which has contributed remarkable advancement in cooling performance of automotive engine [152, 153, 154]. It can be observed that higher heat transfer coefficient is obtained with increasing the loading of GNPs, as $\sim 108\%$ enhancement is achieved at 0.5 vol.% which is very significant for inlet temperatures of 35°C and 45°C [154]. Comparing enhancement of $\sim 108\%$ and 83% in convective heat transfer coefficients of studies [154] and [152], it can be observed that former investigation has the better cooling performance at same inlet temperature of 35°C. Furthermore, the pressure drop increases with increasing the loading of GNPs whereas with the increase of inlet temperature from 35°C to 45°C, the pressure drop decreases at constant loading and flow rate [153]. The increase in pressure drop is significantly more influenced by mass flow rate rather than GNPs loading. Here, the authors suggest that further investigations are needed for different base fluid, varying loading, and inlet temperature across the car radiator. The detail descriptions studies are provided in Table 6.

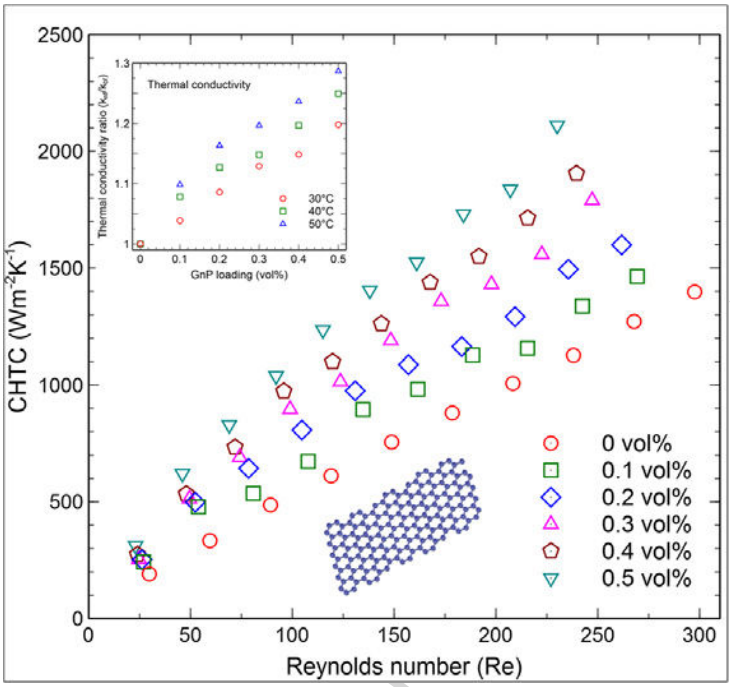

Figure 18: Effect of Re number and CHTC at various loading of GNPs, from Ref. [153], reused with permission from Elsevier license number 4385231493845.

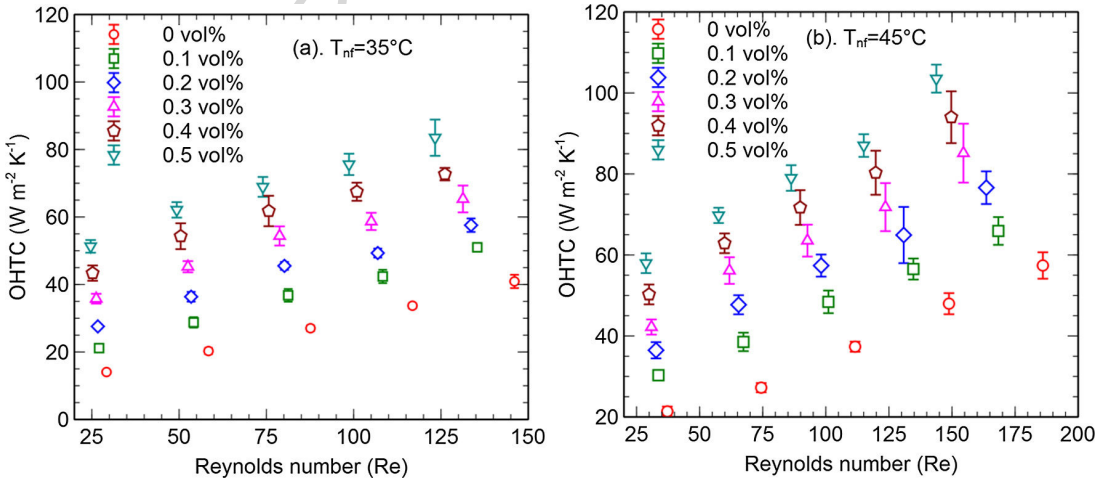

Figure 19: Enhancement in OHTC as function of Re for various loading of GNPs, from Ref. [154], reused with permission from Elsevier license number 4385231269869.

Table 6: Graphene based nanofluids for automotive engine cooling.

Ref.	NPs	SM	PS	CONC.	BF	SFTs	PM	pH	Charac. Tech.	Findings
[152]	CNDG	Hummers method	N/A	0–0.01 wt.%	DI water–EG	N/A	Two–step method	N/A	X–ray photoelectron spectroscopy, Raman spectroscopy	The results found the enhancement of thermal and electrical conductivity as well the heat transfer enhancement. The enhancement in heat transfer coefficient and thermal conductivity was achieved of 83% and 19.4%, respectively, at weight concentration of 0.01 wt.%.
[153]	GNPs	Supplied by manufacturer	t=5–10nm d=15μm	0.1 $-$ $-$0.5%	Water-EG mixture	SDC	Two-step method	N/A	Vibration-vis absorption spectroscopy, Zeta potential test	They found the enhancement in convective heat transfer coefficient of 20% and 51% for inlet temperatures of 35°C and 45°C. The pressure drop was increased from 3.07 $-$ $-$4.88 kPa by increasing GNPs from 0–0.5% at 35°C while it increased from 3.02 $-$ $-$4.04 kPa at 45°C for 100 g/s.
[154]	GNPs	Supplied by manufacturer	t=5–10nm d=15μm	0.1–0.5%	Water–EG mixture	SDC	Two–step method	N/A	Vibration-vis absorption spectroscopy, Zeta potential test	The result found that both convective and overall heat transfer coefficient increased by increasing mass flow rate, inlet temperature and concentration of GNPs. The maximum enhancement in overall heat transfer coefficient was obtained about $\sim$ 108% and $\sim$ 81% at 35°C and 45°C, respectively, for 0.5 vol.%, 62.5 g/s and 5 m/s.

6.4. Micro/Mini–channels

A few studies have reported use of minichannel with GE based nanofluids for thermal system applications. Ahammed et al. [155] conducted an experimental study for entropy generation and heat transfer analysis for multiport minichannel heat exchanger coupled with a thermoelectric cooler. Hybrid nanofluid containing Al_2O_3 nanoparticles and GNSs under two different heat fluxes of 6250 W/m^2 and 25000 W/m^2, and *Re* number range from 200 to 1000, were investigated in an multiport minichannel shown in Figure 20. Results showed a remarkable contribution in heat transfer and thermodynamics performance by increasing cooling performance of thermoelectric cooler by 72% and decreasing the total entropy generation of 31.86% using GNSs/water nanofluid in comparison of hybrid and Al_2O_3 nanofluids. Furthermore, the maximum enhancement of 88.62% was achieved in convective heat transfer coefficient of with GNSs/water nanofluid whereas it was 63.13% and 31.89% using hybrid and Al_2O_3 nanofluids, respectively. The results of increase of pressure drop also revealed that GNSs/water has the least drop of 11.17% as compared to hybrid and Al_2O_3 nanofluids having 20.35% and 33.14%, respectively. The effect of flow boiling heat transfer and resulting surface deposition analysis of GO/water nanofluid in microchannels was investigated by Zhang et al. [156]. The results of heat transfer and surface deposition were presented under varying concentration of $0 - 0.05\%$ and showed that higher concentration had lower heat transfer coefficient. Additionally, non–porous structure surface deposition was formed with GO nanofluid which blocked the nucleation sites and had a negative effect on heat transfer coefficient. The results of energy dispersive spectrometer confirmed that GO was partly reduced chemically during boiling process which causes the surface deposition.

6.4.1. Discussion

The micro and minichannels are widely used for various industrial applications for thermal management, energy conversion and harvesting. Researchers [155, 156] contributed a remarkable advancement phase change heat transfer performance through GE based nanofluids. It can be clearly suggested that thermal performance of GNSs nanofluid is better in comparison with Al_2O_3 and hybrid (GNSs+Al_2O_3) nanofluids. The results of coefficient of performance, entropy generation, convective heat transfer coefficient, pressure drop, device and surface temperature with minichannel have the better enhancement with GNSs/water nanofluid than Al_2O_3 and hybrid (GNSs+Al_2O_3) nanofluids [155]. Additionally, it is also observed that GO based nanofluid causes the surface deposition on the surface of microchannel which can block active nucleation sites and becomes thicker with the increase of nanoparticles concentrations [156]. The surface deposition process in microchannels is because of physical interaction and absorption between the nanoparticles which depend on fluid flow, higher temperature and concentration. The detailed summary of GE based nanofluids are tabulated in Table 7.

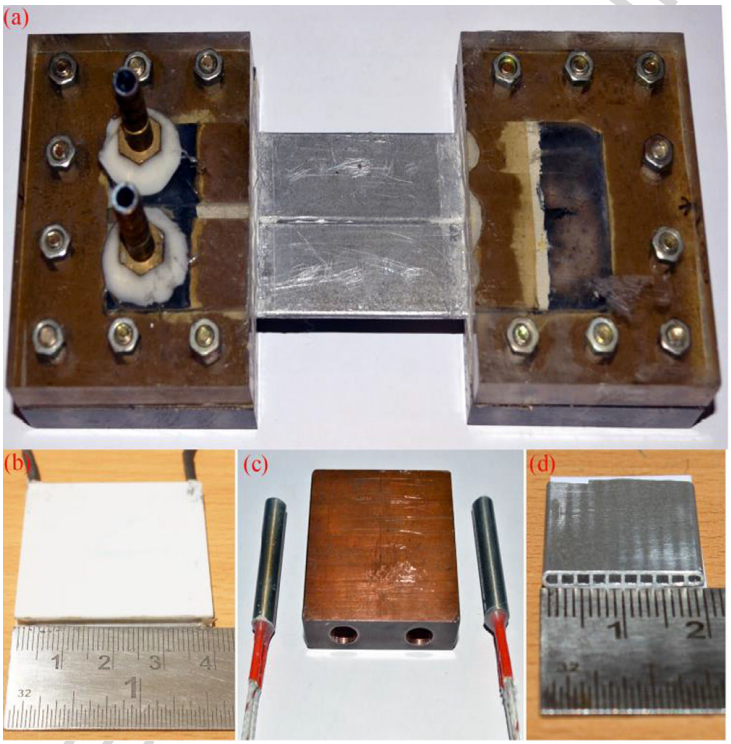

Figure 20: Photograph of multiport minichannel: (a) Two pass multiport minichannel, (b) thermo-electric module, (c) heat simulator with cartridge heater, (d) multiport minichannel, from Ref. [155], reused with permission from Elsevier license number 4385240361991.

Table 7: Graphene based nanofluids with micro/minichannels.

Ref.	**NPs**	**SM**	**PS**	**CONC.**	**BF**	**SFTs**	**PM**	**pH**	**Charac. Tech.**	**Findings**
[155]	Al_2O_3, GNSs	Supplied by manufacturer	(GNSs: t=5nm) (Al_2O_3: d=50μm)	0.1%	DW	Not used	Two–step method	N/A	Ultrasonic homogenizer, TEM	They found the coefficient of performance of 72%, reduced the device temperature and wall surface temperature of 4.7°C and 5.3°C, respectively. The entropy generation decreased by 31.86%, convective heat transfer coefficient was enhanced by 88.62% using GNSs/water nanofluid.
[156]	GONSs	Hummers method	t=1.4–2.3nm	0–0.05%	water	N/A	Two–step method	11.7	Zeta potential	The higher concentration of GO had lower heat transfer coefficient and surface deposition had a negative effect on heat transfer coefficient. The enhancement of critical heat flux was found from $13.2-25\%$.

6.5. Heat exchanger

The heat exchanger is a widely used equipment in industry and especially in process plants e.g. refineries, power plants, cooling towers, fertilizers, car engines and many other thermal applications. The fundamental challenge is the effective cooling and heating of processing fluids inside the heat exchangers. The conventional way to enhance the heat transfer rate is to increase the surface area but here the cost comes the major parameter. Several studies available on effective cooling of heat exchanger with GE based nanofluids based on flow regime (i.e. laminar to turbulent) [157, 158], flow arrangement (i.e. parallel, cross and counter) [159, 160] and construction (i.e. shell and tube, tube–in–tube, plate type) [157, 161, 162, 125].

In the laminar flow regime, Ghozatloo et al. [157] explored the thermal conductivity and enhancement of convective heat transfer coefficient of a shell and tube heat exchanger using GNSs/water nanofluid. The varying trend in thermal conductivity was observed with the increase of loading of GNSs. Thermal conductivity was increased by 15%, 29.2% and 12.6% at 0.05 wt.%, 0.075 wt.% and 0.1 wt.% weight percentages of GNSs, respectively, at 25°C. Similarly, the heat transfer coefficient was increased by 15.3% and 23.9% at temperature of 25°C and 38°C, respectively, with the increase of loading of GNSs from 0.025 wt.% to 0.1 wt.%. By increasing the temperature from 25°C to 38°C, the 13.1% increase in heat transfer coefficient was achieved.

Under turbulent and counter–flow regimes, NDG nanosheets aqueous solution was moved along a double–pipe heat exchanger between a Reynolds number of $5,000$ and $15,000$ by Goodarzi et al. [159]. Thermal performance enhancement was determined after analysing the total and convective heat transfer coefficient, percentage of wall temperature reduction, pressure drop and pumping power. Figure 21 shows the average enhancement of heat heat transfer coefficient and a 16.2% enhancement was obtained at 0.06 wt.% for $Re = 15,000$.

Under turbulent and cross–flow regimes, Ranjbarzadeh et al.[158, 160] examined the heat transfer and friction coefficient of the GO/water flowing nanofluid through a circular profile tube and acting as a cooling heat exchanger. The increasing trend in heat transfer coefficient was observed with increasing Re number from 5250 to $36,500$. Maximum enhancement in heat transfer coefficient and friction coefficient of 40.3% and 16%, respectively, was obtained by increasing the Re number and loading of GO. Additionally, opposite trends were observed between Re and ratio of convective heat transfer coefficient. With increase of Re number at constant loading of GO, the ratio of convective heat transfer coefficient decreases which proved the higher thermal efficiency of thermal systems operating at low Re numbers or laminar flow regime [158]. Further, under cross-flow and Re number range ($3800 \leq Re \leq 21500$), the enhancement in Nusselt number, friction factor, and heat transfer performance coefficient of 51.4%, 21%, and 42.2% was achieved, respectively, using GO/water nanofluid at 0.2% volume concentration [160].

Under all three flow regimes (i.e. laminar, transition and turbulent), Selvam et al. [161] explored the effect of convective heat transfer coefficient and pressure drop of a tube–in–tube heat exchanger passing through the GNPs/water+EG nanofluid. A maximum enhancement of 170% at 0.5% volume concentration in convective heat transfer coefficient was achieved in turbulent flow regime whereas, the maximum pressure drop was predicted in laminar flow region. Additionally, it was summarized that

enhancement in heat transfer coefficient and Nusselt number depends on Reynolds number, GE loading, and inlet temperature, as shown in Figure 22.

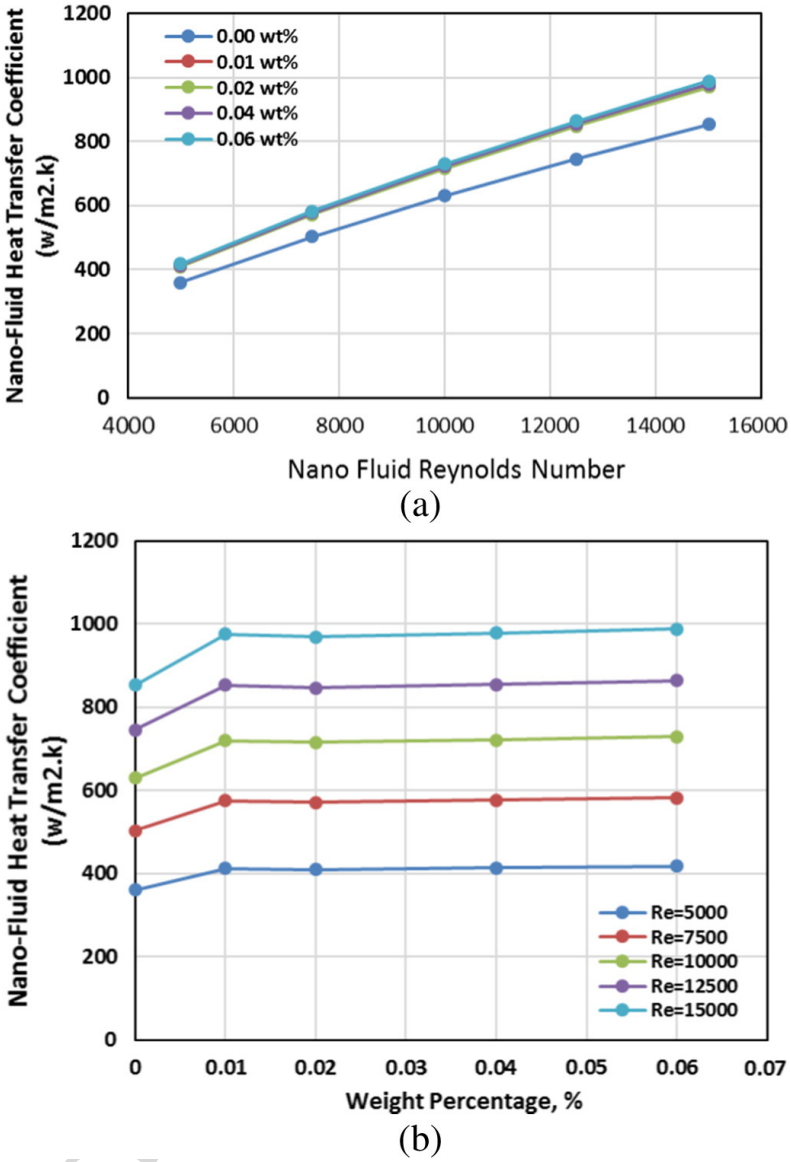

Figure 21: Convective heat transfer coefficient enhancement versus *Re* number at different weight percentages, from Ref. [159], reused with permission from Elsevier license number 4385240646030.

In addition, the thermal performance effects of graphene based hybrid nanofluids flowing through the heat exchanger have been investigated. Kumar et al. [162] synthesized water based nanofluids of dispersing TiO_2, Al_2O_3, ZnO, CeO_2, ($Cu+Al_2O_3$), MWCNT, and GNPs nanoparticles and carried out the energetic and exergetic performance parameters of a plate heat exchanger (PHE). A maximum enhancement in heat transfer coefficient of 53% was achieved with MWCNT/water nanofluid whereas it was 39.93% for GNPs/water nanofluid. The exergetic analysis further showed that the maximum reduction of exergy destruction was achieved by MWCNTs and GNPs based fluids of 75.91% and 62.59%, respectively, at 0.75 vol.% concentration. Recently, Wang et al. [125] carried out the heat transfer and pressure drop characteristics of a miniature plate heat exchanger (MPHE) by flowing the EG and water

(50 wt.% and 50 wt.%) base fluids with GNPs at four weight concentrations of 0.01, 0.1, 0.5 and 1.0 wt.%. The authors proposed the empirical correlation of Nu number for MPHE as follows:

$$Nu = 0.3759 Re^{0.6814} Pr^{n} \tag{7}$$

where the ranges of Re and Pr numbers are $10 < Re < 900$ and $5.5 < Pr < 8.5$, respectively. The n is 0.3 for hot fluid and 0.4 for cold fluid. Figure 23 shows that convective heat transfer coefficient was only enhanced by the same amount as the increase in the thermal conductivity of GNPs nanofluid. From the results, a maximum heat transfer enhancement of 4% was observed compared to the base fluid keeping pumping power constant from weight concentration range of 0.01 to 0.1 wt.%.

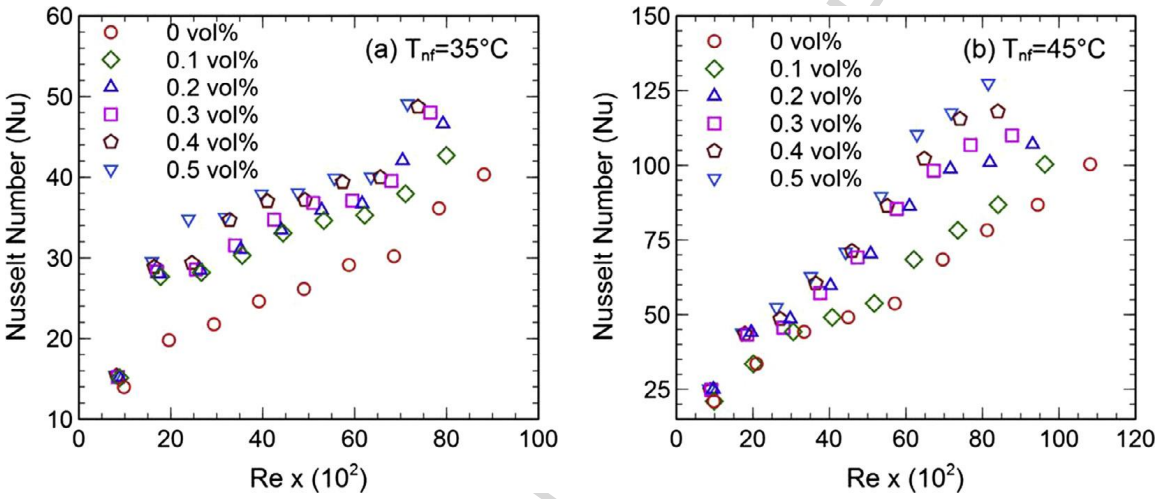

Figure 22: Variation of Nusselt number as a function of Reynolds number at inlet temperature of (a) 35°C and (b) 45°C, from Ref. [161], reused with permission from Elsevier license number 4463600209728.

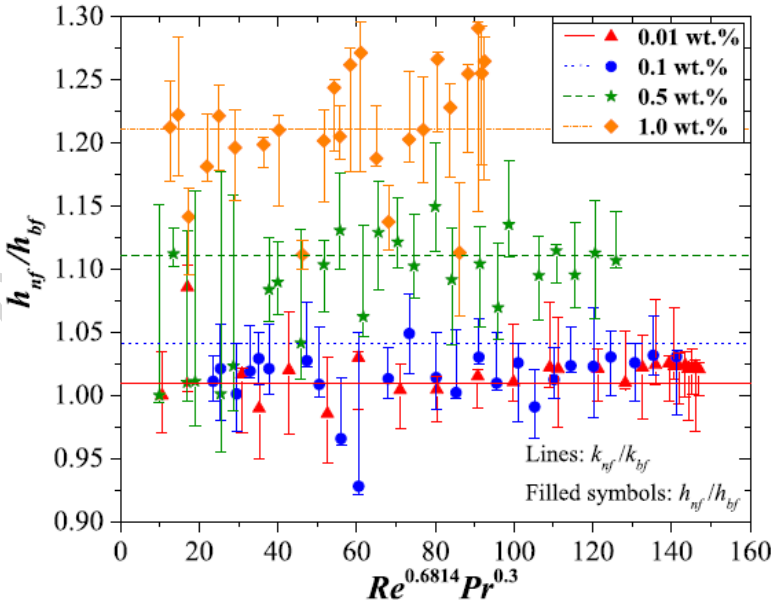

Figure 23: Comparison between heat transfer coefficient and thermal conductivity, from Ref. [125], reused with permission from Elsevier.

6.5.1. Discussion

Tremendous utilization of graphene based nanofluids have been under investigation for various types of heat exchangers under different flow arrangement and flow regimes. From the researchers investigations [157, 159], it can be seen that with the increment of loading GNSs to water enhances the convective heat transfer coefficient at a constant Reynolds number. Additionally, increasing Reynolds number and concentration of GNSs cause the increase in friction factor resulting in rise the pressure drop and pumping power. With GNSs/water based nanofluid the maximum enhancement in convective heat transfer has been reported of 23.9% at 0.1 wt.% weight concentration and 38°C temperature. Whereas the maximum reported enhancements in convective transfer coefficient with GO/water nanofluid are 40.3% and 42.2% at volume fractions of 0.1% and 0.2%, respectively [160]. With GNPs based nanofluid, the 170% enhancement in heat transfer coefficient is achieved at 0.5 vol.% of GNPs with water and EG host fluids [161]. Here, authors emphasize that enhancement in heat transfer coefficient as well as in Nusselt number in purely loading of graphene based nanomaterial, flow arrangement and regime, and inlet temperature, see Figures 21 and 22. The detail summary of GE based nanofluid passing through the heat exchangers are described in Table 8.

Table 8: Graphene based nanofluids with heat exchangers.

Ref.	NPs	SM	PS	CONC.	BF	SFTs	PM	pH	Charac. Tech.	Findings
[157]	GNSs	CVD	N/A	0.05 wt.% 0.075 wt.% 0.1 wt.%	DI water	N/A	Two–step method	N/A	SEM, Raman spectroscopy	Thermal conductivity was increased by 15%, 29.2% and 12.6% at 0.05 wt.%, 0.075wt% and 0.1 wt.% weight percentages of GNSs, respectively, at 25°C. Similarly, the heat transfer coefficient was increased by 15.3% and 23.9% at temperature of 25°C and 38°C, respectively, with the increase of loading of GNSs from 0.025 wt.% to 0.1 wt.%.
[79]	NDG	Modified Hummers method	d<45μm	0.01% 0.02% 0.04% 0.06%	DW	Triton X-100	Two–step method	11	UV-vis spectrometer, Zeta potential test, FESEM, TEM, XPS	The authors reported the average enhancement of heat transfer coefficient of 16.2% at 0.06 wt.% for Re=15000.
[163]	GE-NPs	Hummers method	N/A	0.005% 0.01% 0.02%	Water	PVP	Two–step method	N/A	AFM, UV-vis spectrometer	The results showed the 10.3% enhancement of thermal conductivity, 6.04% enhancement of heat transfer coefficient and pressure drop remained unchanged.
[139]	GNPs	Supplied by manufacturer	N/A	0.025% 0.05% 0.075% 0.1%	DW	Not used	Two–step method	N/A	UV-vis spectrometer, Zeta potential test	The convective heat transfer coefficient and pressure drop increased from $13-160$% and $0.4-14.6$%, respectively, as due to flow rate and heat flux increased.
[164]	GNPs	Supplied by manufacturer	t=2nm d=2μm	0.025% 0.05% 0.075% 0.1%	DW	Not used	Two–step method	N/A	UV-vis spectrometer, Zeta potential test	The authors found the thermal performance enhancement in range of 7.96% and 25%. The Nusselt number increased with the increase of Re number and heat flux. The increase of Nusselt number was up to 75%, 79%, and 83% at heat fluxes of 8231, 10351, and 12320 W/m^2 and 0.1 wt.%. The pressure drop increased by 0.4% to 14.6%.

[165]	GNs	Hummers method	t=1.4–2.3nm	0.005–0.02 vol.%	DW	PVP	Two–step method	N/A	AFM	The maximum enhancement of thermal conductivity and heat transfer coefficient were obtained of 10.3% and 14.2%, respectively, at 0.02 vol.% concentration.
[166]	GNPs	Supplied by manufacturer	N/A	0–0.2%	Water–EG	N/A	Two–step method	N/A	DSC	The authors determined the thermophysical properties and heat transfer as well pressure drop characteristics of annular channel using GNPs/water-EG nanofluid.
[162]	TiO_2 Al_2O_3 ZnO CeO_2 (Cu+Al_2O_3) GNPs MWCNT	Supplied by manufacturer	N/A	0.5–2.0 vol.%	Water	CTAB	Two–step method	N/A	N/A	The maximum enhancement in heat transfer coefficient of 53% was achieved with MWCNT/water nanofluid whereas it was 39.93% for GNPs/water nanofluid. The exergetic analysis further showed that maximum reduction of exergy destruction was achieved by MWCNTs and GNPs based fluids of 75.91% and 62.59%, respectively, at 0.75 vol.% concentration.
[158]	GO	Supplied by manufacturer	t=3.4–7nm d=2μm	0–0.2%	Water	N/A	Two–step method	9	Zeta potential test, Sedimentation photograph capturing	The heat transfer coefficient and friction factor were increased 40.3% and 16%, respectively. The thermal conductivity enhancement was obtained 28% and thermal performance coefficient increased 1.148, maximally.
[160]	GO	Supplied by manufacturer	t=3.4–7nm d=2μm	0–0.2%	Water	N/A	Two–step method	9	Zeta potential analyser, Sedimentation photograph capturing	With the range of Reynolds number ($3800 \leq Re \leq 21500$), the enhancement in Nusselt number, friction factor, and heat transfer performance coefficient were achieved of 51.4%, 21%, and 42.2% using GO/water nanofluid at 0.2% volume concentration.
[161]	GNPs	Supplied by manufacturer	t=5–10nm d=15μm	0.1–0.5%	Water+EG	SDC	Two–step method	N/A	SEM	The results presented the maximum enhancement of convective heat transfer coefficient of 170% at 0.5 vol.%.
[125]	GNPs	Supplied by manufacturer	t=2nm d=2μm	0.01, 0.1, 0.5, 1.0 wt.%	Water+EG	Triton X-100	Two–step method	N/A	SEM, Zeta potential test, Thermal constant analyzer	The maximum heat transfer enhancement was observed of 4% compared to the base fluid keeping pumping power constant from weight concentration range of 0.01 to 0.1 wt.%.

6.6. Boiling heat transfer

Studies have been reported on boiling heat transfer under different regimes and boiling parameters with graphene based nanofluids [167]. Pool boiling heat transfer is still under investigation to increase or decrease the rate of heat transfer. There are several studies on the transient pool boiling heat transfer using GNPs with DW, which report the enhancement in critical heat flux (CHF) and boiling heat transfer coefficient. The enhancement of pool boiling heat transfer can be accomplished by (a) modifying the heat of channel surface conditions (b) modifying heater size, shape, material, diameter and orientation, (c) degree of surface wetting, (d) sub-cooling of liquid, (e) changing the added surfactants (f) enhancing the properties of liquid and (g) bubble transport while flow and pool boiling regime [168].

Zhang et al. [169, 170, 156] carried out pool and flow boiling heat transfer performance using GONs and GO nanomaterials dispersed in water. The effect of transient pool boiling was observed under weight fractions of 0.0001 wt.% and 0.0002 wt.% and is was found that the enhancement in critical heat fluxes (CHF) was 13.2% and 25% during quenching of surface. The wettability of the quenched surfaces was observed to improve with increase concentration of GONs [169].

The quenching experiments were carried out with copper spheres at various dilute concentration of GONs from 0.0001 wt.% to 0.0010 wt.% and observed the non–monotonous enhancement in CHF by increasing the concentration of GONs. A maximum enhancement in CHF of 25% was obtained at 0.0002 wt.% of GONs [169]. The non–monotonously behaviour in enhancement of CHF firstly, is because of the deposition layers of GONs on the quenches surface with the increase of concentration of GONs and secondly, the non-trivial effect of suspended GONs especially at higher concentrations. Using microchannels with GO/water nanofluids, the authors further studied the flow boiling and resulting surface deposition process [156]. A negative effect on heat transfer coefficient was identified because of surface deposition of GO, which was caused to increase the CHF.

Park and his co–authors [171, 172, 173, 174, 175] examined the effect of flow and pool boiling on critical heat transfer using GE, GONs, Al_2O_3, SiO_2, ZnO, SiC and CuO nanoparticles with different base fluids i.e. DW, Boric acid, LiOH, TSP, and R-123 in different investigation, summarized in Table 9. Park et al. [174], examined the difference of CHF with MWCNTs and GE in pool–boiling CHF with spray-deposition. It was found that MWCNTs and GE based nanofluids had maximum pool–boiling CHF of 20% and 21.94% at 19.8° and 21.7° contact angles, respectively, with heat transfer surface, as shown in Figure 24.

Based on the contact angle with heat transfer surface, the following correlation was proposed offering 7% or less error within contact angle of $0-49.4°$ to determine the CHF by introducing a correction factor (C_{cf}) to Kandlikar's predicted model:

$$q_{CHF} = C_{cf} h_{fg} \rho_g^{1/4} \left(\frac{1+\cos\beta}{16}\right) \left[\frac{2}{\pi} + \frac{\pi}{4}(1+\cos\beta)\cos\phi\right] [\sigma g(\rho_l - \rho_g)]^{1/4} \tag{8}$$

$$C_{cf} = 1.154 \exp(-0.1 \sin\beta) \tag{9}$$

where h_{fg}, ρ_g, ρ_l, β, ϕ, σ, and g are the evaporative latent heat (kJ/kg), vapor density (kg/m^3),

liquid density (kg/m^3), contact angle of heat transfer surface (°), basic contact angle of heat transfer surface, surface tension (N/m), and gravitational acceleration (m/s^2), respectively.

Yudong et al. [176] found the homogeneous nucleation rate of DI water whereas the heterogeneous nucleation rate was found by increasing GO nanoparticles concentration. The supercooling of GO nanofluid of 7.98, 7.93, 3.05, and 3.03 K were obtained for four different concentrations of GO and reduced by more than 74% which recommended fluids for cold storage applications. Fan et al. [177] studied experimentally the effect of concentration under transient boiling heat transfer. It was found that quenching was accelerated by increasing concentration ratio; further the CHF was enhanced more than 16 kW/m^2 at 0.1 wt.% concentration due to increase of surface roughness, as shown in Figure 25. Cheedarala et al. [178] conducted different thermophysical analysis and determined the CHF value of CuO:GO-NCs-NFs and found a 160% enhancement of CHF at 0.06 wt.%.

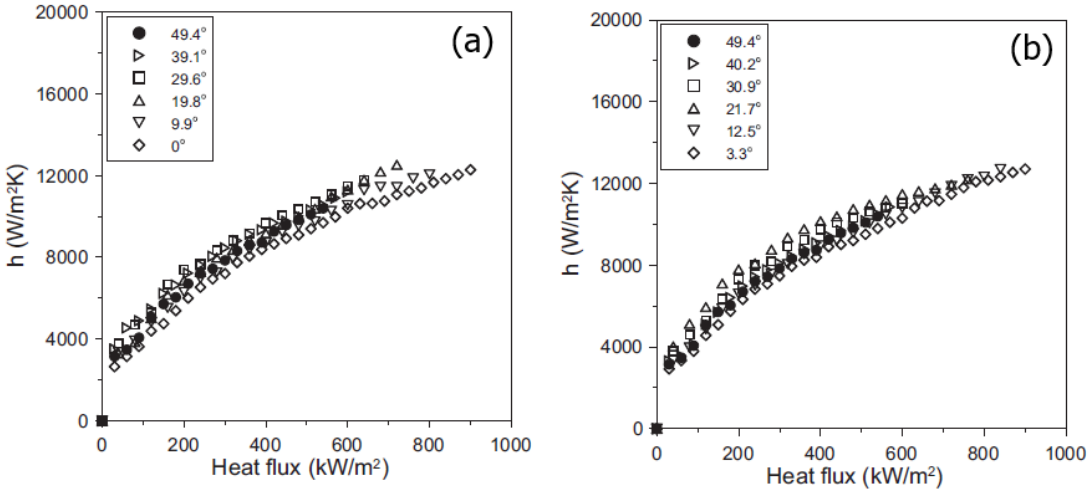

Figure 24: Comparison of CHF as a function of contact angles variation with (a)- MWCNT deposition, (b)-GE deposition, from Ref. [174], reused with permission from Elsevier license number 4385321420739.

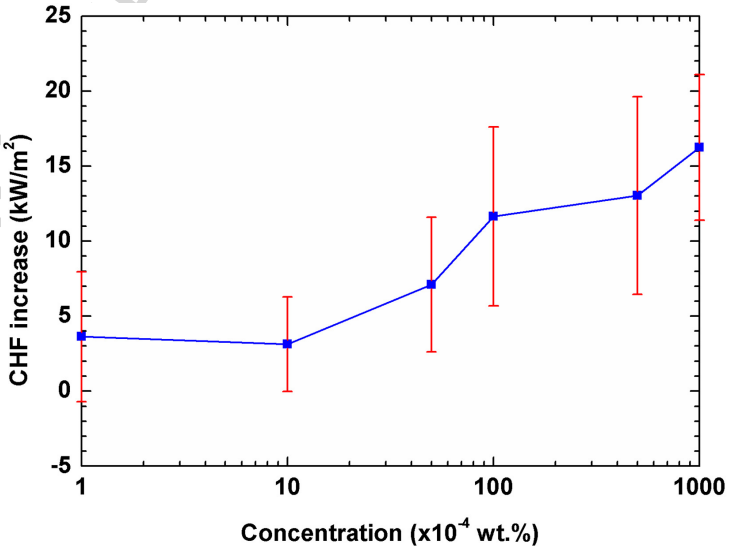

Figure 25: Enhancement of CHF with weight concentration of GON nanofluid, from Ref. [177], reused with permission from Elsevier.

6.6.1. Discussion

The detail findings in the enhancement of boiling heat transfer coefficient to enhance the critical heat flux based on graphene nanofluids have been reported in Table 9. It can be seen from the investigation by researchers [169, 170, 156, 171, 172, 173, 174, 175, 176, 177, 178] on pool and flow boiling heat transfer that enhancement in CHF varies with increasing concentration of loading, contact angle and surface temperature. Additionally, surface modification plays a significant role in pool boiling CHF enhancement, which requires lower concentration of nanoparticle resulting in reduced deposition layers. The varying trends in CHF is further justified by the surface morphology of the deposited layers of graphene based nanoparticles on quenched surfaces. The higher enhancement in CHF is because of the formation of ordered porous structure of GO compared to other metallic nanoparticles while boiling on heated surface [172, 173, 178]. The deposition analysis proved that increased concentration of GO resulted in thicker deposition layer due to the absorption of nanoparticles and interaction of nanoparticles [169, 172].

The deposition formation especially of GO can be explained on the basis of DLVO theory. GO can be reduced after continuously flowing through the heated surface, which makes the oxygen containing functional groups more hydrophilic. According to DLVO theory, that oxygen containing functional groups can give the H^+ in alkaline solutions and possess negative charges [156]. The enhancement of CHF for GE nanofluids is based on surface wettability and the capillarity of the GE deposited layer and modulation of wavelength in ordered porous surface structure [171].

Table 9: Graphene based nanofluids for boiling heat transfer applications.

Ref.	NPs	SM	PS	CONC.	BF	SFTs	PM	pH	Charac. Tech.	Findings
[169]	GONs	Supplied by manufacturer	t=0.55–1.2nm	0.0001 wt.% 0.0002 wt.%	Water	N/A	Two–step method	N/A	TEM, UV-vis spectrometer	The transient pool boiling CHF enhancement was investigated and observed the increment of 13.2% and 25% further wettability of the quenched surfaces was observed to improve with the increase of concentration of GNPs.
[170]	GONs	Supplied by manufacturer	N/A	0.0001% 0.0002% 0.005% 0.0010%	DW	Not used	Two–step method	N/A	DLS, TEM, UV-vis spectrometer, SEM	They found the consistent enhancement of CHF with variation of surface wettability. The maximum enhancement in CHF of 25% was obtained at 0.0002 wt.% of GONs.
[156]	GONs	Hummers method	t=1.4–2.3nm	0-0.05%	water	N/A	Two–step method	11.7	Zeta potential test	Authors found the partly reduction of GO during boiling and non-porous surface disposition was found at different concentration and flow rates. The enhancement of critical heat flux was found from $13.2-25\%$.
[171]	GE, GONs	Modified Hummers method	t<45μm	0.001vol.%	DW	N/A	Two–step method	N/A	SEM	The authors found that GO nanofluid had higher enhancement of CHF of 179% than GN nanofluid which was 84% than pure water.
[172]	GO, Al_2O_3, SiO_2	Modified Hummers method	N/A	0.0001vol.%	Boric acid, LiOH, TSP, DW	N/A	Two–step method	N/A	Zeta potential test	The authors carried out pool boiling CHF enhancement experiments for nuclear reactor cooling using GE/water nanofluid for 0° and 90°. The results found the enhancement of CHF about at 40% (minimum) at 90° and 200% (maximum) at 0°, respectively.
[173]	GO	Modified Hummers method	t=0.8–1.0nm	0.0001vol.%	DW	N/A	Two–step method	N/A	N/A	The results showed that CHF was enhanced up to 20%, wettability was not improved with a thin coating layer, more heat dissipation was observed from the graphene coated heat surface.

[174]	MWCNT, GE	Chemical reformation process	(GE: t=6–8nm, d=15μm), (MWCNT: d=10–15nm)	0.1%	DW	Not used	Two–step method	7	SEM	The results found that MWCNTs and GE based nanofluids had maximum pool-boiling CHF of 20% and 21.94% at 19.8° and 21.7° contact angles, respectively.
[175]	ZnO, SiC, Al_2O_3, GO, CuO	Hummers method	(ZnO: t=40–100nm), (SiC: t<100nm), (Al_2O_3: t<50nm), (GO: t<45μm), (CuO: t=23–37nm)	0.01%	DW R-123	Not Used	Two–step method	N/A	N/A	The authors found that CHF was increased $90-160\%$.
[176]	GNSs	Supplied by manufacturer	t=0.8–1.2nm d=1–5μm	0.1%, 0.2%, 0.3%, 0.5%	DW	N/A	Two–step method	3.91, 3.85, 3.45, 3.38	Laser size and zeta potential tests	The supercooling of GO nanofluid were obtained of 7.98, 7.93, 3.05, and 3.03 K for four different concentrations of GO and reduced by more than 74% which recommended fluids for cold storage applications.
[179]	GO-Fe_3O_4	Simplified Hummers method	N/A	0.5%	DW	Tannic acid, Iron salt	Two–step method	10	Light transmission method	The authors experimentally examined that the thermal conductivity increased up to 11% adding GO-Fe_3O_4, the viscosity decreased with increase of temperature, and with influence of magnetic field the convective heat transfer coefficient increased up to 82%.
[177]	GONs	Supplied by manufacturer	t=0.55–1.2nm, d=0.5–3μm	0–0.1%	DI water	Not used	Two-step method	N/A	DLS, SEM, AFM, TEM	The results found that quenching was accelerated by increasing concentration ratio further the CHF was enhanced more than 16 kW/m^2 at 0.1 wt.% concentration due to increase of surface roughness.

[178]	CuO+GO	Hummers method	100nm	0.006 wt.% 0.03 wt.% 0.06 wt.%	DI water	Not used	Two–step method	7	FESEM, TEM, surface roughness average, XRD, FT-IR, Raman spectra, AFM, XPS	The authors found the 160% enhancement of CHF at 0.06 wt.% of CuO+GO nanocomposite nanofluid.

6.7. Solar collectors

Several studies have been reported on direct absorption solar collector (DASC) and flat plate solar collector (FPSC) with graphene based nanofluid, focusing on the enhancement of the absorption of solar irradiation. So far, researchers have investigated GE, GNPs, RGO, GO and hybrid graphene based nanofluids with DASC and FPSC to examine solar–to–thermal energy conversion and performance.

Using GE/oil based nanofluid through DASC, Wang et al. [180] examined the dispersion stability, thermal conductivity and kinetic viscosity by varying mass fraction of GE. The enhanced thermal conductivity and reduction in kinetic viscosity were observed in comparison with pure oil. Additionally, the GE/oil based nanofluid had high absorption, high extinction and low scattering coefficient. The highest heat collection efficiency was achieved with GE/oil nanofluid at low input fluid temperature and deceased linearly with the increase of inlet fluid temperature at stable radiation and mass concentration.

Vakili et al. [181, 182] used GNPs/DI-water nanofluid through the volumetric solar collector for domestic water heating at varying weight concentrations and mass flow rates. The results revealed that the collector efficiency increases with the increase of weight concentration. Maximum collector efficiencies of 83.5%, 89.7%, and 93.2% were achieved at weight fractions of 0.0005 wt.%, 0.001 wt.%, and 0.005 wt.%, respectively, at a mass flow rate of 0.015 kg/s [181]. The findings show that the GNP/DI–water has good absorption as well as thermal conductivity ability for solar–to–thermal energy systems for residential applications.

Optical characteristics of GO/EG nanofluids to directly absorb solar radiation collectors were investigated by Rose et al. [183] for a volume fraction range of $0.004 - 0.016$ vol.%. An optimum concentration of 0.012 vol.% of GO showed the minimum reflectance and high absorption over the visible spectral range. Using GO/DI–water nanofluid for low temperature DASCs, Lavasani and Vakili [184] investigated the thermo–optical properties with weight concentrations of 0.001 wt.%, 0.005 wt.%, 0.015 wt.%, and 0.045 wt.%. A significant improvement in absorbing solar energy of 99.6% was obtain at optimum weight concentration of 0.045 wt.% for 3 cm nanofluid layer thickness, as shown in Figure 26.

Based on the RGO/water+EG nanofluid through the DASC, Shende and Ramaprabhu [185] determined the optical and thermal properties. The presented results of optical properties revealed that RGO dispersed nanofluid had significant potential to absorb the solar energy and could be very effective for DASC for direct solar–to–thermal conversion. Enhancements in thermal conductivity for water and EG base nanofluids of 18.5% and 17.8% were achieved, respectively, at 50°C for 0.03%. A comparison of three different nanoparticles, GE, GO, and RGO dispersed in water was examined by Chen et al. [186] through irradiating process to evaluate the performance of DASCs. After performing the stability test analysis, RGO/water nanofluid was shown to have the better stability along with high optical absorption and thermal conductivity thus making it more suitable for photo–thermal conversion than the GO/water and GE/water nanofluids at constant loading. Figure 27 shows the comparison of RGO, GO, and GE water based nanofluids and peak photo–thermal conversion efficiencies of 96.93% and 52% at 30°C and 75°C, respectively, were achieved by the RGO/water nanofluid.

The hybrid nanofluids based of GO and Au have been utilized for solar vapor generation which is green, efficient and provides a direct approach to harvest the solar energy. Fu et al. [187] prepared GO–Au/water

nanofluid to generate the solar steam. With 15.6 wt.% loading of GO–Au nanoparticles, a 59.2% steam generation efficiency was achieved which was 2.6 times higher than pure water, whose conversion efficiency was 16.2%. Additionally, steam generation efficiency was enhanced by 10.8% with pure GO nanofluid after dispersing only 15.6 wt.% concentration of Au nanoparticles. The highest temperature of 27.2°C was achieved with 15 wt.% weight percentage of GO+Au nanofluid, which was higher than from pure GO nanofluid and pure water. Figure 28 shows the schematic of GO and Au nanoparticles mechanism of photo–thermal conversion and solar steam generation with different conversion processes. The results revealed that GO sheets could be reduced into GE sheet under solar irradiation which provided a new, clean, green and efficient way to reduce the GO sheet only using natural sunlight in comparison with conventional reduction methods.

A few studies have been reported on FPSC for direct solar–to–thermal energy conversion. Vincely and Natarajan [188] examined the thermophysical properties of GO/DI–water nanofluid for a FPSC under forced convection. The thermal performance of FPSC was investigated in terms of overall heat transfer coefficient, friction factor and collector efficiency under laminar flow. The overall heat transfer coefficient was enhanced by 8.03%, 10.93%, 11.5% at mass concentrations of 0.005, 0.01, 0.02, respectively. Additionally, collector efficiency enhancement of 7.3% was obtained with mass concentration of 0.02 and mass flow rate of 0.0167 kg/s by using GO/DI–water nanofluid. Using hybrid nanofluids flowing through FPSC, Verma et al. [189] evaluated the thermal performance to find out the energy and exergy analysis by varying the mass flow rate at an optimum concentration of $\sim$ 0.75 vol.%. A maximum enhancement in exergy efficiency for MWCNTs/water nanofluid of 29.32% was obtained and followed by 21.64%, 16.67%, 10.86%, 6.97% and 5.74% for GE, CuO, Al_2O_3, TiO_2 and SiO_2 based nanofluids, respectively. In a similar trend, the maximum drop in entropy generation of 65.55% was observed for the MWCNTs/water nanofluid, followed by GE, CuO, Al_2O_3, TiO_2 and SiO_2 based nanofluids with 57.89%, 48.32%, 36.84%, 24.49% and 10.04%, respectively. Figure 29 illustrates the results between efficiency and volume concentration of different types of nanoparticles of FPSC. It can been seen that MWCNT has the highest efficiency of 23.47% followed by GE, CuO, Al_2O_3, TiO_2 and SiO_2 based nanofluids with maximum efficiency of 16.97%, 12.64%, 8.28%, 5.09% and 4.08%, respectively.

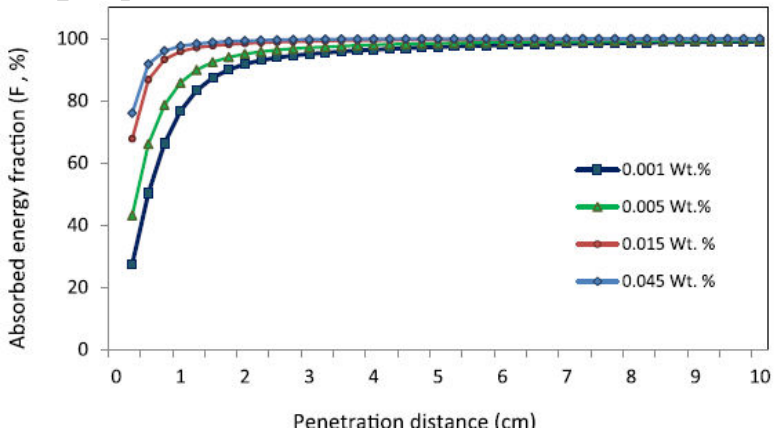

Figure 26: Absorbed energy fraction with different heights of nanofluid layers, from Ref. [184], reused with permission from Elsevier license number 4385340468381.

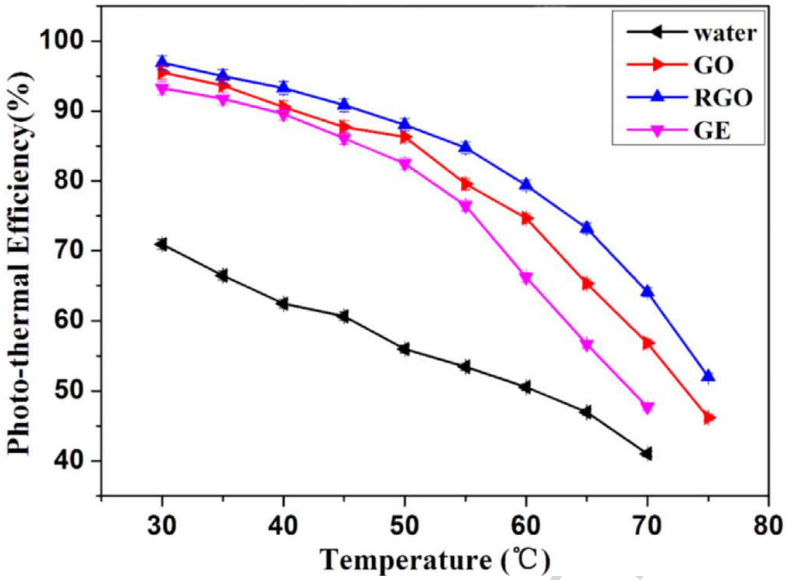

Figure 27: Relation between photo-thermal efficiency and temperature with water and nanofluids, from Ref. [186], reused with permission from Elsevier license number 4385340128764.

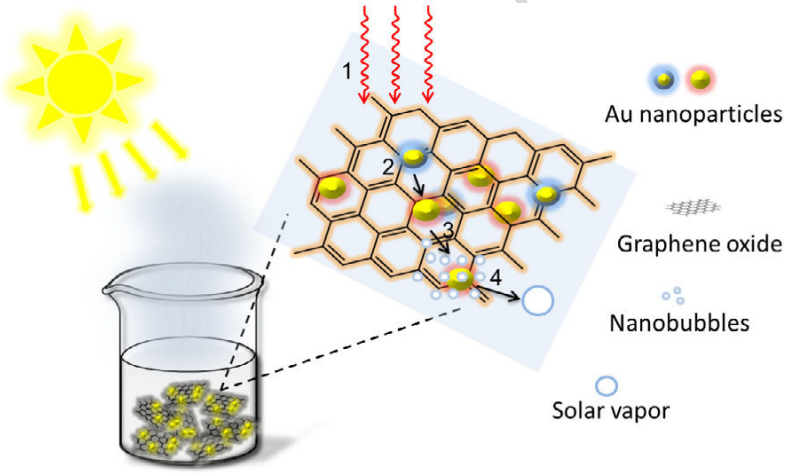

Figure 28: Schematic of Au+GO nanoparticles enhanced solar steam generation: (1) Irradiation (2) Absorption (3) vaporization (4) coalescence of nanobubbles, from Ref. [187], reused with permission from Elsevier license number 4385330962718.

6.7.1. Discussion

Investigations have been conducted with various GE based nanomaterials for both DASC and FPSC [180, 181, 182, 183, 184, 185, 186, 187, 188, 189]. Firstly, it can be seen that solar–to–thermal energy conversion and heat transfer performance with GE based nanofluids have significant improvement as compare to the base fluid to enhance the system thermal efficiency. The GE based nanofluid with high viscous based fluid, such as oil, have more potential to absorb the solar energy, which leads to an increase in the heat collection efficiency [180]. Despite this, non–aqueous nanofluids experience higher pressure drop, friction coefficient and pumping power, which decreases the overall heat transfer performance of the solar collector. Using GNPs based aqueous nanofluids at maximum concentration and mass flow rate of 0.005 wt.% and 0.015 kg/s, respectively, a collector efficiency of 93.2% is achieved [181], which shows the significant potential of aqueous nanofluids to achieve the best solar–to–thermal energy conversion.

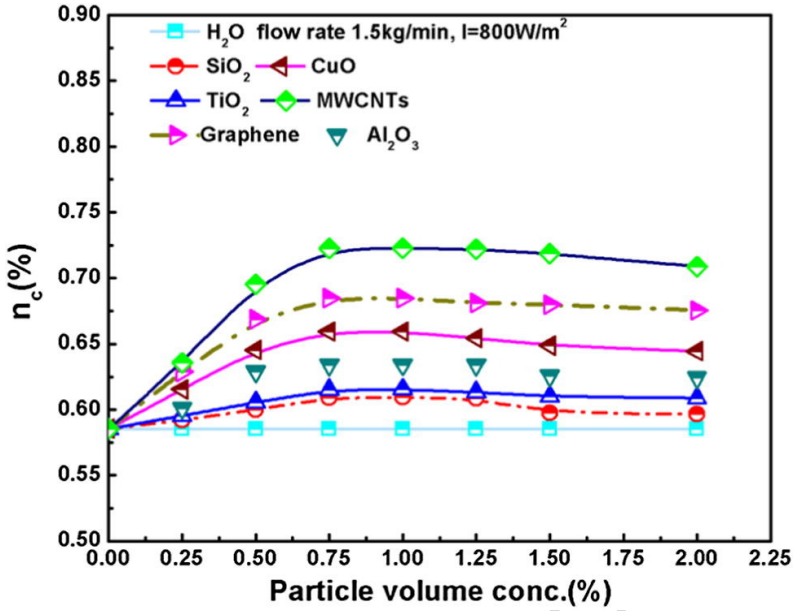

Figure 29: The graph between the FPSC and volume concentrations of nanoparticles, from Ref. [189], reused with permission from Elsevier license number 4385330694188.

Using GO/DI–water based nanofluids, a photo–thermal conversion of 99.6% is achieved at 0.045 wt.% of GO nanoparticles [184]. Further comparing the results of RGO, GO and GE, the highest photo–thermal conversion of 96.93% is seen by RGO/water nanofluid, as shown in Figure 27. Similarly, comparing the results of single or hybrid GO–Au nanoparticles reveal that the maximum thermal performance in terms of solar steam generation can be achieved with GO nanofluid [187, 188]. This proves that oxides based GE nanofluids have more potential to harvest solar energy for thermal systems. Notwithstanding, the authors suggest to further explore the GE based nanoparticles with metallic and metallic oxides nanoparticles by varying the concentration, inlet temperature, flow rate, pumping power both for aqueous and non-aqueous nanofluids. Table 10 summarises the effect of GE based nanofluids application with DASC and FPSC.

Table 10: Graphene based nanofluids with solar collectors.

Ref.	NPs	SM	PS	CONC.	BF	SFTs	PM	pH	Charac. Tech.	Findings
[190]	Graphite	Supplied by manufacturer	t>10nm	0.00001–0.1%	Water	SDS	Two–step method	N/A	UV-vis spectrometer	The authors found that over 95% of solar irradiation could be absorbed.
[191]	Graphite	N/A	d=50–300nm	0.00001–0.5%	Water	N/A	N/A	N/A	N/A	The finding concluded that using graphite nanofluids more than 50% solar irradiation could be absorbed.
[192]	GE, Al	N/A	d=5nm	0.02% 0.09%	Therminol VP-1	N/A	N/A	N/A	N/A	The authors found the maximum temperature of 265°C.
[193]	Graphite	Supplied by manufacturer	d=50–300nm	0.01vol.%	Water	Texatherm oil	Two–step method	N/A	UV-vis spectrometer, SEM	The results showed the enhancement of outlet temperature and efficiency around $30-100$ K and $2-25\%$, respectively.
[194]	GE	N/A	N/A	N/A	Water, Acetone	N/A	N/A	N/A	N/A	The resulted revealed that exergy efficiency was improved by 21% whereas the entropy generation was decreased by 4%. Further, authors suggested that GE/water nanofluid had lower entropy generation.
[195]	GE	Supplied by manufacturer	N/A	0.0005–0.01%	$[HMIM]BF_4$	Not used	Two–step method	N/A	N/A	The results found that receiver efficiency was increased with solar concentration and receiver height, whereas it was decreased with GE concentration.
[196]	MWCNTs, RGO	Hummers method	N/A	0.005–0.03%	DI water, EG	PEG, SLS	Two–step method	N/A	XRD, FESEM, XPS, UV-vis spectrometer, TEM	The results showed that thermal conductivity was enhanced by 17.7% and 15.1% using DI water and EG.

[197]	GNPs, SWCNT, GE	Supplied by manufacturer	(GNP: t<30nm, d <2nm), (GE: t=0.8nm, d=0.8–2μm)	0.005% 0.01%	$[BMIM]BF_4$	N/A	Two–step method	N/A	TEM, UV-vis-NIR spectrometer, DSC	It was found that GE-nanofluid had highest thermal conductivity than GNPs and SWCNT, further GE dispersed nanofluid had the lowest transmittance and highest extinction coefficient.
[198]	Au, Cu, Al, graphite, SiO_2/Au	N/A	d=10–150nm	0–100%	Water	N/A	N/A	N/A	N/A	The numerical proposed the multiple type of nanofluid with water for solar radiation to observe the effect of concentrations, diameters, height of the container and temperature.
[181]	GNPs	Supplied by manufacturer	t=2nm, d<2μm	0.0005wt.% 0.001wt.% 0.005wt.%	DI water, EG	N/A	Two-step method	N/A	TEM, XRD, Zeta potential test	The maximum collector efficiencies were achieved of 83.5%, 89.7%, and 93.2% at weight fractions of 0.0005 wt.%, 0.001 wt.%, and 0.005 wt.%, respectively, at mass flow rate of 0.015 kg/s.
[182]	GNPs	Supplied by manufacturer	t=2nm d<2μm	0.00025wt.% 0.0005wt.% 0.001wt.% 0.005wt.%	DI water, EG	N/A	Two–step method	N/A	TEM, XRD, Zeta potential test	The results showed that by increasing GNPs ratio increased both of absorption and thermal conductivity of nanofluid.
[188]	GO	Modified Hummers method	N/A	0.005% 0.01% 0.02%	DI water	Not used	Two–step method	N/A	XRD, UV-vis spectrometer, SEM, FESEM, FT-IR, Raman spectra	The results showed the collector efficiency of 7.3% with mass concentration of 0.02 and mass flow rate of 0.0167 kg/s. Further, it was observed that the collector efficiency was increased by increasing mass concentration and flow rate.
[183]	GO	Supplied by manufacturer	t=5nm	0.004% 0.008% 0.012% 0.013% 0.014% 0.016%	EG	N/A	Two–step method	N/A	UV-vis Spectrometer	It was achieved of 0.012 vol.% optimum concentration for minimum reflectance and high absorption.

[184]	GNPs	Supplied by manufacturer	t=3.4–7nm d=10–50nm	0.001wt.% 0.005wt.% 0.015wt.% 0.045wt.%	DI water	Not used	Two–step method	N/A	SEM, XRD, Zeta potential test, UV-vis-NIR Spectrometer, transient hot–wire method	The presented results showed that for 0.045 wt.% of GNPs the energy absorbing ability was 99.6%.
[185]	RGO	Hummers method	N/A	0.005%, 0.01% 0.03%	DI water, Water+EG	Not used	Two–step method	neutral	XRD, SEM, TEM, FT-IR, UV-vis-NIR Spectrometer	The results presented the enhancement of thermal conductivity of DI water and EG based nanofluids was 18.5% and 17.8%, respectively, at 50°C for 0.03%.
[187]	GO, Au	Hummers and Marcano	N/A	Au=15.6%, GO=0.5%	Water	Not used	Two–step method	N/A	Zeta potential test, UV-vis absorption spectrometer, TEM, SEM, FT-IR	With 15.6$wt.$% loading of GO-Au nanoparticles, the 59.2% steam generation efficiency was achieved. Steam efficiency of GO–Au nanofluids was 10.8% higher than pure GO nanofluid.
[199]	GE	Supplied by manufacturer	N/A	0.05 wt.% 0.07 wt.% 0.10 wt.% 0.20 wt.% 0.25 wt.%	DI water	Not used	Two–step method	N/A	N/A	The results showed that the maximum voltage, output power, and conversion efficiency were obtained of 11.29%, 21.55%, and 3.5%, respectively.
[186]	GO, RGO	Supplied by manufacturer	(GO: t=0.55–1.2nm d=0.5–3nm), (GE: t=0.8nm, d=0.8–2μm)	0.02%	DW	PVP	Two–step method	N/A	XPS, Zeta potential test, UV-vis-NIR spectrometer, DSC, TEM	The results revealed that RGO/water nanofluid was possessed in 340s from GO/water nanofluid, further it was showed the photo-thermal conversion efficiency of 96.93% and 52% at 30°C and 75°C, respectively.
[200]	GO	Supplied by manufacturer	t=0.55–1.2nm d=0.5–3nm	0.001–0.1%	DW	N/A	Two–step method	N/A	XPS, Zeta potential test, UV-vis-NIR spectrometer, DSC, TEM	The maximum photo-thermal efficiency of 97.45% and 48.92% at 30°C and 80°C, respectively, was achieved, also showed good dispersion stability and optical absorption property.

[180]	GE, CuO	Supplied by manufacturer	t=0.8–1.2nm d=0.5–2μm	0.02%, 0.05%, 0.1%, 0.2%, 0.5%, 1.0%	Oil	Not used	Two–step method	N/A	Microscope imaging system	It was concluded thermal conductivity was enhanced and kinetic viscosity was reduced, further, the GE–oil based nanofluid had the high absorption, high extinction and low scattering coefficient.
[189]	TiO_2, Al_2O_3, CuO, SiO_2, GE, MWCNTs	Supplied by manufacturer	t=20–45nm	0.25–2.0%	DW	Triton X-100	Two–step method	N/A	Zeta potential test, TEM	The results concluded that using MWCNTs/water nanofluid, a solar collector could be more economical.

7. Conclusions and Recommendations for Future Research

This review article focuses on the comprehensive features of graphene nanofluids and their recent advances of morphological, transport properties and significantly the industrial applications. From the literature, it has been shown that most of the research is focused on the thermal aspects, especially thermal conductivity and heat transfer enhancements. This study also covers the fundamental of synthesis, preparation and stability features of graphene nanofluids. Stability is one the major issue in the preparation of nanofluids for commercial applications.

Further, the effective parameters, namely concentration, particle size and shape, material, purity level, motion, temperature, morphology, shear rate which influence the thermal conductivity and viscosity of graphene nanofluid are discussed. In addition to this review study focuses on recent, major applications of graphene nanofluids such as electronics cooling, boiling heat transfer, solar collectors, heat pipe, heat exchangers and minichannel.

The results and concluded remarks of each section are presented in tabular form, which helps to highlight the key features and findings of each study. It has been noted that thermal conductivity has been enhanced with the increase of loading and temperature and has a linear relationship. From the review of electronics cooling, it has been found there are only few studies available for the thermal management of high heat flux generating electronics devices with graphene and more research is needed in future with different optimized geometries and flow conditions. Similarly there are few studies available on heat pipe, heat exchangers and minichannels.

This work has covered the preparation and stability, fundamental characterization properties, effective parameters, and potential industrial applications of graphene nanomaterials based nanofluids. However, there are still some potential areas which need to be explored. Although, the heat transfer rate of graphene materials based nanofluids is higher than the other metal and metal oxide nanoparticles based nanofluids, there is further needed to improve the design and performance of thermal systems. Following are the major future directions which need to be explored:

- The stability of nanofluids has been a major and challenging issue so far, which limits the applications of nanofluids in heat transfer applications. Therefore, further research is needed to find the optimum methods to enhance thermal and chemical stability of graphene based nanofluids on the basis of optimum and compatible amount of various surfactants and surface modification techniques of nanoparticles.

- Although, a detailed summary on thermophysical properties of graphene based nanofluids has been presented in this work, there is still a need to explore the accumulative effect of morphological, thermal and fluid parameters.

- The effect of size, shape, amount of nanoparticles of different graphene based nanomaterials (i.e. GO, RGO GQD, GNPs, GONs etc.) nanofluids require further investigation with different host fluids after performing optimization. This will not only increase the thermal and flow performance but also lead to reduce the production challenges of nanofluids.

- Most of the research has only focused on the thermal and rheological behaviour of graphene based nanofluids. So, there is a critical need to investigate the compatibility of graphene nanofluids with other materials to study the corrosion phenomenon in various high temperature thermal applications.

- Phase change heat transfer phenomenon such as condensation and boiling heat transfer, latent heat of condensation and vaporization, and relevant thermodynamics parameters at low and high temperatures are further area suggested to study.

- There is a huge potential available to study the thermophysical properties of hybrid nanofluids considering various graphene based nanomaterials, mentioned above, by changing the various effective parameters such as nanoparticles concentration, size, aspect ratio, temperature, and host fluids under varying heat and flow regimes. Furthermore, investigation can be focused to highlight the main parameters that affect the thermophysical properties of graphene based nanomaterials hybrid nanofluids.

- The optimum amount and type of surfactant are required to address critically on the basis of both aqueous and non-aqueous for single and hybrid graphene based nanofluids.

- Very limited applications of graphene based nanofluids have been explored especially on thermal management area. Therefore, the authors encourage further research to investigate the heat transfer performance of graphene nanofluids for thermal management of high-heat-flux electronic device, batteries, fuel cells, and solar-to-thermal energy harvesting systems.

- Optimizations of key parameters of the different applications are needed to be carried out to overcome the challenges related to synthesis, production, rheological, morphological and thermal properties, to study the effective transport phenomenon of heat and mass transfer and commercial applications.

- Finally, there is a need of to develop theoretical models to explain the empirical data on the basis of various parameters that affect the heat transfer performance of graphene based nanofluids.

References

[1] W. S. Hummers Jr, R. E. Offeman, Preparation of graphitic oxide, Journal of the American Chemical Society 80 (6) (1958) 1339–1339.

[2] F. Schffel, Chapter 2 - the atomic structure of graphene and its few-layer counterparts, in: J. H. Warner, F. Schffel, A. Bachmatiuk, M. H. Rmmeli (Eds.), Graphene, Elsevier, 2013, pp. 5 – 59. doi:https://doi.org/10.1016/B978-0-12-394593-8.00002-3.
URL https://www.sciencedirect.com/science/article/pii/B9780123945938000023

[3] A. Eatemadi, H. Daraee, H. Karimkhanloo, M. Kouhi, N. Zarghami, A. Akbarzadeh, M. Abasi, Y. Hanifehpour, S. W. Joo, Carbon nanotubes: properties, synthesis, purification, and medical applications., Nanoscale research letters 9 (1) (2014) 393–393.

[4] M. REGI, 6 - synthesis, characterization and application of carbon nanotubes: the case of aerospace engineering, in: P. Brown, , K. Stevens (Eds.), Nanofibers and Nanotechnology in Textiles, Woodhead Publishing Series in Textiles, Woodhead Publishing, 2007, pp. 113 – 193. doi:https://doi.org/10.1533/9781845693732.2.113.
URL https://www.sciencedirect.com/science/article/pii/B9781845691059500066

[5] H. Shinohara, A. Tiwari, Graphene: An Introduction to the Fundamentals and Industrial Applications, John Wiley & Sons, 2015.

[6] S. Iijima, Helical microtubules of graphitic carbon, nature 354 (6348) (1991) 56–58.

[7] S. Stankovich, D. A. Dikin, R. D. Piner, K. A. Kohlhaas, A. Kleinhammes, Y. Jia, Y. Wu, S. T. Nguyen, R. S. Ruoff, Synthesis of graphene-based nanosheets via chemical reduction of exfoliated graphite oxide, carbon 45 (7) (2007) 1558–1565.

[8] C.-Y. Su, Y. Xu, W. Zhang, J. Zhao, X. Tang, C.-H. Tsai, L.-J. Li, Electrical and spectroscopic characterizations of ultra-large reduced graphene oxide monolayers, Chemistry of Materials 21 (23) (2009) 5674–5680.

[9] S. Angayarkanni, J. Philip, Review on thermal properties of nanofluids: recent developments, Advances in colloid and interface science 225 (2015) 146–176.

[10] A. M. Dimiev, Graphene oxide: Fundamentals and applications, John Wiley & Sons, 2016.

[11] K. S. Novoselov, A. K. Geim, S. V. Morozov, D. Jiang, Y. Zhang, S. V. Dubonos, I. V. Grigorieva, A. A. Firsov, Electric field effect in atomically thin carbon films, science 306 (5696) (2004) 666–669.

[12] T. Zhang, Q. Xue, S. Zhang, M. Dong, Theoretical approaches to graphene and graphene-based materials, Nano Today 7 (3) (2012) 180–200. doi:10.1016/j.nantod.2012.04.006.

[13] D. G. Papageorgiou, I. A. Kinloch, R. J. Young, Mechanical properties of graphene and graphene-based nanocomposites, Progress in Materials Science 90 (2017) 75–127. doi:10.1016/j.pmatsci.2017.07.004.

[14] R. Agromayor, D. Cabaleiro, A. A. Pardinas, J. P. Vallejo, J. Fernandez-Seara, L. Lugo, Heat transfer performance of functionalized graphene nanoplatelet aqueous nanofluids, Materials 9 (6) (2016) 455.

[15] E. J. Duplock, M. Scheffler, P. J. D. Lindan, Hallmark of perfect graphene, Physical Review Letters 92 (22). doi:10.1103/physrevlett.92.225502.

[16] A. A. Balandin, Thermal properties of graphene and nanostructured carbon materials, Nature Materials 10 (8) (2011) 569–581. doi:10.1038/nmat3064.

[17] M.-Y. Li, C.-H. Chen, Y. Shi, L.-J. Li, Heterostructures based on two-dimensional layered materials and their potential applications, Materials Today 19 (6) (2016) 322–335. doi:10.1016/j.mattod.2015.11.003.

[18] P. Suvarnaphaet, S. Pechprasarn, Graphene-based materials for biosensors: a review, Sensors 17 (10) (2017) 2161.

[19] P. Wick, A. E. Louw-Gaume, M. Kucki, H. F. Krug, K. Kostarelos, B. Fadeel, K. A. Dawson, A. Salvati, E. Vázquez, L. Ballerini, M. Tretiach, F. Benfenati, E. Flahaut, L. Gauthier, M. Prato, A. Bianco, Classification framework for graphene-based materials, Angewandte Chemie International Edition 53 (30) (2014) 7714–7718. doi:10.1002/anie.201403335.

[20] B. Brodie, Note sur un nouveau procédé pour la purification et la désagrégation du graphite, Ann. Chim. Phys 45 (1855) 351–353.

[21] B. C. Brodie, Xiii. on the atomic weight of graphite, Philosophical Transactions of the Royal Society of London 149 (1859) 249–259. arXiv:http://rstl.royalsocietypublishing.org/content/149/249.full.pdf+html, doi:10.1098/rstl.1859.0013.
URL http://rstl.royalsocietypublishing.org/content/149/249.short

[22] B. Brodie, Sur le poids atomique du graphite, Ann. Chim. Phys 59 (466) (1860) e472.

[23] B. Brodie, Ueber das atomgewicht des graphits, European Journal of Organic Chemistry 114 (1) (1860) 6–24.

[24] L. Staudenmaier, Verfahren zur darstellung der graphitsäure, European Journal of Inorganic Chemistry 32 (2) (1899) 1394–1399.

[25] V. Kohlschütter, P. Haenni, Zur kenntnis des graphitischen kohlenstoffs und der graphitsäure, Zeitschrift für anorganische und allgemeine Chemie 105 (1) (1919) 121–144.

[26] U. Hofmann, A. Frenzel, Quellung von graphit und die bildung von graphitsäure, European Journal of Inorganic Chemistry 63 (5) (1930) 1248–1262.

[27] H. Hamdi, Zur kenntnis der kolloidchemischen eigenschaften des humus. dispersoidchemische beobachtungen an graphitoxid., Kolloid Beihefte 54 (1942) 554643.

[28] U. Hofmann, E. König, Untersuchungen über graphitoxyd, Zeitschrift für anorganische und allgemeine Chemie 234 (4) (1937) 311–336.

[29] E. Sadeghinezhad, M. Mehrali, R. Saidur, M. Mehrali, S. T. Latibari, A. R. Akhiani, H. S. C. Metselaar, A comprehensive review on graphene nanofluids: recent research, development and applications, Energy Conversion and Management 111 (2016) 466–487.

[30] W. Yu, X. Guo, W. Xu, An improved score interval with a modified midpoint for a binomial proportion, Journal of Statistical Computation and Simulation 84 (5) (2014) 1022–1038.

[31] A. K. Singh, V. S. Raykar, Microwave synthesis of silver nanofluids with polyvinylpyrrolidone (pvp) and their transport properties, Colloid and Polymer Science 286 (14-15) (2008) 1667–1673.

[32] M. T. Jamal-Abad, A. Zamzamian, M. Dehghan, Experimental studies on the heat transfer and pressure drop characteristics of cu–water and al–water nanofluids in a spiral coil, Experimental Thermal and Fluid Science 47 (2013) 206–212.

[33] G. Paul, S. Sarkar, T. Pal, P. Das, I. Manna, Concentration and size dependence of nano-silver dispersed water based nanofluids, Journal of colloid and interface science 371 (1) (2012) 20–27.

[34] H.-t. Zhu, Y.-s. Lin, Y.-s. Yin, A novel one-step chemical method for preparation of copper nanofluids, Journal of colloid and interface science 277 (1) (2004) 100–103.

[35] C.-H. Lo, T.-T. Tsung, L.-C. Chen, Shape-controlled synthesis of cu-based nanofluid using submerged arc nanoparticle synthesis system (sanss), Journal of Crystal Growth 277 (1) (2005) 636–642.

[36] H. Zhu, D. Han, Z. Meng, D. Wu, C. Zhang, Preparation and thermal conductivity of cuo nanofluid via a wet chemical method, Nanoscale research letters 6 (1) (2011) 181.

[37] C.-H. Lo, T.-T. Tsung, L.-C. Chen, C.-H. Su, H.-M. Lin, Fabrication of copper oxide nanofluid using submerged arc nanoparticle synthesis system (sanss), Journal of Nanoparticle Research 7 (2) (2005) 313–320.

[38] X. Wei, H. Zhu, T. Kong, L. Wang, Synthesis and thermal conductivity of cu 2 o nanofluids, International Journal of Heat and Mass Transfer 52 (19) (2009) 4371–4374.

[39] L. Wang, M. Quintard, Nanofluids of the future, Advances in transport phenomena (2009) 179–243.

[40] X.-Q. Wang, A. S. Mujumdar, A review on nanofluids-part ii: experiments and applications, Brazilian Journal of Chemical Engineering 25 (4) (2008) 631–648.

[41] K. Solangi, S. Kazi, M. Luhur, A. Badarudin, A. Amiri, R. Sadri, M. Zubir, S. Gharehkhani, K. Teng, A comprehensive review of thermo-physical properties and convective heat transfer to nanofluids, Energy 89 (2015) 1065–1086.

[42] M. Mehrali, E. Sadeghinezhad, S. T. Latibari, S. N. Kazi, M. Mehrali, M. N. B. M. Zubir, H. S. C. Metselaar, Investigation of thermal conductivity and rheological properties of nanofluids containing graphene nanoplatelets, Nanoscale research letters 9 (1) (2014) 15.

[43] E. Sadeghinezhad, M. Mehrali, S. T. Latibari, M. Mehrali, S. N. Kazi, C. S. Oon, H. S. C. Metselaar, Experimental investigation of convective heat transfer using graphene nanoplatelet based nanofluids under turbulent flow conditions, Industrial & Engineering Chemistry Research 53 (31) (2014) 12455–12465. doi:10.1021/ie501947u.

[44] M. N. M. Zubir, A. Badarudin, S. Kazi, N. M. Huang, M. Misran, E. Sadeghinezhad, M. Mehrali, N. Yusoff, Highly dispersed reduced graphene oxide and its hybrid complexes as effective additives for improving thermophysical property of heat transfer fluid, International Journal of Heat and Mass Transfer 87 (2015) 284–294.

[45] W. Yu, H. Xie, L. Chen, Nanofluids, in: Smart nanoparticles technology, InTech, 2012.

[46] W. Yu, H. Xie, A review on nanofluids: preparation, stability mechanisms, and applications, Journal of Nanomaterials 2012 (2012) 1.

[47] M. Mehrali, E. Sadeghinezhad, M. M. Rashidi, A. R. Akhiani, S. T. Latibari, M. Mehrali, H. S. C. Metselaar, Experimental and numerical investigation of the effective electrical conductivity of nitrogen-doped graphene nanofluids, Journal of Nanoparticle Research 17 (6) (2015) 267.

[48] H. Zhu, C. Zhang, Y. Tang, J. Wang, B. Ren, Y. Yin, Preparation and thermal conductivity of suspensions of graphite nanoparticles, Carbon 45 (1) (2007) 226–228.

[49] M. N. M. Zubir, A. Badarudin, S. Kazi, N. M. Huang, M. Misran, E. Sadeghinezhad, M. Mehrali, N. Yusoff, Highly dispersed reduced graphene oxide and its hybrid complexes as effective additives for improving thermophysical property of heat transfer fluid, International Journal of Heat and Mass Transfer 87 (2015) 284–294.

[50] M. N. M. Zubir, A. Badarudin, S. Kazi, N. M. Huang, M. Misran, E. Sadeghinezhad, M. Mehrali, N. Syuhada, S. Gharehkhani, Experimental investigation on the use of reduced graphene oxide and its hybrid complexes in improving closed conduit turbulent forced convective heat transfer, Experimental Thermal and Fluid Science 66 (2015) 290–303.

[51] Z. Sun, S. Pöller, X. Huang, D. Guschin, C. Taetz, P. Ebbinghaus, J. Masa, A. Erbe, A. Kilzer, W. Schuhmann, et al., High-yield exfoliation of graphite in acrylate polymers: A stable few-layer graphene nanofluid with enhanced thermal conductivity, Carbon 64 (2013) 288–294.

[52] M. Mehrali, E. Sadeghinezhad, S. T. Latibari, M. Mehrali, H. Togun, M. Zubir, S. Kazi, H. S. C. Metselaar, Preparation, characterization, viscosity, and thermal conductivity of nitrogen-doped graphene aqueous nanofluids, Journal of materials science 49 (20) (2014) 7156–7171.

[53] N. Ahammed, L. G. Asirvatham, S. Wongwises, Effect of volume concentration and temperature on viscosity and surface tension of graphene–water nanofluid for heat transfer applications, Journal of Thermal Analysis and Calorimetry 123 (2) (2016) 1399–1409.

[54] W. S. Sarsam, A. Amiri, S. Kazi, A. Badarudin, Stability and thermophysical properties of non-covalently functionalized graphene nanoplatelets nanofluids, Energy Conversion and Management 116 (2016) 101–111.

[55] A. M. Haque, S. Kwon, J. Kim, J. Noh, S. Huh, H. Chung, H. Jeong, An experimental study on thermal characteristics of nanofluid with graphene and multi-wall carbon nanotubes, Journal of Central South University 22 (8) (2015) 3202–3210.

[56] W. Yu, H. Xie, D. Bao, Enhanced thermal conductivities of nanofluids containing graphene oxide nanosheets, Nanotechnology 21 (5) (2009) 055705.

[57] W. Yu, H. Xie, X. Wang, X. Wang, Significant thermal conductivity enhancement for nanofluids containing graphene nanosheets, Physics Letters A 375 (10) (2011) 1323–1328.

[58] L. Chen, H. Xie, Y. Li, W. Yu, Nanofluids containing carbon nanotubes treated by mechanochemical reaction, Thermochimica Acta 477 (1) (2008) 21–24.

[59] T. Missana, A. Adell, On the applicability of dlvo theory to the prediction of clay colloids stability, Journal of Colloid and Interface Science 230 (1) (2000) 150–156.

[60] I. Popa, G. Gillies, G. Papastavrou, M. Borkovec, Attractive and repulsive electrostatic forces between positively charged latex particles in the presence of anionic linear polyelectrolytes, The Journal of Physical Chemistry B 114 (9) (2010) 3170–3177.

[61] R. Sadri, M. Hosseini, S. Kazi, S. Bagheri, N. Zubir, G. Ahmadi, M. Dahari, T. Zaharinie, A novel, eco-friendly technique for covalent functionalization of graphene nanoplatelets and the potential of their nanofluids for heat transfer applications, Chemical Physics Letters 675 (2017) 92–97.

[62] D. Cabaleiro, L. Colla, S. Barison, L. Lugo, L. Fedele, S. Bobbo, Heat transfer capability of (ethylene glycol+ water)-based nanofluids containing graphene nanoplatelets: Design and thermophysical profile, Nanoscale research letters 12 (1) (2017) 53.

[63] S. Wang, C. Wang, X. Ji, Towards understanding the salt-intercalation exfoliation of graphite into graphene, RSC Advances 7 (82) (2017) 52252–52260.

[64] J. Liu, C. Xu, L. Chen, X. Fang, Z. Zhang, Preparation and photo-thermal conversion performance of modified graphene/ionic liquid nanofluids with excellent dispersion stability, Solar Energy Materials and Solar Cells 170 (2017) 219–232.

[65] M. Mehrali, E. Sadeghinezhad, A. R. Akhiani, S. T. Latibari, S. Talebian, A. Dolatshahi-Pirouz, H. S. C. Metselaar, M. Mehrali, An ecofriendly graphene-based nanofluid for heat transfer applications, Journal of Cleaner Production 137 (2016) 555–566.

[66] H. Yarmand, S. Gharehkhani, G. Ahmadi, S. F. S. Shirazi, S. Baradaran, E. Montazer, M. N. M. Zubir, M. S. Alehashem, S. Kazi, M. Dahari, Graphene nanoplatelets–silver hybrid nanofluids for enhanced heat transfer, Energy Conversion and Management 100 (2015) 419–428.

[67] M. Mehrali, E. Sadeghinezhad, M. A. Rosen, S. T. Latibari, M. Mehrali, H. S. C. Metselaar, S. N. Kazi, Effect of specific surface area on convective heat transfer of graphene nanoplatelet aqueous nanofluids, Experimental thermal and fluid science 68 (2015) 100–108.

[68] M. Mehrali, E. Sadeghinezhad, M. A. Rosen, A. R. Akhiani, S. T. Latibari, M. Mehrali, H. S. C. Metselaar, Heat transfer and entropy generation for laminar forced convection flow of graphene nanoplatelets nanofluids in a horizontal tube, International Communications in Heat and Mass Transfer 66 (2015) 23–31.

[69] S. N. Kazi, A. Badarudin, M. N. M. Zubir, H. N. Ming, M. Misran, E. Sadeghinezhad, M. Mehrali, N. I. Syuhada, Investigation on the use of graphene oxide as novel surfactant to stabilize weakly charged graphene nanoplatelets, Nanoscale research letters 10 (1) (2015) 212.

[70] L. G. Asirvatham, S. Wongwises, J. Babu, Heat transfer performance of a glass thermosyphon using graphene–acetone nanofluid, Journal of Heat Transfer 137 (11) (2015) 111502.

[71] A. Amiri, R. Sadri, M. Shanbedi, G. Ahmadi, B. Chew, S. Kazi, M. Dahari, Performance dependence of thermosyphon on the functionalization approaches: an experimental study on thermo-physical properties of graphene nanoplatelet-based water nanofluids, Energy Conversion and Management 92 (2015) 322–330.

[72] S. S. Park, N. J. Kim, Influence of the oxidation treatment and the average particle diameter of graphene for thermal conductivity enhancement, Journal of Industrial and Engineering Chemistry 20 (4) (2014) 1911–1915.

[73] J. S. Park, K. D. Kihm, H. Kim, G. Lim, S. Cheon, J. S. Lee, Wetting and evaporative aggregation of nanofluid droplets on cvd-synthesized hydrophobic graphene surfaces, Langmuir 30 (28) (2014) 8268–8275.

[74] J. Liu, F. Wang, L. Zhang, X. Fang, Z. Zhang, Thermodynamic properties and thermal stability of ionic liquid-based nanofluids containing graphene as advanced heat transfer fluids for medium-to-high-temperature applications, Renewable Energy 63 (2014) 519–523.

[75] X. Li, Y. Chen, S. Mo, L. Jia, X. Shao, Effect of surface modification on the stability and thermal conductivity of water-based sio 2-coated graphene nanofluid, Thermochimica Acta 595 (2014) 6–10.

[76] G.-J. Lee, C. K. Rhee, Enhanced thermal conductivity of nanofluids containing graphene nanoplatelets prepared by ultrasound irradiation, Journal of materials science 49 (4) (2014) 1506–1511.

[77] Z. Hajjar, A. morad Rashidi, A. Ghozatloo, Enhanced thermal conductivities of graphene oxide nanofluids, International Communications in Heat and Mass Transfer 57 (2014) 128–131.

[78] M. Hadadian, E. K. Goharshadi, A. Youssefi, Electrical conductivity, thermal conductivity, and rheological properties of graphene oxide-based nanofluids, Journal of nanoparticle research 16 (12) (2014) 2788.

[79] A. Ghozatloo, M. Shariaty-Niasar, A. Rashidi, Investigation of heat transfer coefficient of ethylene glycol/graphenenanofluid in turbulent flow regime, International Journal of Nanoscience and Nanotechnology 10 (4) (2014) 237–244.

[80] T. Theres Baby, R. Sundara, Synthesis of silver nanoparticle decorated multiwalled carbon nanotubes-graphene mixture and its heat transfer studies in nanofluid, AIP Advances 3 (1) (2013) 012111.

[81] A. Ghozatloo, M. Shariaty-Niasar, A. M. Rashidi, Preparation of nanofluids from functionalized graphene by new alkaline method and study on the thermal conductivity and stability, International Communications in Heat and Mass Transfer 42 (2013) 89–94.

[82] P. Dhar, S. Sen Gupta, S. Chakraborty, A. Pattamatta, S. K. Das, The role of percolation and sheet dynamics during heat conduction in poly-dispersed graphene nanofluids, Applied Physics Letters 102 (16) (2013) 163114.

[83] W. Yu, H. Xie, W. Chen, Experimental investigation on thermal conductivity of nanofluids containing graphene oxide nanosheets, Journal of Applied Physics 107 (9) (2010) 094317.

[84] W. Yu, H. Xie, L. Chen, Y. Li, D. Li, The preparation and thermal conductivities enhacement of nanofluids containing graphene oxide nanosheets, in: 2010 14th International Heat Transfer Conference, American Society of Mechanical Engineers, 2010, pp. 569–573.

[85] T. T. Baby, S. Ramaprabhu, Synthesis and nanofluid application of silver nanoparticles decorated graphene, Journal of Materials Chemistry 21 (26) (2011) 9702–9709.

[86] T. T. Baby, S. Ramaprabhu, Enhanced convective heat transfer using graphene dispersed nanofluids, Nanoscale research letters 6 (1) (2011) 289.

[87] T. T. Baby, S. Ramaprabhu, Investigation of thermal and electrical conductivity of graphene based nanofluids, Journal of Applied Physics 108 (12) (2010) 124308.

[88] T. T. Baby, R. Sundara, Synthesis and transport properties of metal oxide decorated graphene dispersed nanofluids, The Journal of Physical Chemistry C 115 (17) (2011) 8527–8533.

[89] S. Sen Gupta, V. Manoj Siva, S. Krishnan, T. Sreeprasad, P. K. Singh, T. Pradeep, S. K. Das, Thermal conductivity enhancement of nanofluids containing graphene nanosheets, Journal of Applied Physics 110 (8) (2011) 084302.

[90] S. Jyothirmayee Aravind, S. Ramaprabhu, Surfactant free graphene nanosheets based nanofluids by in-situ reduction of alkaline graphite oxide suspensions, Journal of Applied Physics 110 (12) (2011) 124326.

[91] N. Sandeep, Effect of aligned magnetic field on liquid thin film flow of magnetic-nanofluids embedded with graphene nanoparticles, Advanced Powder Technology 28 (3) (2017) 865–875.

[92] A. Hussanan, M. Z. Salleh, I. Khan, S. Shafie, Convection heat transfer in micropolar nanofluids with oxide nanoparticles in water, kerosene and engine oil, Journal of Molecular Liquids 229 (2017) 482–488.

[93] J. Cha, W. Kyoung, Molecular dynamics simulation of the effects of affinity of functional groups and particle-size on the behavior of a graphene sheet in nanofluid, Computational Materials Science 139 (2017) 202–208.

[94] E. Pop, V. Varshney, A. K. Roy, Thermal properties of graphene: Fundamentals and applications, MRS bulletin 37 (12) (2012) 1273–1281.

[95] Z.-S. Wu, G. Zhou, L.-C. Yin, W. Ren, F. Li, H.-M. Cheng, Graphene/metal oxide composite electrode materials for energy storage, Nano Energy 1 (1) (2012) 107–131. doi:10.1016/j.nanoen.2011.11.001.

[96] Y. Zhang, Q. Pei, X. He, Y.-W. Mai, A molecular dynamics simulation study on thermal conductivity of functionalized bilayer graphene sheet, Chemical Physics Letters 622 (2015) 104–108.

[97] P. Keblinski, S. Phillpot, S. Choi, J. Eastman, Mechanisms of heat flow in suspensions of nano-sized particles (nanofluids), International Journal of Heat and Mass Transfer 45 (4) (2002) 855–863. doi:10.1016/s0017-9310(01)00175-2.

[98] S. P. Jang, S. U. S. Choi, Role of brownian motion in the enhanced thermal conductivity of nanofluids, Applied Physics Letters 84 (21) (2004) 4316–4318. doi:10.1063/1.1756684.

[99] P. Keblinski, J. A. Eastman, D. G. Cahill, Nanofluids for thermal transport, Materials Today 8 (6) (2005) 36–44. doi:10.1016/s1369-7021(05)70936-6.

[100] J. H. Warner, F. Schffel, A. Bachmatiuk, M. H. Rmmeli, Chapter 3 - properties of graphene, in: J. H. Warner, F. Schffel, A. Bachmatiuk, M. H. Rmmeli (Eds.), Graphene, Elsevier, 2013, pp. 61 – 127. doi:https://doi.org/10.1016/B978-0-12-394593-8.00003-5.
URL https://www.sciencedirect.com/science/article/pii/B9780123945938000035

[101] A. Cardellini, M. Fasano, M. B. Bigdeli, E. Chiavazzo, P. Asinari, Thermal transport phenomena in nanoparticle suspensions, Journal of Physics: Condensed Matter 28 (48) (2016) 483003. doi:10.1088/0953-8984/28/48/483003.

[102] R. Davis, The effective thermal conductivity of a composite material with spherical inclusions, International Journal of Thermophysics 7 (3) (1986) 609–620.

[103] P. S. Joshi, P. S. Mahapatra, A. Pattamatta, Effect of particle shape and slip mechanism on buoyancy induced convective heat transport with nanofluids, Physics of Fluids 29 (12) (2017) 122001. doi:10.1063/1.4996824.

[104] H. Yarmand, N. W. B. M. Zulkifli, S. Gharehkhani, S. F. S. Shirazi, A. A. Alrashed, M. A. B. Ali, M. Dahari, S. Kazi, Convective heat transfer enhancement with graphene nanoplatelet/platinum hybrid nanofluid, International Communications in Heat and Mass Transfer 88 (2017) 120–125. doi:10.1016/j.icheatmasstransfer.2017.08.010.

[105] G. Huminic, A. Huminic, Hybrid nanofluids for heat transfer applications – a state-of-the-art review, International Journal of Heat and Mass Transfer 125 (2018) 82–103. doi:10.1016/j.ijheatmasstransfer.2018.04.059.

[106] H. D. Koca, S. Doganay, A. Turgut, I. H. Tavman, R. Saidur, I. M. Mahbubul, Effect of particle size on the viscosity of nanofluids: A review, Renewable and Sustainable Energy Reviews 82 (2018) 1664–1674. doi:10.1016/j.rser.2017.07.016.

[107] H. Zhu, C. Zhang, S. Liu, Y. Tang, Y. Yin, Effects of nanoparticle clustering and alignment on thermal conductivities of fe 3 o 4 aqueous nanofluids, Applied Physics Letters 89 (2) (2006) 023123.

[108] H. Ş. Aybar, M. Sharifpur, M. R. Azizian, M. Mehrabi, J. P. Meyer, A review of thermal conductivity models for nanofluids, Heat Transfer Engineering 36 (13) (2015) 1085–1110.

[109] J.-H. Lee, S.-H. Lee, C. Choi, S. Jang, S. Choi, A review of thermal conductivity data, mechanisms and models for nanofluids, International Journal of Micro-Nano Scale Transport.

[110] J. Maxwell, A treatise on electricity and magnetism, Clarendon Press, Oxford, UK, Vol. 1 (1881) p. 435.

[111] V. D. Bruggeman, Berechnung verschiedener physikalischer konstanten von heterogenen substanzen. i. dielektrizitätskonstanten und leitfähigkeiten der mischkörper aus isotropen substanzen, Annalen der physik 416 (7) (1935) 636–664.

[112] R. L. Hamilton, O. Crosser, Thermal conductivity of heterogeneous two-component systems, Industrial & Engineering chemistry fundamentals 1 (3) (1962) 187–191.

[113] Z. Hashin, S. Shtrikman, A variational approach to the theory of the effective magnetic permeability of multiphase materials, Journal of applied Physics 33 (10) (1962) 3125–3131.

[114] D. J. Jeffrey, Conduction through a random suspension of spheres, in: Proceedings of the Royal Society of London A: Mathematical, Physical and Engineering Sciences, Vol. 335, The Royal Society, 1973, pp. 355–367.

[115] E. J. Wasp, J. P. Kenny, R. L. Gandhi, Solid–liquid flow: slurry pipeline transportation.[pumps, valves, mechanical equipment, economics], Ser. Bulk Mater. Handl.;(United States) 1 (4).

[116] D. Hasselman, L. F. Johnson, Effective thermal conductivity of composites with interfacial thermal barrier resistance, Journal of Composite Materials 21 (6) (1987) 508–515.

[117] C.-W. Nan, R. Birringer, D. R. Clarke, H. Gleiter, Effective thermal conductivity of particulate composites with interfacial thermal resistance, Journal of Applied Physics 81 (10) (1997) 6692–6699.

[118] S. Aberoumand, A. Jafarimoghaddam, M. Moravej, H. Aberoumand, K. Javaherdeh, Experimental study on the rheological behavior of silver-heat transfer oil nanofluid and suggesting two empirical based correlations for thermal conductivity and viscosity of oil based nanofluids, Applied Thermal Engineering 101 (2016) 362–372.

[119] M. Afrand, D. Toghraie, N. Sina, Experimental study on thermal conductivity of water-based fe 3 o 4 nanofluid: development of a new correlation and modeled by artificial neural network, International Communications in Heat and Mass Transfer 75 (2016) 262–269.

[120] A. M. Khdher, N. A. C. Sidik, W. A. W. Hamzah, R. Mamat, An experimental determination of thermal conductivity and electrical conductivity of bio glycol based al 2 o 3 nanofluids and development of new correlation, International Communications in Heat and Mass Transfer 73 (2016) 75–83.

[121] L. Yang, X. Xu, W. Jiang, K. Du, A new thermal conductivity model for nanorod-based nanofluids, Applied Thermal Engineering 114 (2017) 287–299.

[122] L. Yang, X. Xu, A renovated hamilton–crosser model for the effective thermal conductivity of cnts nanofluids, International Communications in Heat and Mass Transfer 81 (2017) 42–50.

[123] A. A. Nadooshan, An experimental correlation approach for predicting thermal conductivity of water-eg based nanofluids of zinc oxide, Physica E: Low-dimensional Systems and Nanostructures 87 (2017) 15–19.

[124] A. Parsian, M. Akbari, New experimental correlation for the thermal conductivity of ethylene glycol containing al2o3–cu hybrid nanoparticles, Journal of Thermal Analysis and Calorimetry 1–9.

[125] Z. Wang, Z. Wu, F. Han, L. Wadsö, B. Sundén, Experimental comparative evaluation of a graphene nanofluid coolant in miniature plate heat exchanger, International Journal of Thermal Sciences 130 (2018) 148–156.

[126] A. Ghadimi, R. Saidur, H. Metselaar, A review of nanofluid stability properties and characterization in stationary conditions, International Journal of Heat and Mass Transfer 54 (17) (2011) 4051–4068.

[127] Gaganpreet, S. Srivastava, Effect of aggregation on thermal conductivity and viscosity of nanofluids, Applied Nanoscience 2 (3) (2012) 325–331. doi:10.1007/s13204-012-0082-z.

[128] P. Namburu, D. Kulkarni, A. Dandekar, D. Das, Experimental investigation of viscosity and specific heat of silicon dioxide nanofluids, Micro & Nano Letters 2 (3) (2007) 67–71.

[129] C. Nguyen, F. Desgranges, N. Galanis, G. Roy, T. Maré, S. Boucher, H. A. Mintsa, Viscosity data for al2o3–water nanofluidhysteresis: is heat transfer enhancement using nanofluids reliable?, International Journal of Thermal Sciences 47 (2) (2008) 103–111.

[130] J. B. Mena, A. A. U. de Moraes, Y. R. Benito, G. Ribatski, J. A. R. Parise, Extrapolation of al 2 o 3–water nanofluid viscosity for temperatures and volume concentrations beyond the range of validity of existing correlations, Applied thermal engineering 51 (1) (2013) 1092–1097.

[131] K. Suganthi, K. Rajan, Temperature induced changes in zno–water nanofluid: zeta potential, size distribution and viscosity profiles, International Journal of Heat and Mass Transfer 55 (25) (2012) 7969–7980.

[132] A. Turgut, I. Tavman, M. Chirtoc, H. Schuchmann, C. Sauter, S. Tavman, Thermal conductivity and viscosity measurements of water-based tio2 nanofluids, International Journal of Thermophysics 30 (4) (2009) 1213–1226.

[133] J. Chevalier, O. Tillement, F. Ayela, Rheological properties of nanofluids flowing through microchannels, Applied physics letters 91 (23) (2007) 233103.

[134] Y. Yang, A. Oztekin, S. Neti, S. Mohapatra, Characterization and convective heat transfer with nanofluids, in: ASME/JSME 2011 8th thermal engineering joint conference, American Society of Mechanical Engineers, 2011, pp. T30087–T30087.

[135] S. Halelfadl, P. Estellé, B. Aladag, N. Doner, T. Maré, Viscosity of carbon nanotubes water-based nanofluids: Influence of concentration and temperature, International Journal of Thermal Sciences 71 (2013) 111–117.

[136] W. Yu, H. Xie, L. Chen, Y. Li, Investigation of thermal conductivity and viscosity of ethylene glycol based zno nanofluid, Thermochimica Acta 491 (1) (2009) 92–96.

[137] B. C. Pak, Y. I. Cho, Hydrodynamic and heat transfer study of dispersed fluids with submicron metallic oxide particles, Experimental Heat Transfer an International Journal 11 (2) (1998) 151–170.

[138] Y. Xuan, W. Roetzel, Conceptions for heat transfer correlation of nanofluids, International Journal of heat and Mass transfer 43 (19) (2000) 3701–3707.

[139] E. Sadeghinezhad, M. Mehrali, S. Tahan Latibari, M. Mehrali, S. Kazi, C. S. Oon, H. S. C. Metselaar, Experimental investigation of convective heat transfer using graphene nanoplatelet based nanofluids under turbulent flow conditions, Industrial & Engineering Chemistry Research 53 (31) (2014) 12455–12465.

[140] F. Perrozzi, S. Prezioso, L. Ottaviano, Graphene oxide: from fundamentals to applications, Journal of Physics: Condensed Matter 27 (1) (2014) 013002.

[141] F. Li, X. Jiang, J. Zhao, S. Zhang, Graphene oxide: A promising nanomaterial for energy and environmental applications, Nano Energy 16 (2015) 488–515. doi:10.1016/j.nanoen.2015.07.014.

[142] I. Mudawar, Assessment of high-heat-flux thermal management schemes, IEEE Transactions on Components and Packaging Technologies 24 (2) (2001) 122–141. doi:10.1109/6144.926375.

[143] H. M. Ali, W. Arshad, Effect of channel angle of pin-fin heat sink on heat transfer performance using water based graphene nanoplatelets nanofluids, International Journal of Heat and Mass Transfer 106 (2017) 465–472.

[144] W. Arshad, H. M. Ali, Graphene nanoplatelets nanofluids thermal and hydrodynamic performance on integral fin heat sink, International Journal of Heat and Mass Transfer 107 (2017) 995–1001.

[145] T. Tharayil, L. G. Asirvatham, V. Ravindran, S. Wongwises, Thermal performance of miniature loop heat pipe with graphene–water nanofluid, International Journal of Heat and Mass Transfer 93 (2016) 957–968. doi:10.1016/j.ijheatmasstransfer.2015.11.011.

[146] T. Tharayil, L. G. Asirvatham, M. J. Dau, S. Wongwises, Entropy generation analysis of a miniature loop heat pipe with graphene–water nanofluid: Thermodynamics model and experimental study, International Journal of Heat and Mass Transfer 106 (2017) 407–421. doi:10.1016/j.ijheatmasstransfer.2016.08.035.

[147] M. Mehrali, E. Sadeghinezhad, R. Azizian, A. R. Akhiani, S. T. Latibari, M. Mehrali, H. S. C. Metselaar, Effect of nitrogen-doped graphene nanofluid on the thermal performance of the grooved copper heat pipe, Energy Conversion and Management 118 (2016) 459–473. doi:10.1016/j.enconman.2016.04.028.

[148] E. Sadeghinezhad, M. Mehrali, M. A. Rosen, A. R. Akhiani, S. T. Latibari, M. Mehrali, H. S. C. Metselaar, Experimental investigation of the effect of graphene nanofluids on heat pipe thermal performance, Applied Thermal Engineering 100 (2016) 775–787. doi:10.1016/j.applthermaleng.2016.02.071.

[149] X. Su, M. Zhang, W. Han, X. Guo, Experimental study on the heat transfer performance of an oscillating heat pipe with self-rewetting nanofluid, International Journal of Heat and Mass Transfer 100 (2016) 378–385. doi:10.1016/j.ijheatmasstransfer.2016.04.094.

[150] H. Yarmand, S. Gharehkhani, S. F. S. Shirazi, A. Amiri, M. S. Alehashem, M. Dahari, S. Kazi, Experimental investigation of thermo-physical properties, convective heat transfer and pressure drop of functionalized graphene nanoplatelets aqueous nanofluid in a square heated pipe, Energy Conversion and Management 114 (2016) 38–49. doi:10.1016/j.enconman.2016.02.008.

[151] K. M. Kim, I. C. Bang, Effects of graphene oxide nanofluids on heat pipe performance and capillary limits, International Journal of Thermal Sciences 100 (2016) 346–356.

[152] A. Amiri, M. Shanbedi, B. Chew, S. Kazi, K. Solangi, Toward improved engine performance with crumpled nitrogen-doped graphene based water–ethylene glycol coolant, Chemical Engineering Journal 289 (2016) 583–595. doi:10.1016/j.cej.2015.12.083.

[153] C. Selvam, D. M. Lal, S. Harish, Enhanced heat transfer performance of an automobile radiator with graphene based suspensions, Applied Thermal Engineering 123 (2017) 50–60. doi:10.1016/j.applthermaleng.2017.05.076.

[154] C. Selvam, R. S. Raja, D. M. Lal, S. Harish, Overall heat transfer coefficient improvement of an automobile radiator with graphene based suspensions, International Journal of Heat and Mass Transfer 115 (2017) 580–588. doi:10.1016/j.ijheatmasstransfer.2017.08.071.

[155] N. Ahammed, L. G. Asirvatham, S. Wongwises, Entropy generation analysis of graphene–alumina hybrid nanofluid in multiport minichannel heat exchanger coupled with thermoelectric cooler, International Journal of Heat and Mass Transfer 103 (2016) 1084–1097. doi:10.1016/j.ijheatmasstransfer.2016.07.070.

[156] C. Zhang, L. Zhang, H. Xu, D. Wang, B. Ye, Investigation of flow boiling performance and the resulting surface deposition of graphene oxide nanofluid in microchannels, Experimental Thermal and Fluid Science 86 (2017) 1–10.

[157] A. Ghozatloo, A. Rashidi, M. Shariaty-Niassar, Convective heat transfer enhancement of graphene nanofluids in shell and tube heat exchanger, Experimental Thermal and Fluid Science 53 (2014) 136–141. doi:10.1016/j.expthermflusci.2013.11.018.

[158] R. Ranjbarzadeh, A. Karimipour, M. Afrand, A. H. M. Isfahani, A. Shirneshan, Empirical analysis of heat transfer and friction factor of water/graphene oxide nanofluid flow in turbulent regime through an isothermal pipe, Applied Thermal Engineering 126 (2017) 538–547.

[159] M. Goodarzi, A. Kherbeet, M. Afrand, E. Sadeghinezhad, M. Mehrali, P. Zahedi, S. Wongwises, M. Dahari, Investigation of heat transfer performance and friction factor of a counter-flow double-pipe heat exchanger using nitrogen-doped, graphene-based nanofluids, International Communications in Heat and Mass Transfer 76 (2016) 16–23. doi:10.1016/j.icheatmasstransfer.2016.05.018.

[160] R. Ranjbarzadeh, A. M. Isfahani, M. Afrand, A. Karimipour, M. Hojaji, An experimental study on heat transfer and pressure drop of water/graphene oxide nanofluid in a copper tube under air cross-flow: Applicable as a heat exchanger, Applied Thermal Engineering 125 (2017) 69–79.

[161] C. Selvam, T. Balaji, D. M. Lal, S. Harish, Convective heat transfer coefficient and pressure drop of water-ethylene glycol mixture with graphene nanoplatelets, Experimental Thermal and Fluid Science 80 (2017) 67–76.

[162] V. Kumar, A. K. Tiwari, S. K. Ghosh, Effect of variable spacing on performance of plate heat exchanger using nanofluids, Energy 114 (2016) 1107–1119.

[163] H. Akhavan-Zanjani, M. Saffar-Avval, M. Mansourkiaei, M. Ahadi, F. Sharif, Turbulent convective heat transfer and pressure drop of graphene–water nanofluid flowing inside a horizontal circular tube, Journal of dispersion science and technology 35 (9) (2014) 1230–1240.

[164] E. Sadeghinezhad, H. Togun, M. Mehrali, P. S. Nejad, S. T. Latibari, T. Abdulrazzaq, S. Kazi, H. S. C. Metselaar, An experimental and numerical investigation of heat transfer enhancement for graphene nanoplatelets nanofluids in turbulent flow conditions, International Journal of Heat and Mass Transfer 81 (2015) 41–51.

[165] H. Akhavan-Zanjani, M. Saffar-Avval, M. Mansourkiaei, F. Sharif, M. Ahadi, Experimental investigation of laminar forced convective heat transfer of graphene–water nanofluid inside a circular tube,

International Journal of Thermal Sciences 100 (2016) 316–323. doi:10.1016/j.ijthermalsci.2015.10.003.

[166] H. K. Arzani, A. Amiri, H. K. Arzani, S. B. Rozali, S. N. Kazi, A. Badarudin, Toward improved heat transfer performance of annular heat exchangers with water/ethylene glycol-based nanofluids containing graphene nanoplatelets, Journal of Thermal Analysis and Calorimetry 126 (3) (2016) 1427–1436. doi:10.1007/s10973-016-5663-8.

[167] N. Zuber, Hydrodynamic aspects of boiling heat transfer (thesis), Tech. rep., Ramo-Wooldridge Corp., Los Angeles, CA (United States); Univ. of California, Los Angeles, CA (United States) (1959).

[168] S. S. Murshed, C. N. De Castro, M. Lourenço, M. Lopes, F. Santos, A review of boiling and convective heat transfer with nanofluids, Renewable and Sustainable Energy Reviews 15 (5) (2011) 2342–2354.

[169] L. Zhang, Z. Yu, D. Li, L. Fan, Y. Zhu, R. Hong, Y. Hu, J. Fan, K. Cen, Enhanced critical heat flux during quenching of extremely dilute aqueous colloidal suspensions with graphene oxide nanosheets, Journal of Heat Transfer 135 (5) (2013) 054502.

[170] L. Zhang, L. Fan, Z. Yu, K. Cen, An experimental investigation of transient pool boiling of aqueous nanofluids with graphene oxide nanosheets as characterized by the quenching method, International Journal of Heat and Mass Transfer 73 (2014) 410–414.

[171] S. D. Park, S. Won Lee, S. Kang, I. C. Bang, J. H. Kim, H. S. Shin, D. W. Lee, D. Won Lee, Effects of nanofluids containing graphene/graphene-oxide nanosheets on critical heat flux, Applied Physics Letters 97 (2) (2010) 023103.

[172] S. D. Park, S. W. Lee, S. Kang, S. M. Kim, I. C. Bang, Pool boiling chf enhancement by graphene-oxide nanofluid under nuclear coolant chemical environments, Nuclear Engineering and Design 252 (2012) 184–191.

[173] S. D. Park, I. C. Bang, Flow boiling chf enhancement in an external reactor vessel cooling (ervc) channel using graphene oxide nanofluid, Nuclear Engineering and Design 265 (2013) 310–318.

[174] S.-S. Park, Y. H. Kim, Y. H. Jeon, M. T. Hyun, N.-J. Kim, Effects of spray-deposited oxidized multi-wall carbon nanotubes and graphene on pool-boiling critical heat flux enhancement, Journal of Industrial and Engineering Chemistry 24 (2015) 276–283.

[175] S. D. Park, I. C. Bang, Experimental study of a universal chf enhancement mechanism in nanofluids using hydrodynamic instability, International Journal of Heat and Mass Transfer 70 (2014) 844–850.

[176] L. Yudong, W. Jiangqing, S. Chuangjian, G. Shichao, G. Yongkun, P. Quangui, Nucleation rate and supercooling degree of water-based graphene oxide nanofluids, Applied Thermal Engineering 115 (2017) 1226–1236.

[177] L.-W. Fan, J.-Q. Li, D.-Y. Li, L. Zhang, Z.-T. Yu, K.-F. Cen, The effect of concentration on transient pool boiling heat transfer of graphene-based aqueous nanofluids, International Journal of Thermal Sciences 91 (2015) 83–95.

[178] R. K. Cheedarala, E. J. Park, Y.-B. Park, H. W. Park, Highly wettable cuo: graphene oxide core–shell porous nanocomposites for enhanced critical heat flux, physica status solidi (a) 212 (8) (2015) 1756–1766.

[179] E. Sadeghinezhad, M. Mehrali, A. R. Akhiani, S. T. Latibari, A. Dolatshahi-Pirouz, H. S. C. Metselaar, M. Mehrali, Experimental study on heat transfer augmentation of graphene based ferrofluids in presence of magnetic field, Applied Thermal Engineering 114 (2017) 415–427. doi:10.1016/j.applthermaleng.2016.11.199.

[180] N. Wang, G. Xu, S. Li, X. Zhang, Thermal properties and solar collection characteristics of oil-based nanofluids with low graphene concentration, Energy Procedia 105 (2017) 194–199.

[181] M. Vakili, S. Hosseinalipour, S. Delfani, S. Khosrojerdi, M. Karami, Experimental investigation of graphene nanoplatelets nanofluid-based volumetric solar collector for domestic hot water systems, Solar Energy 131 (2016) 119–130.

[182] M. Vakili, S. Hosseinalipour, S. Delfani, S. Khosrojerdi, Photothermal properties of graphene nanoplatelets nanofluid for low-temperature direct absorption solar collectors, Solar Energy Materials and Solar Cells 152 (2016) 187–191.

[183] B. Rose, H. Singh, N. Verma, S. Tassou, S. Suresh, N. Anantharaman, D. Mariotti, P. Maguire, Investigations into nanofluids as direct solar radiation collectors, Solar Energy 147 (2017) 426–431.

[184] A. Lavasani, M. Vakili, et al., Experimental study of photothermal specifications and stability of graphene oxide nanoplatelets nanofluid as working fluid for low-temperature direct absorption solar collectors (dascs), Solar Energy Materials and Solar Cells 164 (2017) 32–39.

[185] R. C. Shende, S. Ramaprabhu, Application of few-layered reduced graphene oxide nanofluid as a working fluid for direct absorption solar collectors, Journal of Nanoscience and Nanotechnology 17 (2) (2017) 1233–1239. doi:10.1166/jnn.2017.12695.

[186] L. Chen, J. Liu, X. Fang, Z. Zhang, Reduced graphene oxide dispersed nanofluids with improved photo-thermal conversion performance for direct absorption solar collectors, Solar Energy Materials and Solar Cells 163 (2017) 125–133.

[187] Y. Fu, T. Mei, G. Wang, A. Guo, G. Dai, S. Wang, J. Wang, J. Li, X. Wang, Investigation on enhancing effects of au nanoparticles on solar steam generation in graphene oxide nanofluids, Applied Thermal Engineering 114 (2017) 961–968.

[188] D. A. Vincely, E. Natarajan, Experimental investigation of the solar fpc performance using graphene oxide nanofluid under forced circulation, Energy Conversion and Management 117 (2016) 1–11.

[189] S. K. Verma, A. K. Tiwari, D. S. Chauhan, Experimental evaluation of flat plate solar collector using nanofluids, Energy Conversion and Management 134 (2017) 103–115.

[190] R. A. Taylor, P. E. Phelan, T. P. Otanicar, R. Adrian, R. Prasher, Nanofluid optical property characterization: towards efficient direct absorption solar collectors, Nanoscale Research Letters 6 (1) (2011) 225. doi:10.1186/1556-276x-6-225.

[191] S. Ladjevardi, A. Asnaghi, P. Izadkhast, A. Kashani, Applicability of graphite nanofluids in direct solar energy absorption, Solar Energy 94 (2013) 327–334. doi:10.1016/j.solener.2013.05.012.

[192] A. Toppin-Hector, H. Singh, Development of a nano-heat transfer fluid carrying direct absorbing receiver for concentrating solar collectors, International Journal of Low-Carbon Technologies 11 (2) (2013) 199–204. doi:10.1093/ijlct/ctt072.

[193] Z. Luo, C. Wang, W. Wei, G. Xiao, M. Ni, Performance improvement of a nanofluid solar collector based on direct absorption collection (DAC) concepts, International Journal of Heat and Mass Transfer 75 (2014) 262–271. doi:10.1016/j.ijheatmasstransfer.2014.03.072.

[194] Z. Said, M. A. Alim, I. Janajreh, Exergy efficiency analysis of a flat plate solar collector using graphene based nanofluid, IOP Conference Series: Materials Science and Engineering 92 (2015) 012015. doi:10.1088/1757-899x/92/1/012015.

[195] J. Liu, Z. Ye, L. Zhang, X. Fang, Z. Zhang, A combined numerical and experimental study on graphene/ionic liquid nanofluid based direct absorption solar collector, Solar Energy Materials and Solar Cells 136 (2015) 177–186. doi:10.1016/j.solmat.2015.01.013.

[196] R. Shende, R. Sundara, Nitrogen doped hybrid carbon based composite dispersed nanofluids as working fluid for low-temperature direct absorption solar collectors, Solar Energy Materials and Solar Cells 140 (2015) 9–16. doi:10.1016/j.solmat.2015.03.012.

[197] L. Zhang, L. Chen, J. Liu, X. Fang, Z. Zhang, Effect of morphology of carbon nanomaterials on thermo-physical characteristics, optical properties and photo-thermal conversion performance of nanofluids, Renewable Energy 99 (2016) 888–897. doi:10.1016/j.renene.2016.07.073.

[198] T. K. Tullius, Y. Bayazitoglu, Analysis of a hybrid nanofluid exposed to radiation, Numerical Heat Transfer, Part B: Fundamentals 69 (4) (2016) 271–286.

[199] Y. Li, Z. Wu, H. Xie, J. Xing, J. Mao, Y. Wang, Z. Li, Study on the performance of TEG with heat transfer enhancement using graphene-water nanofluid for a TEG cooling system, Science China Technological Sciences 60 (8) (2017) 1168–1174. doi:10.1007/s11431-017-9079-6.

[200] L. Chen, C. Xu, J. Liu, X. Fang, Z. Zhang, Optical absorption property and photo-thermal conversion performance of graphene oxide/water nanofluids with excellent dispersion stability, Solar Energy 148 (2017) 17–24. doi:10.1016/j.solener.2017.03.073.

Highlights

1. Various synthesis and preparation methods of graphene oxide are discussed in detail.
2. Preparation methods of graphene nanofluids with different base fluids are summarized in detail using different techniques.
3. Stability evaluation, enhancement and mechanism methods of graphene nanofluid are described thoroughly.
4. Effective parameters which influence the thermal properties are discussed.
5. The applications of graphene based nanofluid in major heat transfer systems are detailed summarized.

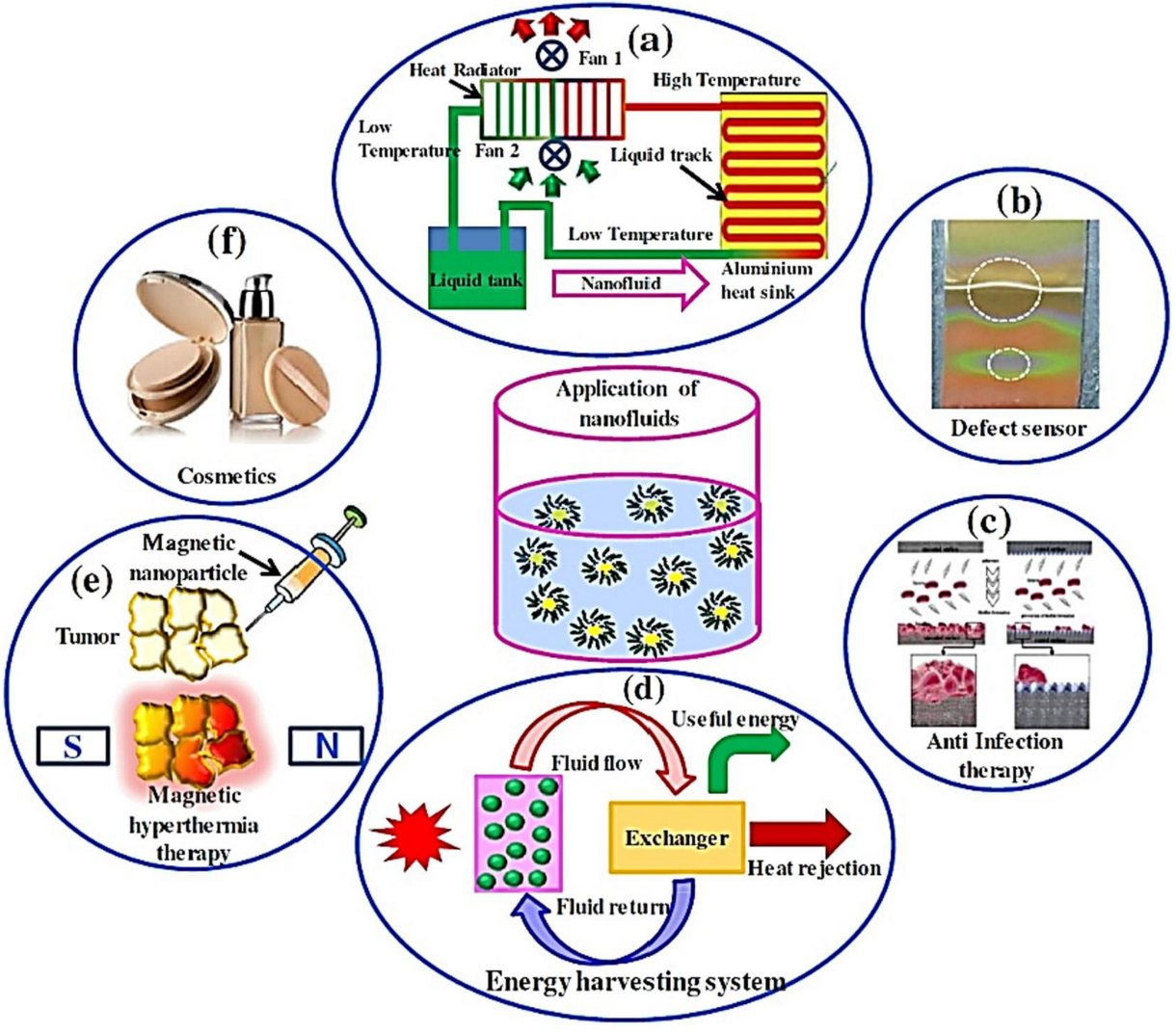
(a)
Fan 1
Heat Radiator
High Temperature
Low Temperature
Fan 2
Liquid track
Low Temperature
Liquid tank
Nanofluid
Aluminium heat sink
(b)
Defect sensor
(c)
Anti Infection therapy
(d)
Useful energy
Fluid flow
Exchanger
Heat rejection
Fluid return
Energy harvesting system
(e)
Magnetic nanoparticle
Tumor
S
N
Magnetic hyperthermia therapy
(f)
Cosmetics
Application of nanofluids

Figure 1

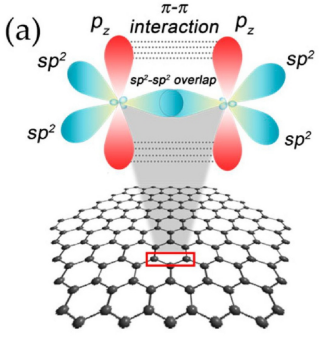

Graphene

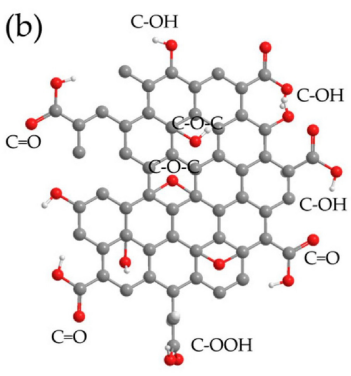

Graphene oxide

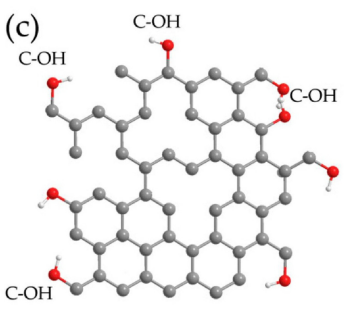

Reduced graphene oxide

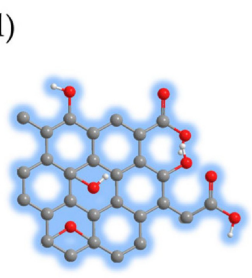

Graphene-based quantum dot

Figure 2

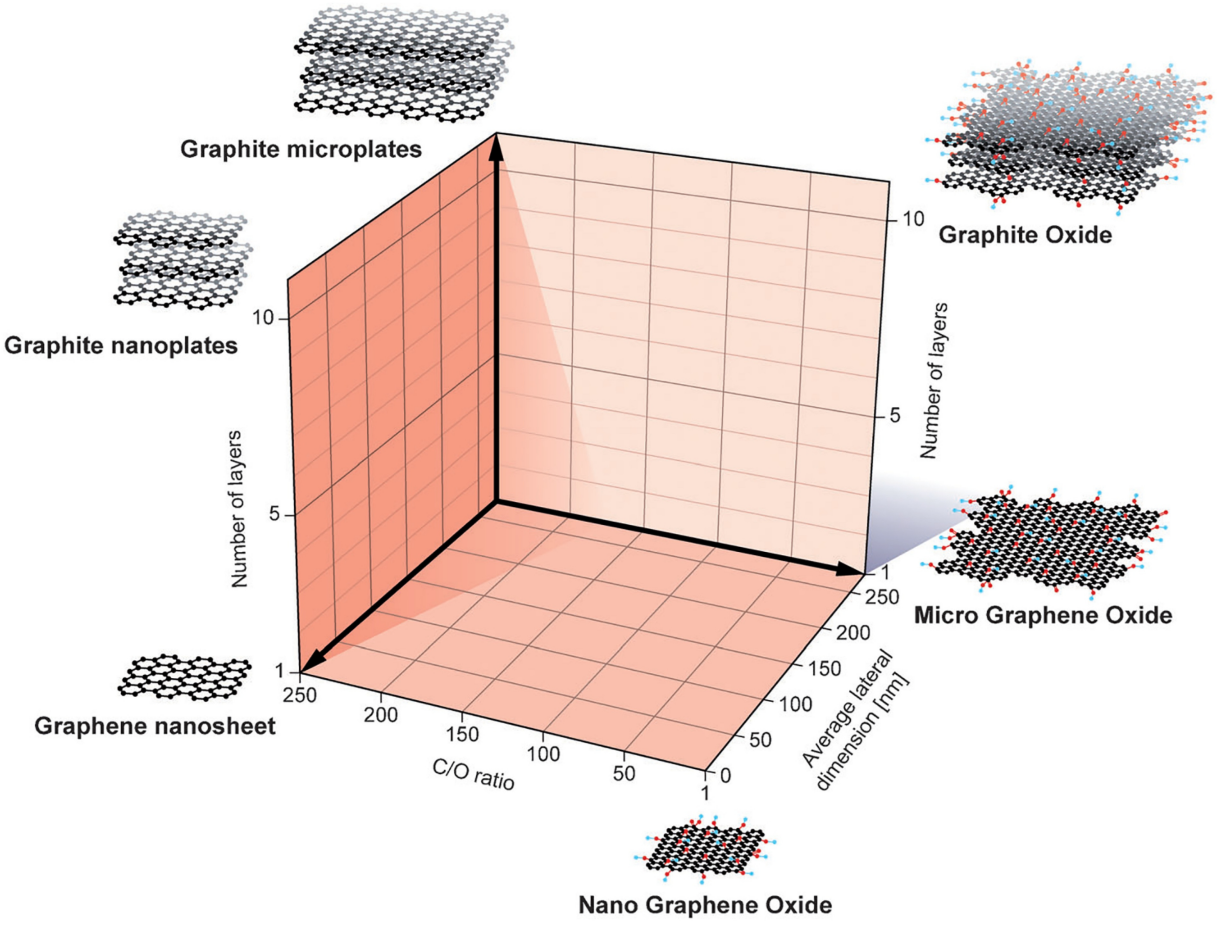
Graphite microplates
Graphite Oxide
Graphite nanoplates
Number of layers
10
5
1
Number of layers
10
5
1
Micro Graphene Oxide
Graphene nanosheet
250
200
150
100
50
1
C/O ratio
250
200
150
100
50
0
Average lateral dimension [nm]
Nano Graphene Oxide

Figure 3

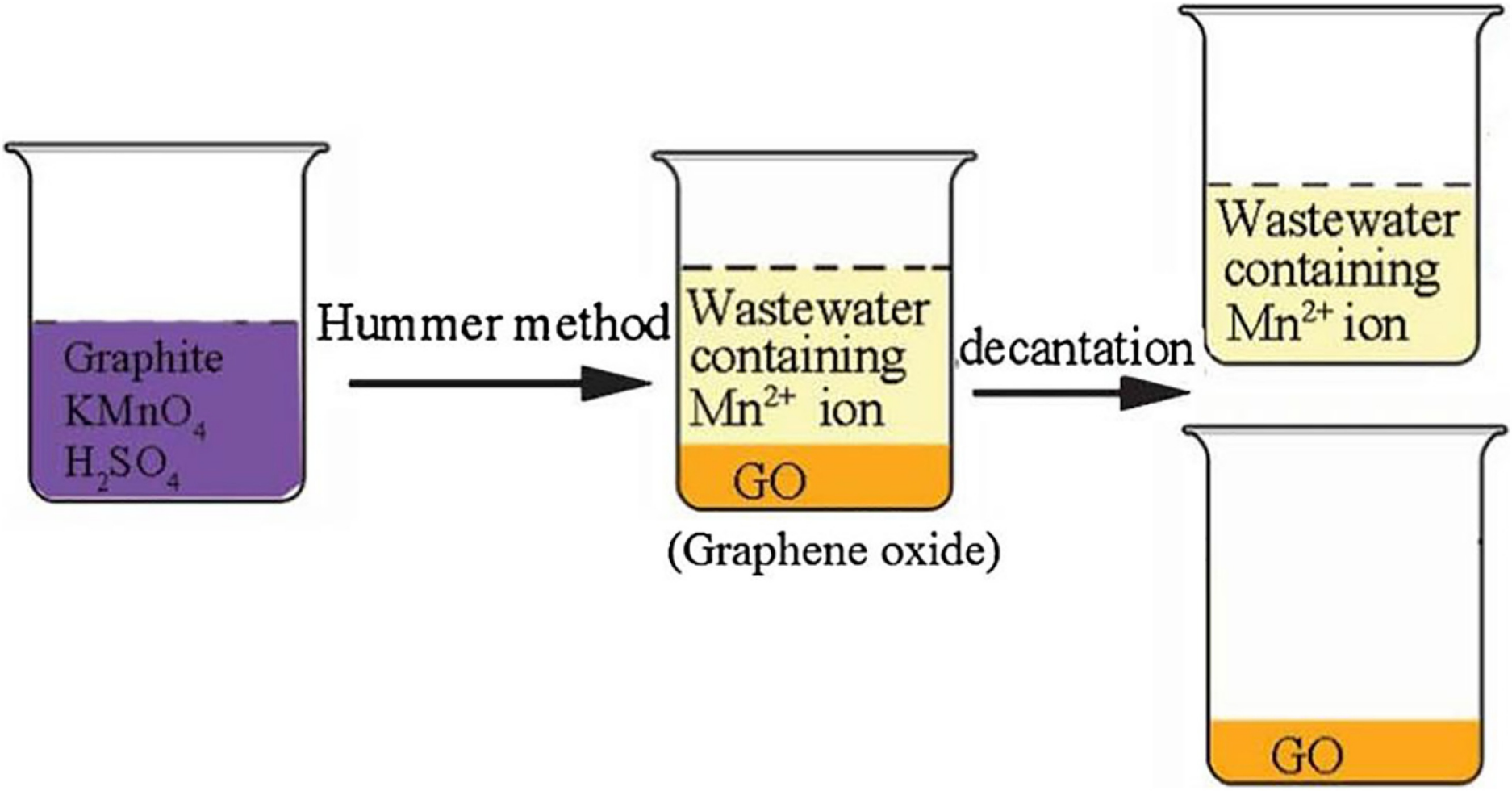
Graphite
KMnO4
H2SO4
Hummer method
Wastewater
containing
Mn2+ ion
GO
(Graphene oxide)
decantation
Wastewater
containing
Mn2+ ion
GO

Figure 4

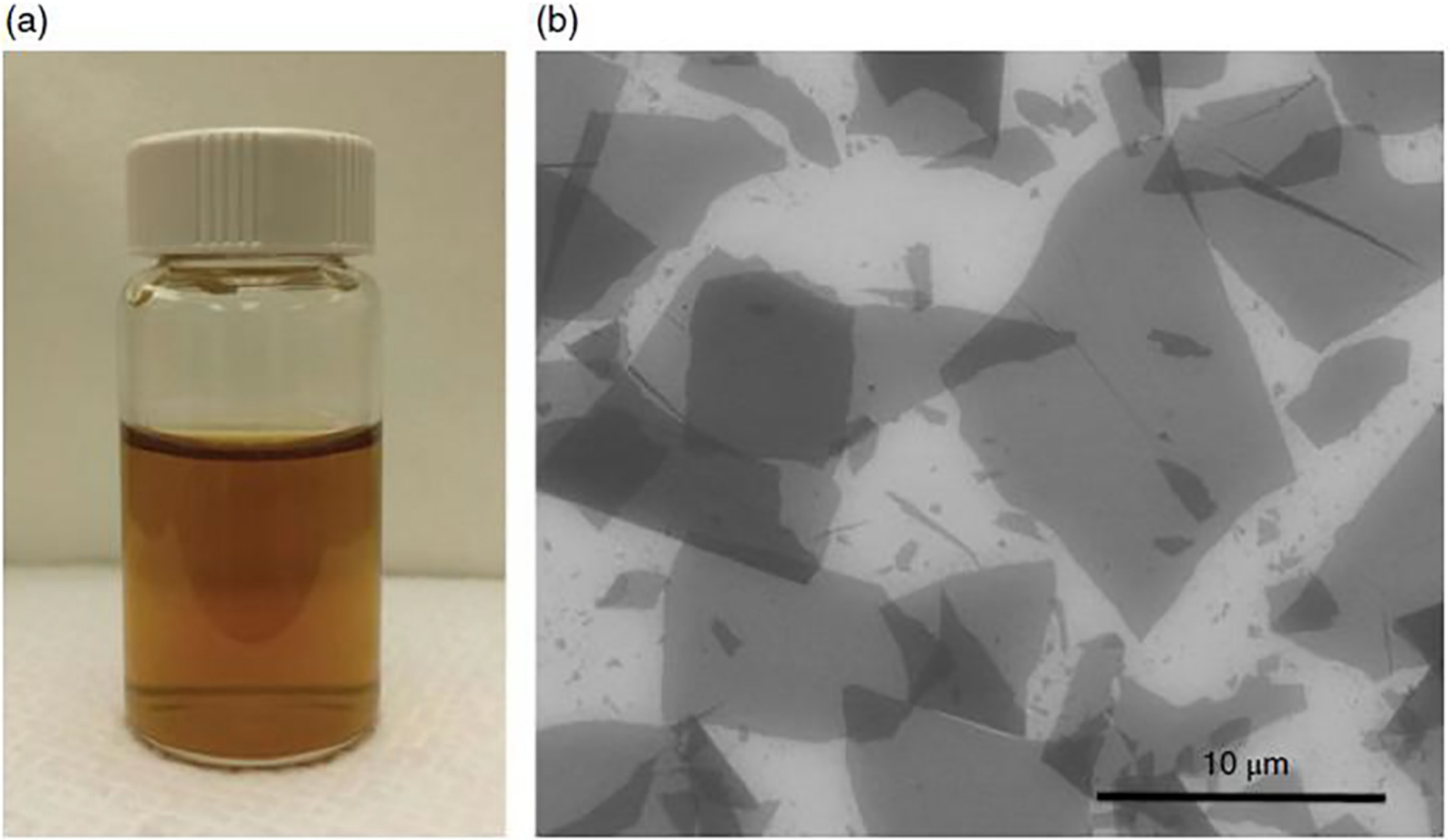

Figure 5

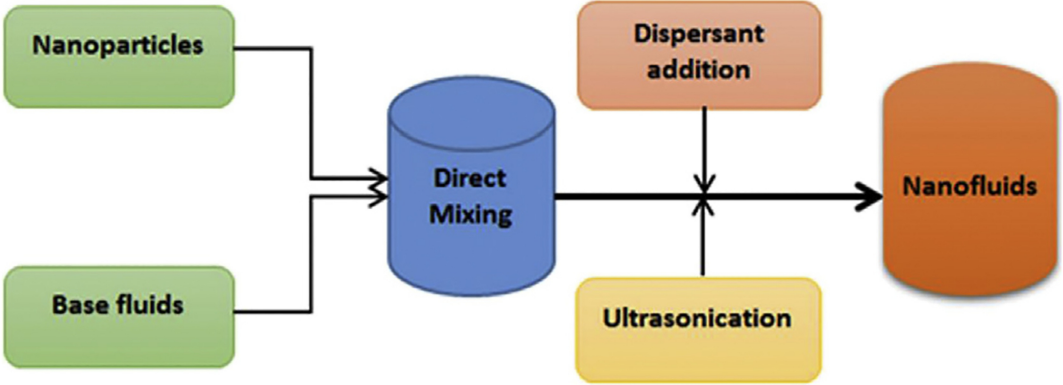
Nanoparticles
Base fluids
Direct Mixing
Dispersant addition
Ultrasonication
Nanofluids

Figure 6

Steric stabilization

Electrostatic stabilization

Figure 7

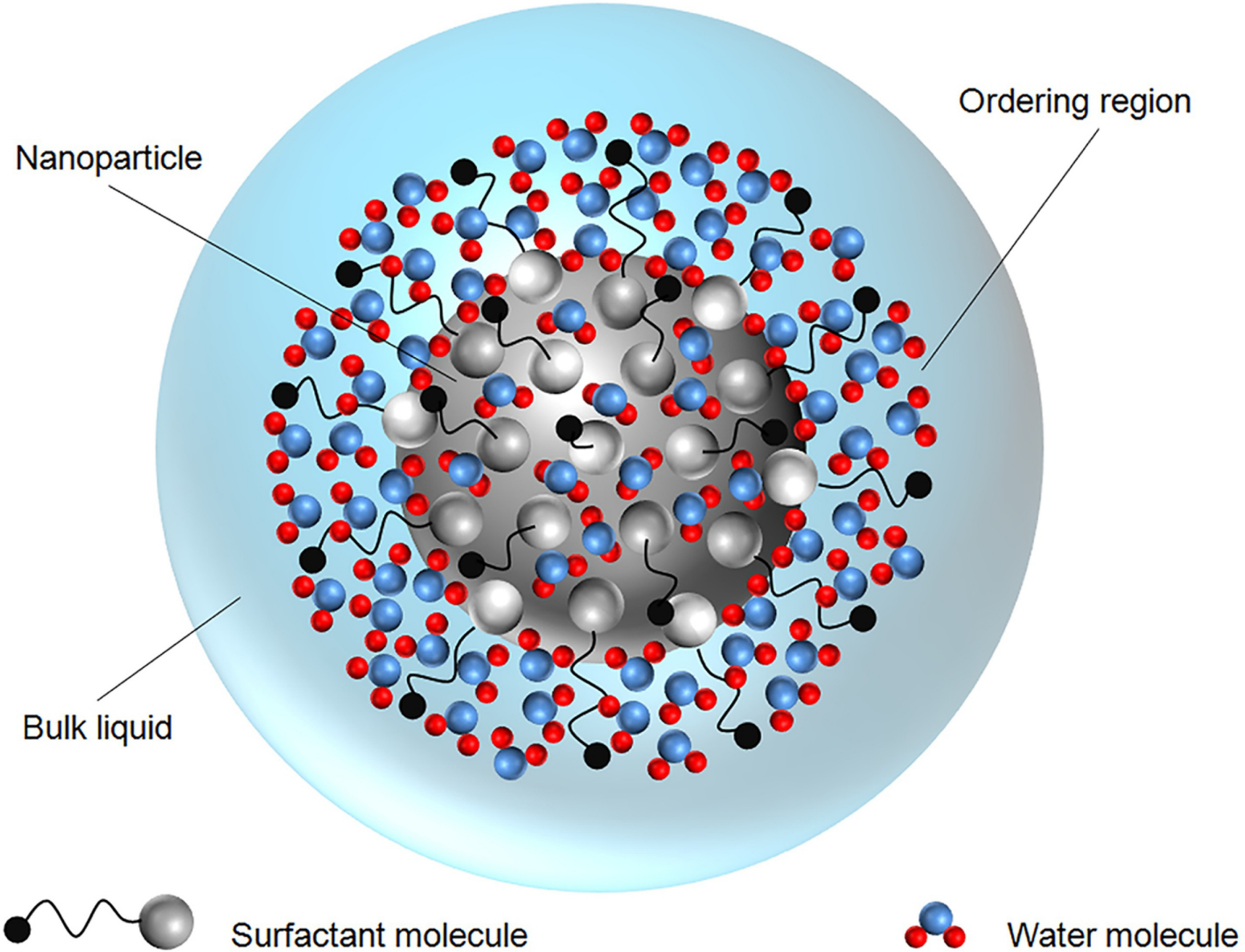
Ordering region
Nanoparticle
Bulk liquid
Surfactant molecule
Water molecule

Figure 8

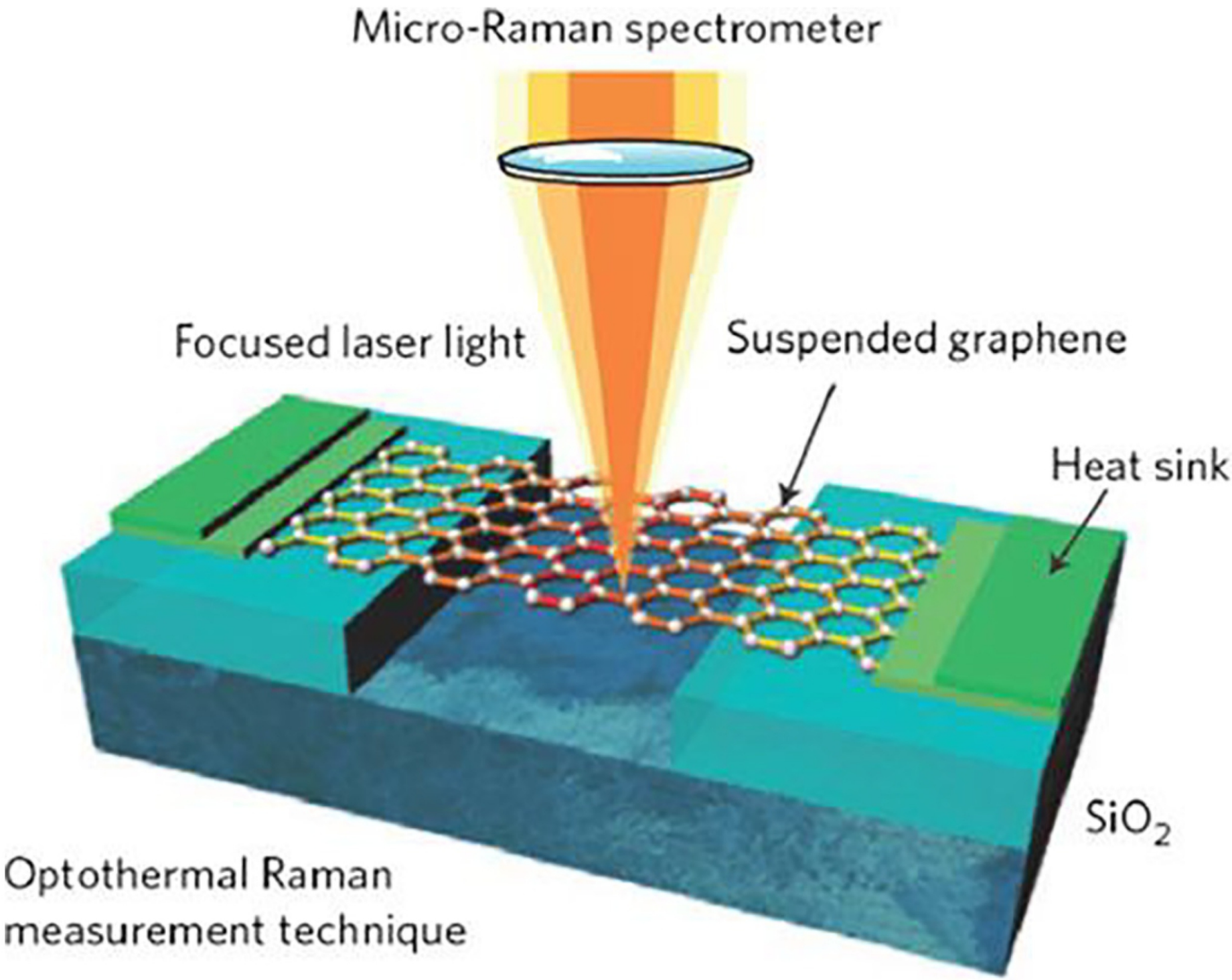
Micro-Raman spectrometer
Focused laser light
Suspended graphene
Heat sink
SiO_2
Optothermal Raman
measurement technique

Figure 9

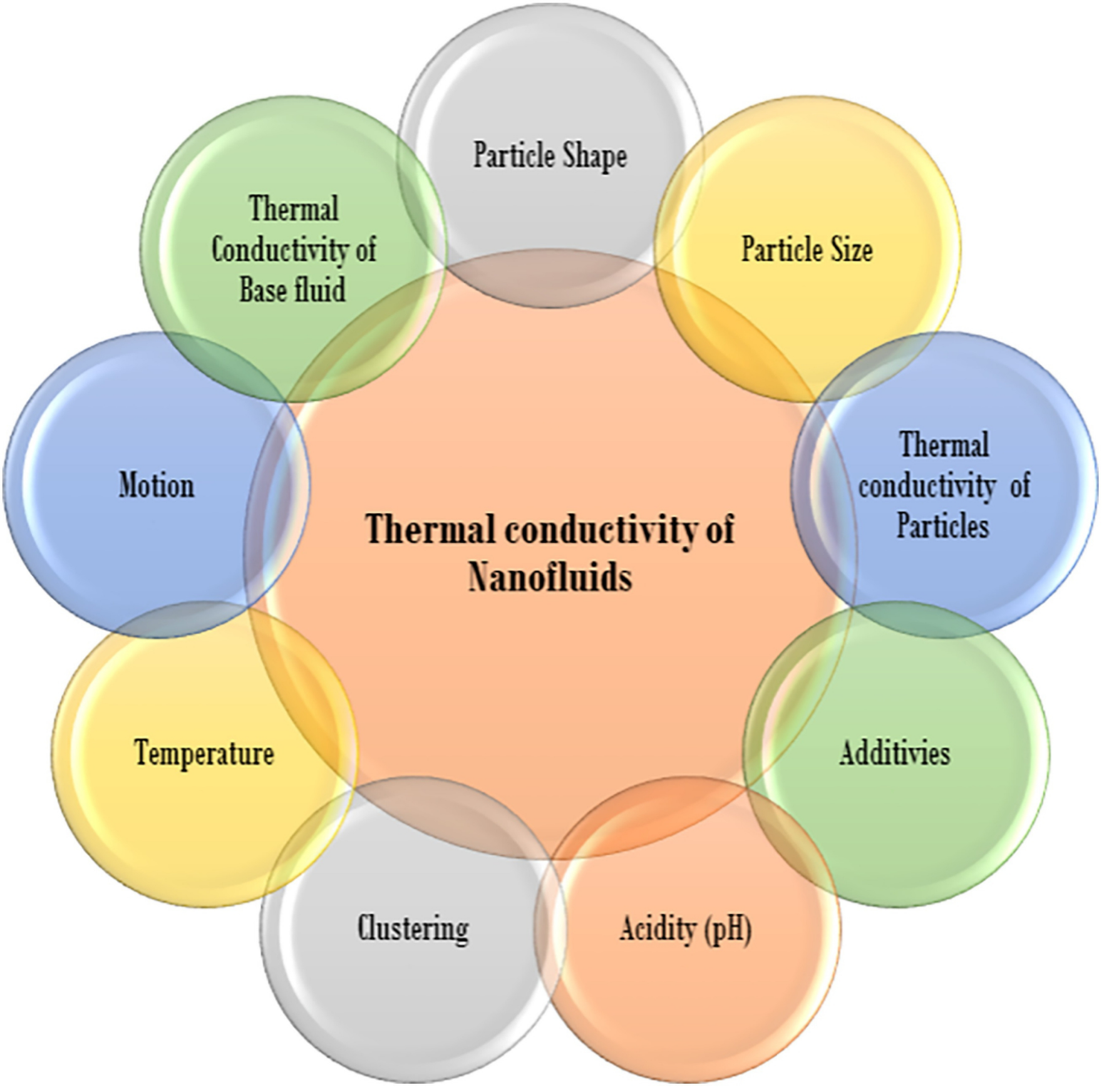
Particle Shape
Particle Size
Thermal conductivity of Particles
Additivies
Acidity (pH)
Clustering
Temperature
Motion
Thermal Conductivity of Base fluid
Thermal conductivity of Nanofluids

Figure 10

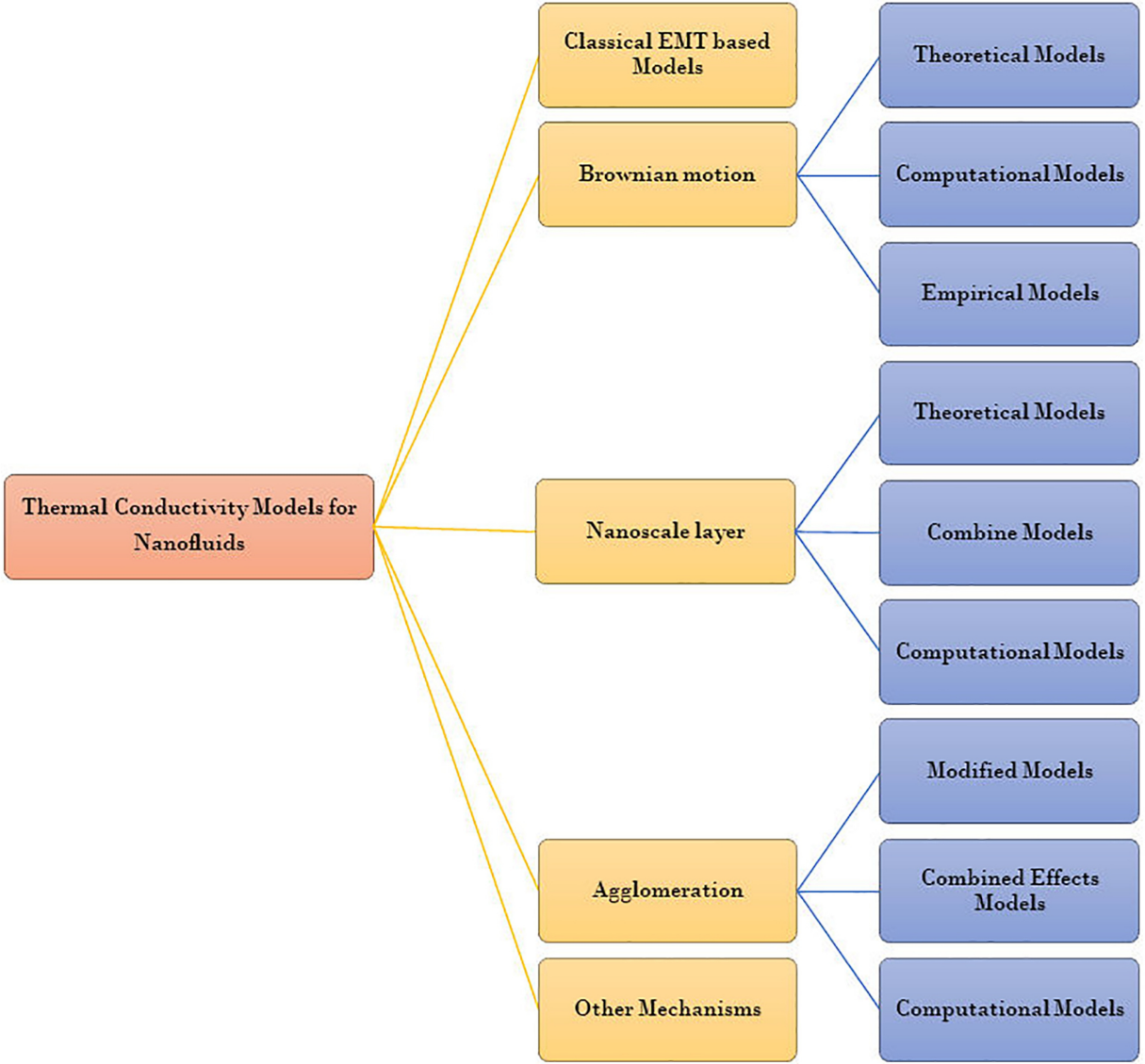
Thermal Conductivity Models for Nanofluids
Classical EMT based Models
Brownian motion
Theoretical Models
Computational Models
Empirical Models
Nanoscale layer
Theoretical Models
Combine Models
Computational Models
Agglomeration
Modified Models
Combined Effects Models
Computational Models
Other Mechanisms

Figure 11

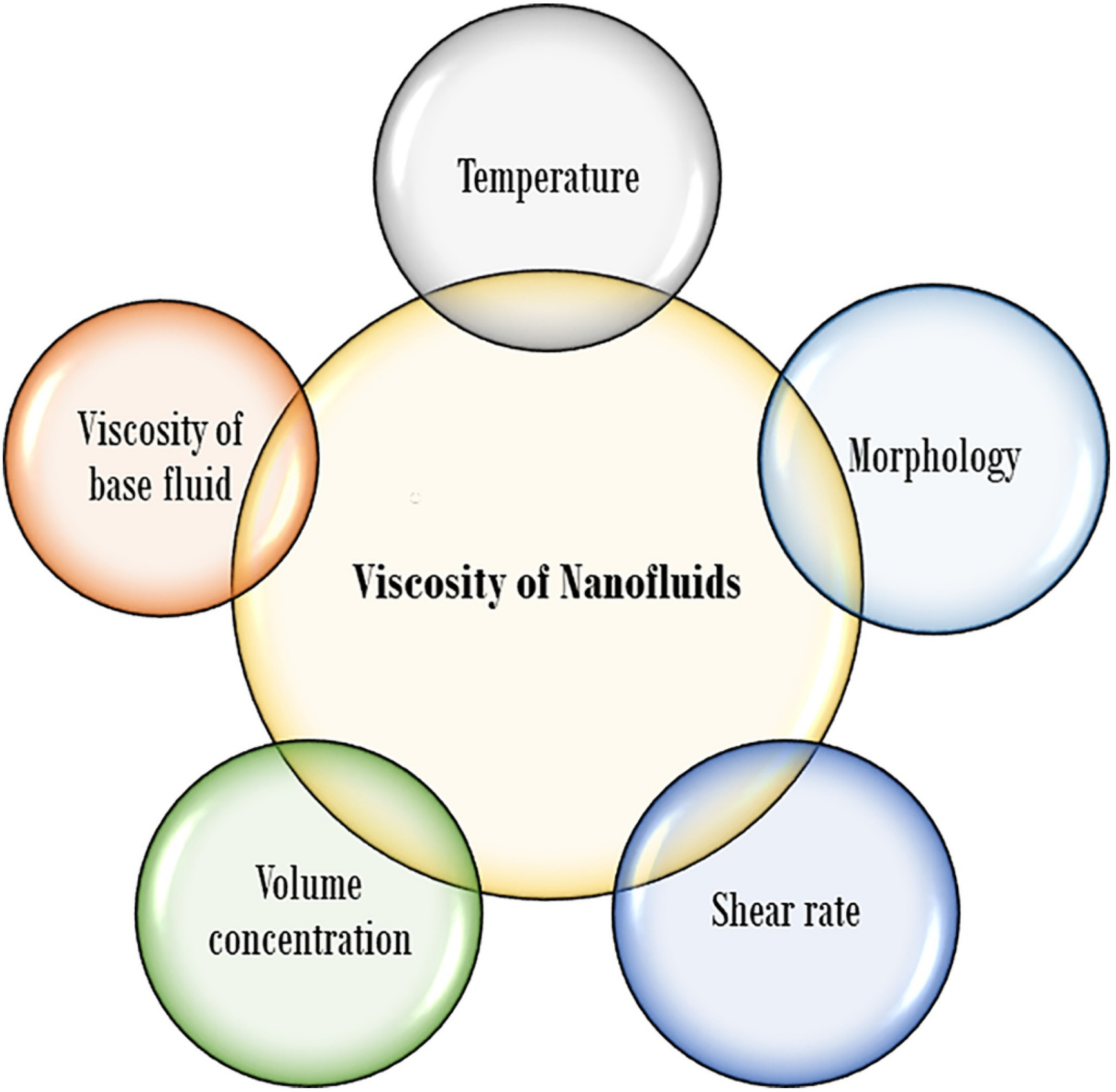
Temperature
Viscosity of base fluid
Morphology
Viscosity of Nanofluids
Volume concentration
Shear rate

Figure 12

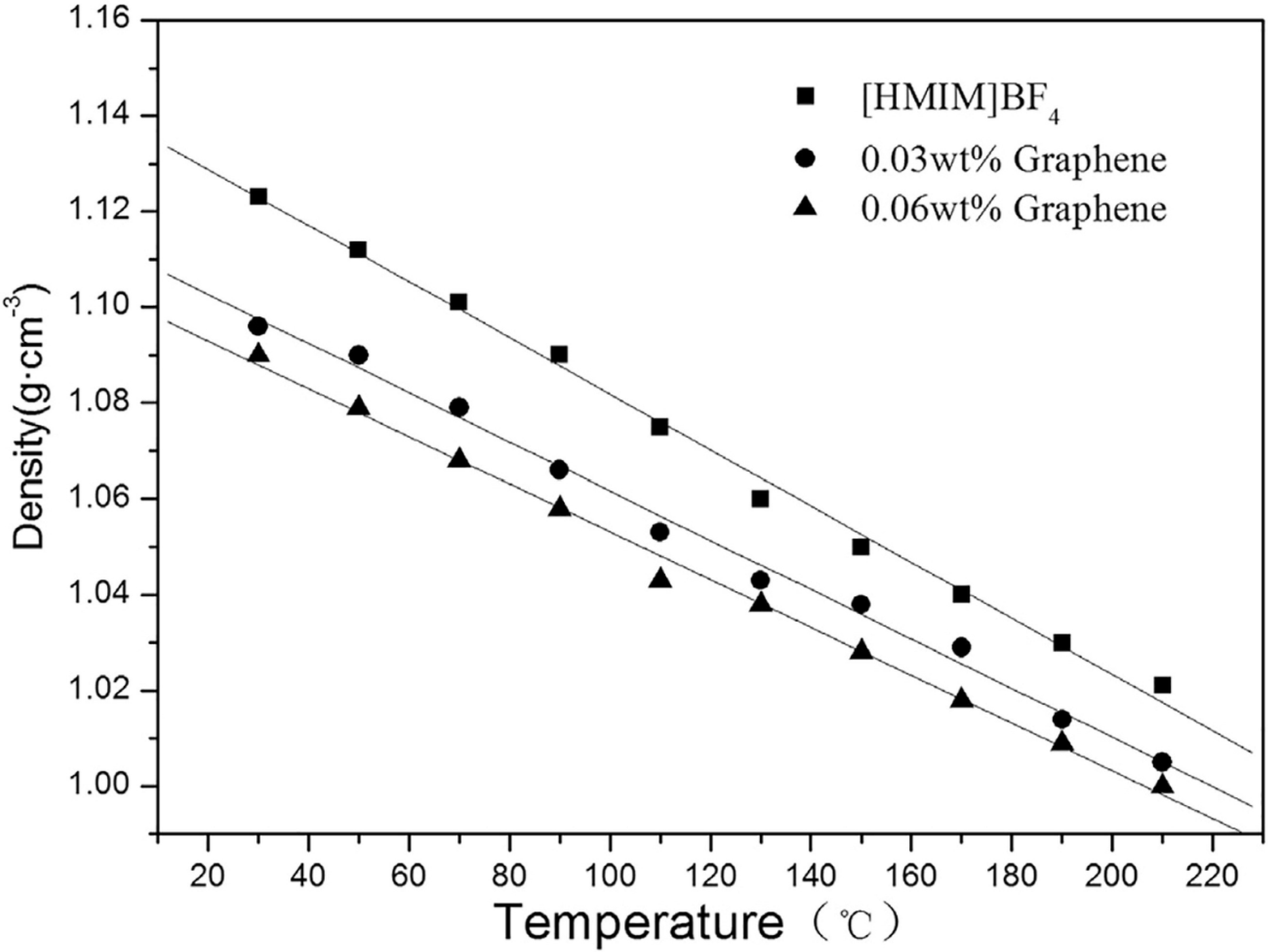
[HMIM]BF4
0.03wt% Graphene
0.06wt% Graphene
Density(g·cm-3)
Temperature（℃）
1.16
1.14
1.12
1.10
1.08
1.06
1.04
1.02
1.00
20
40
60
80
100
120
140
160
180
200
220

Figure 13


Nanofluids Applications
Heat pipe
Electronics Cooling
Engine Cooling
Transmission Oil
Heating and Cooling of building
Welding Cooling
Nuclear system cooling
Solar water heating
Refrigeration
Defense
Space
Biomedical applications
Drilling
Thermal storage
Lubrication
Drag reduction
Solar cells cooling
Exhaust flue gas receovery
Medicine
Laser and microwave tubes
Boiling heat transfer
Diesel combustion
Heat exchanger
Fuel cells
Solar Collector

Figure 14

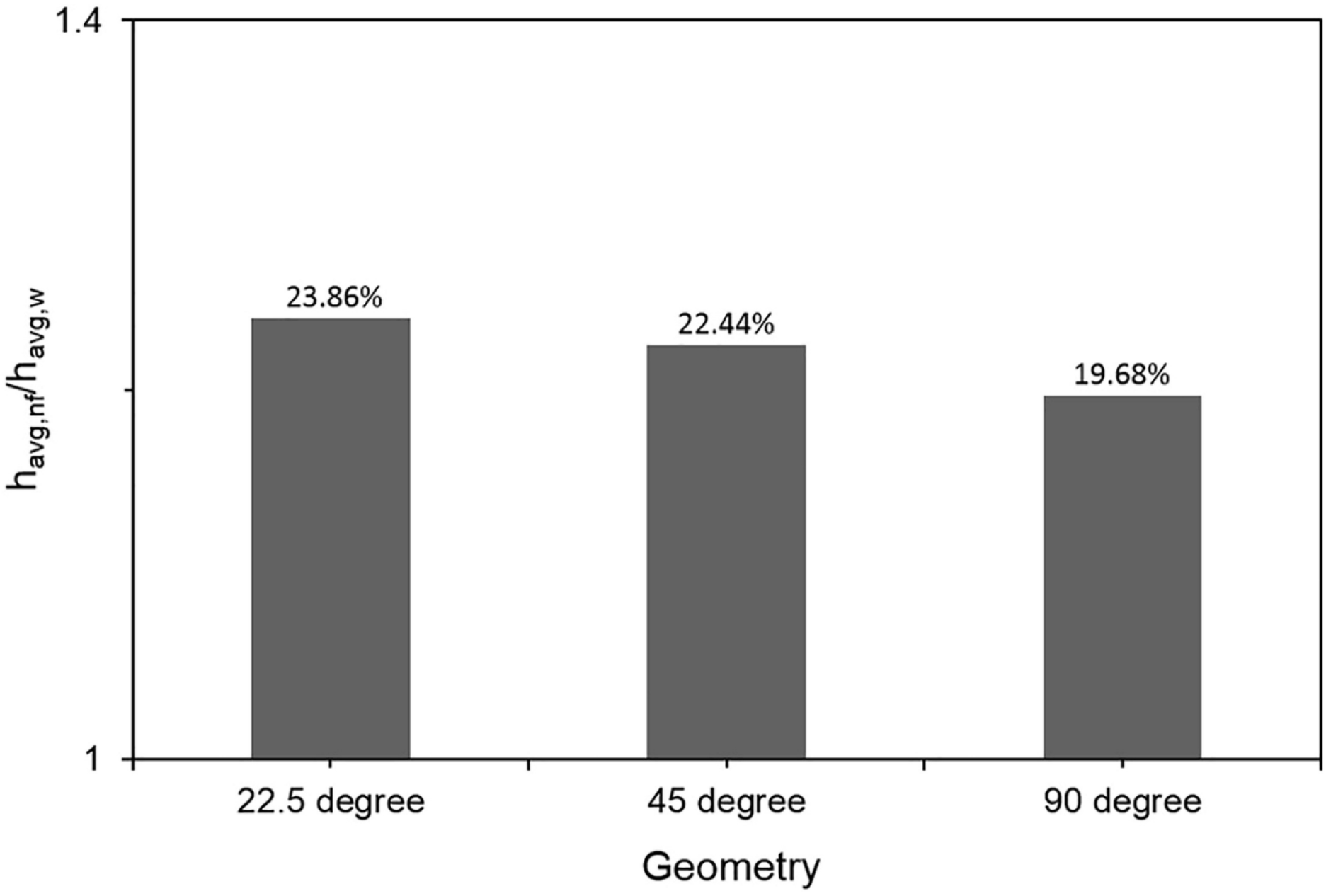
1.4
1
$h_{avg,nf}/h_{avg,w}$
23.86%
22.44%
19.68%
22.5 degree
45 degree
90 degree
Geometry

Figure 15

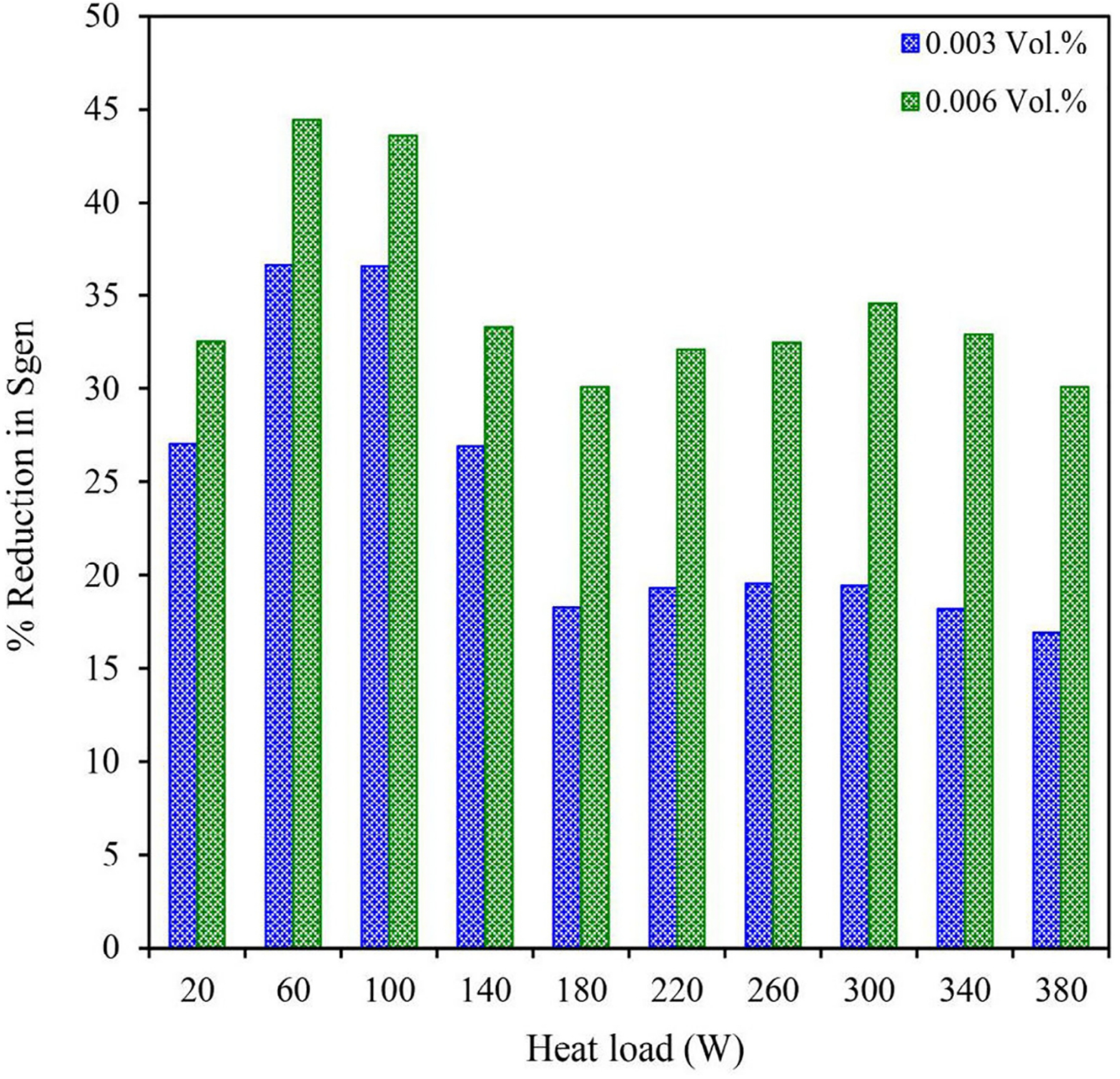
0.003 Vol.%
0.006 Vol.%
% Reduction in Sgen
0
5
10
15
20
25
30
35
40
45
50
20
60
100
140
180
220
260
300
340
380
Heat load (W)

Figure 16

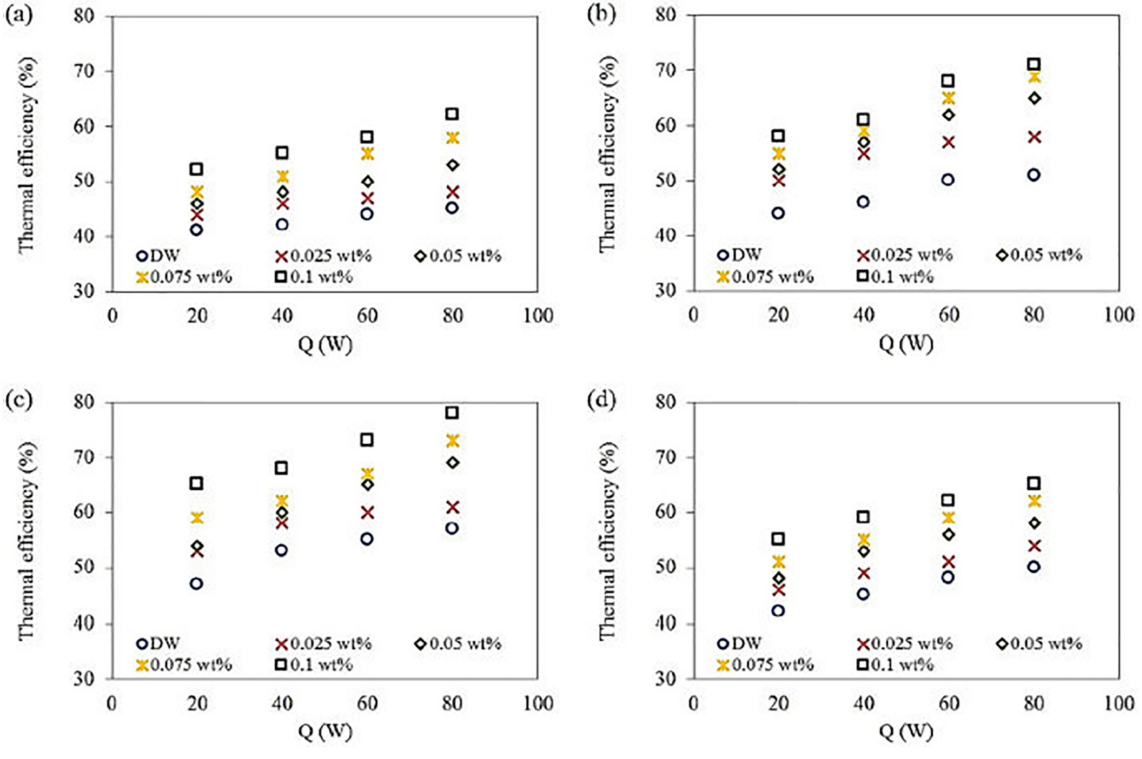

Figure 17

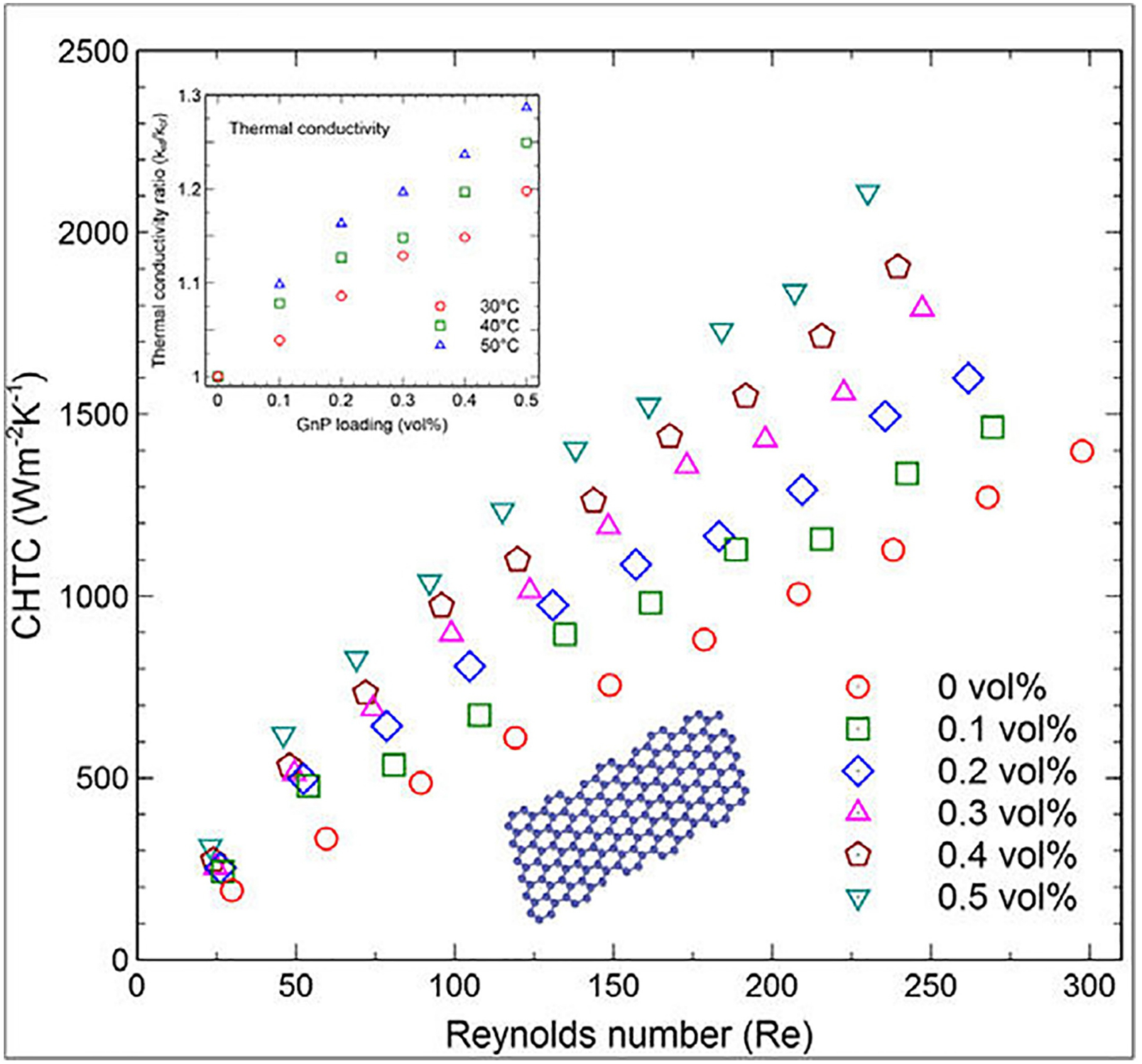
CHTC (Wm-2K-1)
Reynolds number (Re)
0 vol%
0.1 vol%
0.2 vol%
0.3 vol%
0.4 vol%
0.5 vol%
Thermal conductivity
Thermal conductivity ratio (keff/kbf)
GnP loading (vol%)
30°C
40°C
50°C

Figure 18

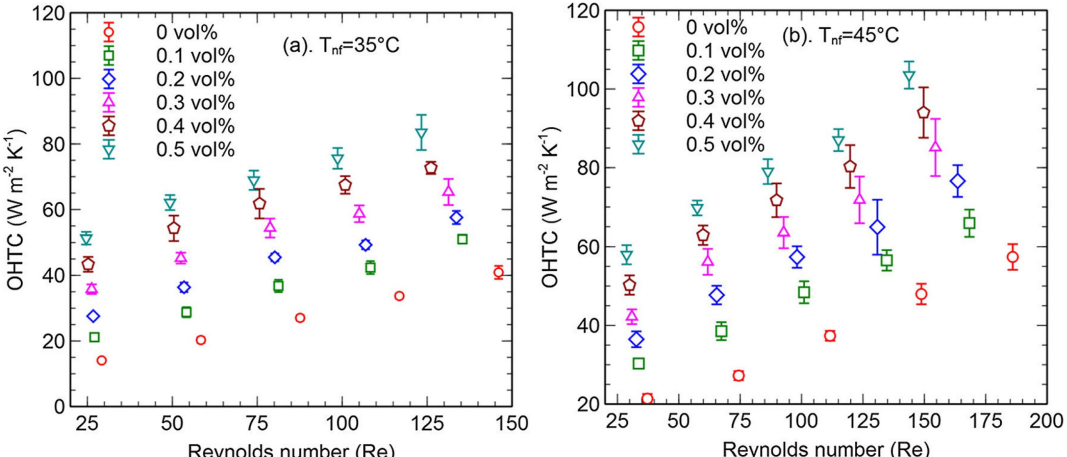
0 vol%
0.1 vol%
0.2 vol%
0.3 vol%
0.4 vol%
0.5 vol%
(a). T_{nf}=35°C
(b). T_{nf}=45°C
OHTC (W m^{-2} K^{-1})
Reynolds number (Re)

Figure 19

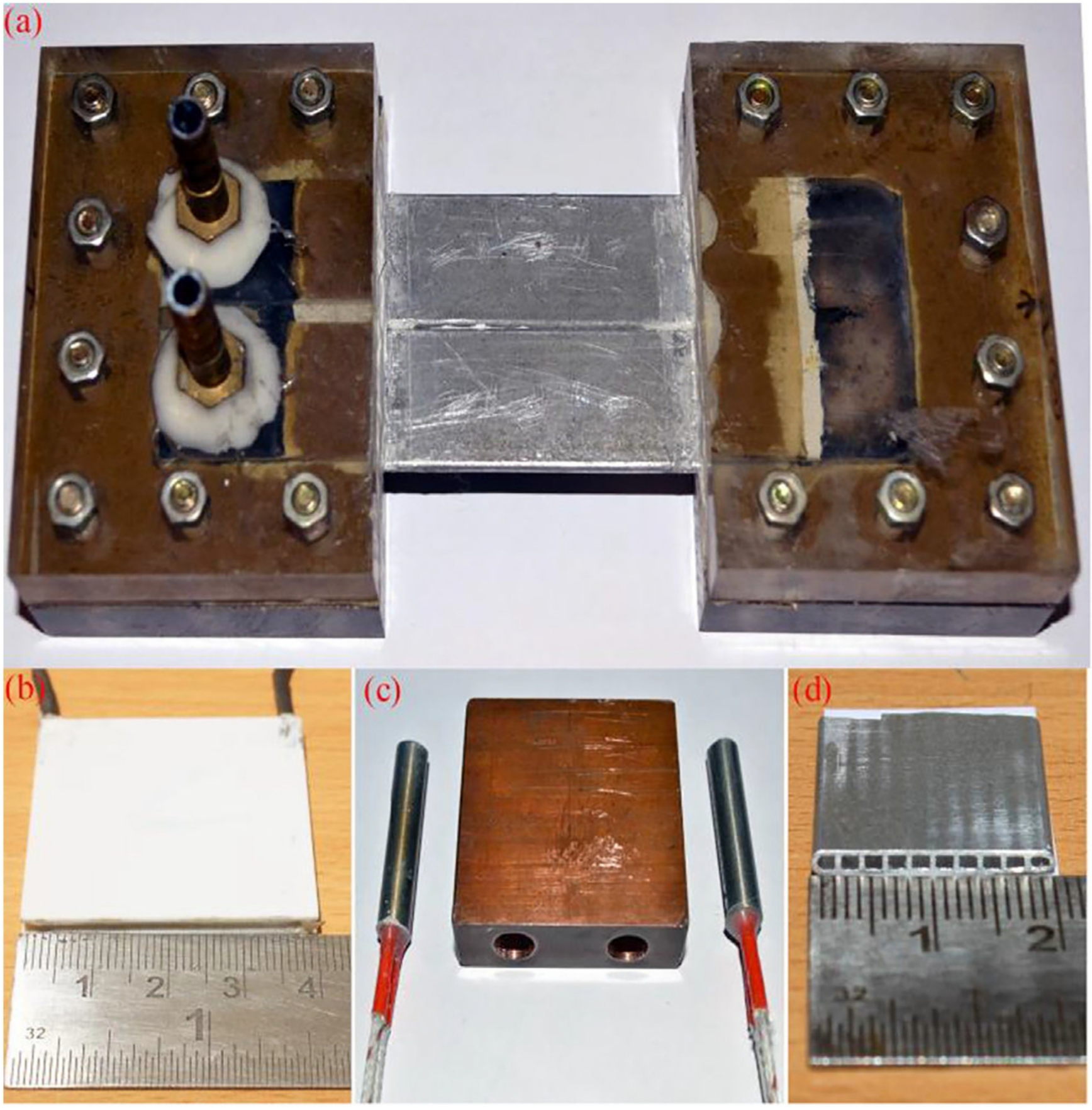

Figure 20

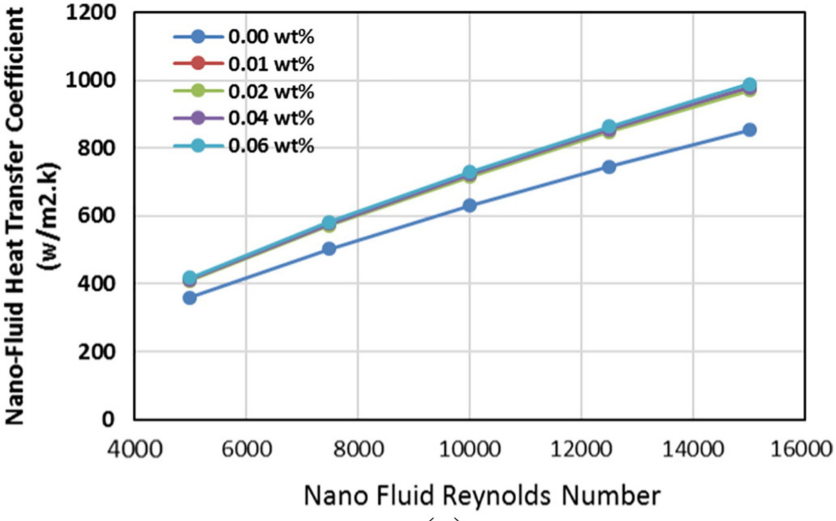
0.00 wt%
0.01 wt%
0.02 wt%
0.04 wt%
0.06 wt%
Nano-Fluid Heat Transfer Coefficient (w/m2.k)
Nano Fluid Reynolds Number
0
200
400
600
800
1000
1200
4000
6000
8000
10000
12000
14000
16000

(a)

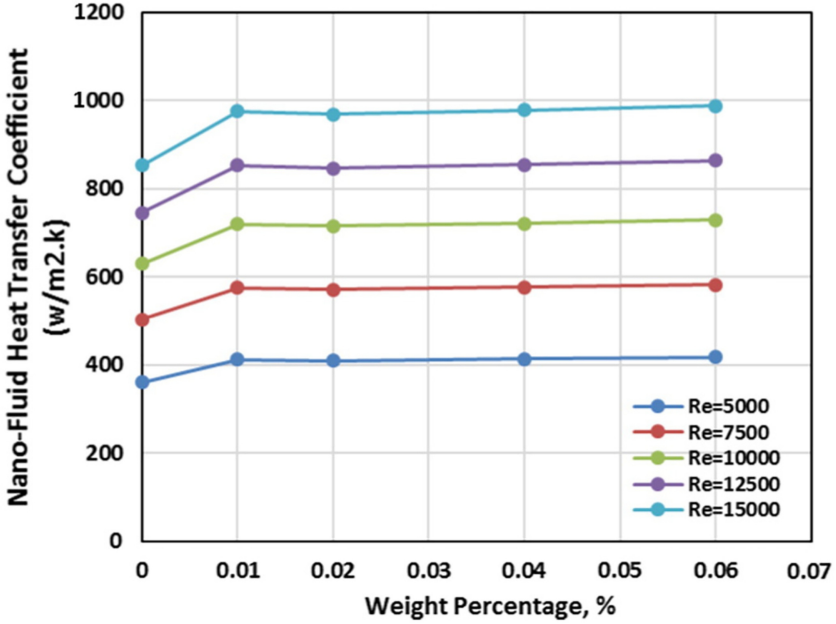
Re=5000
Re=7500
Re=10000
Re=12500
Re=15000
Nano-Fluid Heat Transfer Coefficient (w/m2.k)
Weight Percentage, %
0
200
400
600
800
1000
1200
0
0.01
0.02
0.03
0.04
0.05
0.06
0.07

(b)

Figure 21

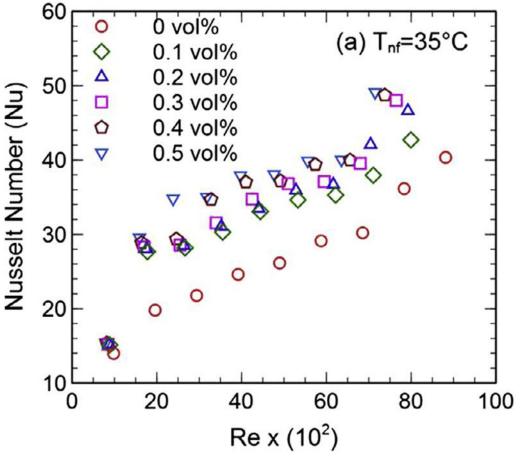
0 vol%
0.1 vol%
0.2 vol%
0.3 vol%
0.4 vol%
0.5 vol%
(a) T_{nf}=35°C
Nusselt Number (Nu)
Re x (10^2)
60
50
40
30
20
10
0
20
40
60
80
100

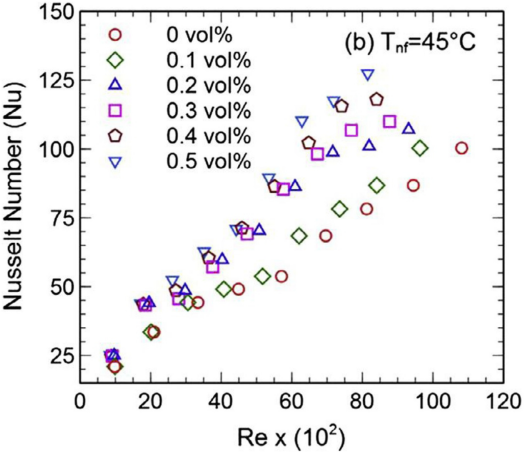
0 vol%
0.1 vol%
0.2 vol%
0.3 vol%
0.4 vol%
0.5 vol%
(b) T_{nf}=45°C
Nusselt Number (Nu)
Re x (10^2)
150
125
100
75
50
25
0
20
40
60
80
100
120

Figure 22

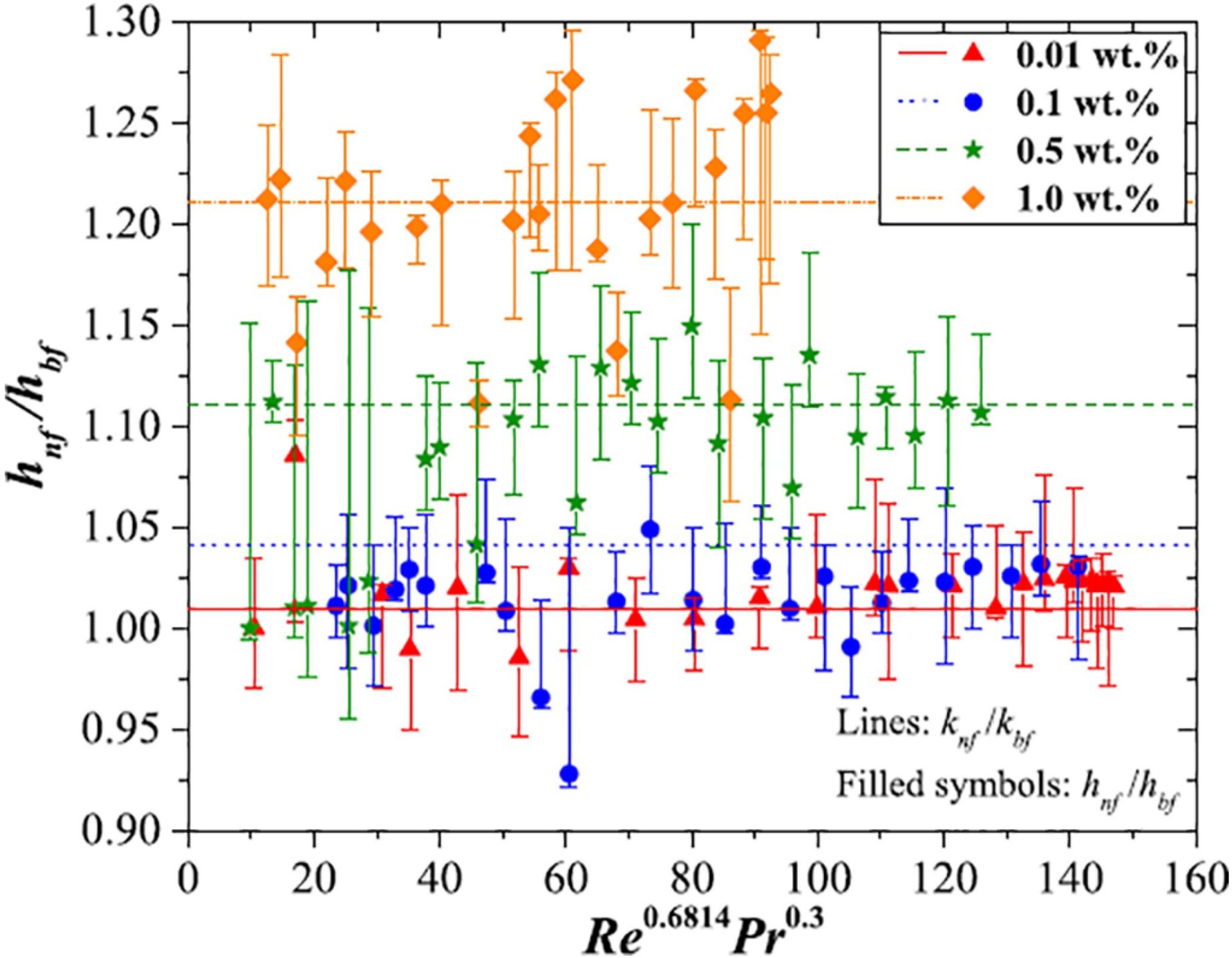
1.30
1.25
1.20
1.15
1.10
1.05
1.00
0.95
0.90
h_{nf}/h_{bf}
0
20
40
60
80
100
120
140
160
$Re^{0.6814}Pr^{0.3}$
0.01 wt.%
0.1 wt.%
0.5 wt.%
1.0 wt.%
Lines: k_{nf}/k_{bf}
Filled symbols: h_{nf}/h_{bf}

Figure 23

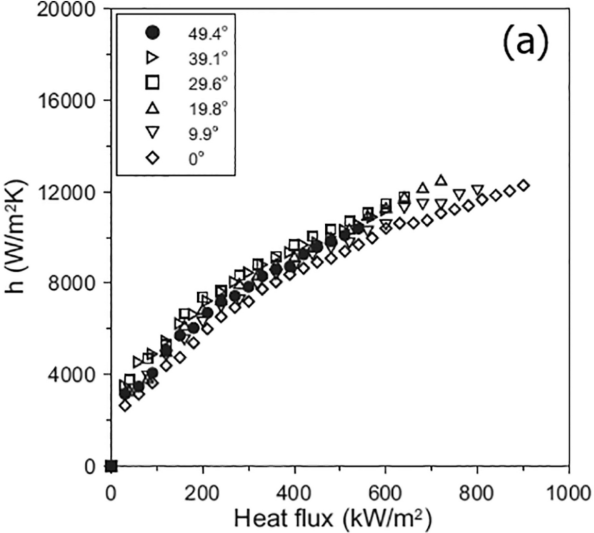
(a)
49.4°
39.1°
29.6°
19.8°
9.9°
0°
h (W/m²K)
Heat flux (kW/m²)
0
4000
8000
12000
16000
20000
0
200
400
600
800
1000

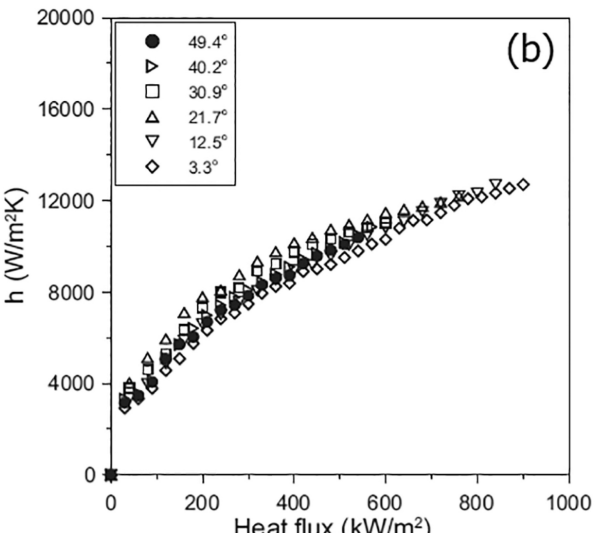
(b)
49.4°
40.2°
30.9°
21.7°
12.5°
3.3°
h (W/m²K)
Heat flux (kW/m²)
0
4000
8000
12000
16000
20000
0
200
400
600
800
1000

Figure 24

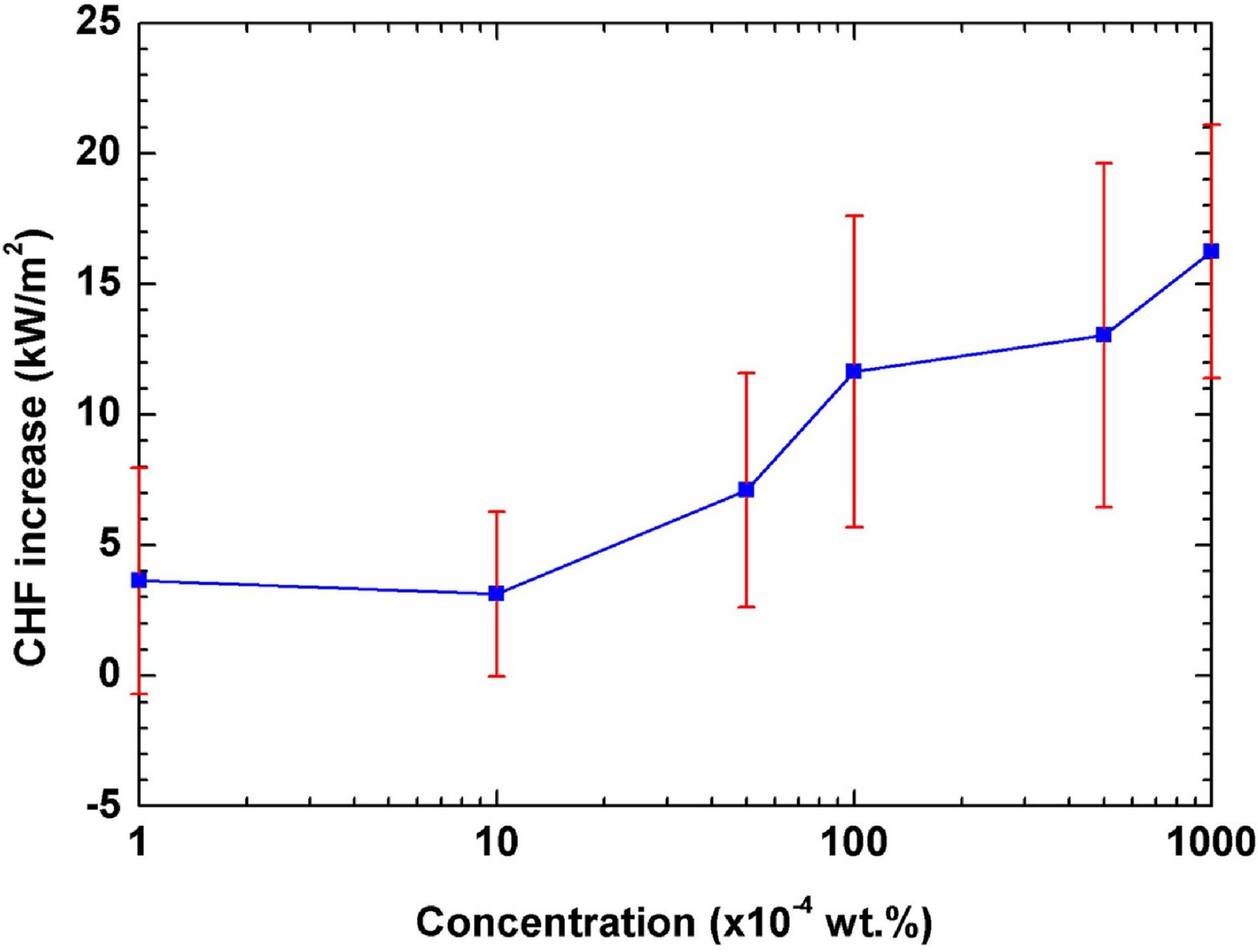
25
20
15
10
5
0
-5
CHF increase (kW/m^2)
1
10
100
1000
Concentration (x10^{-4} wt.%)

Figure 25

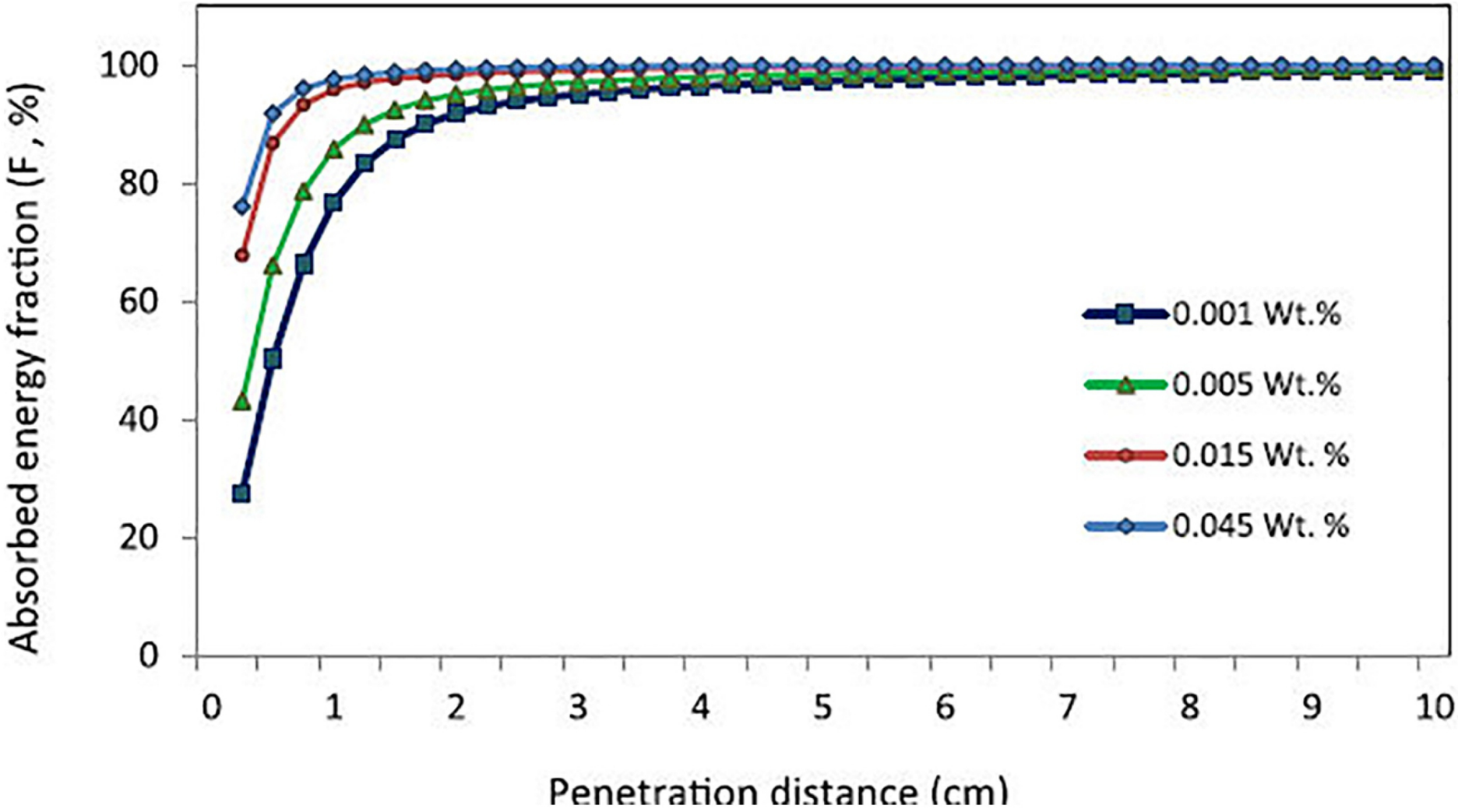
Absorbed energy fraction (F , %)
100
80
60
40
20
0
0
1
2
3
4
5
6
7
8
9
10
Penetration distance (cm)
0.001 Wt.%
0.005 Wt.%
0.015 Wt. %
0.045 Wt. %

Figure 26

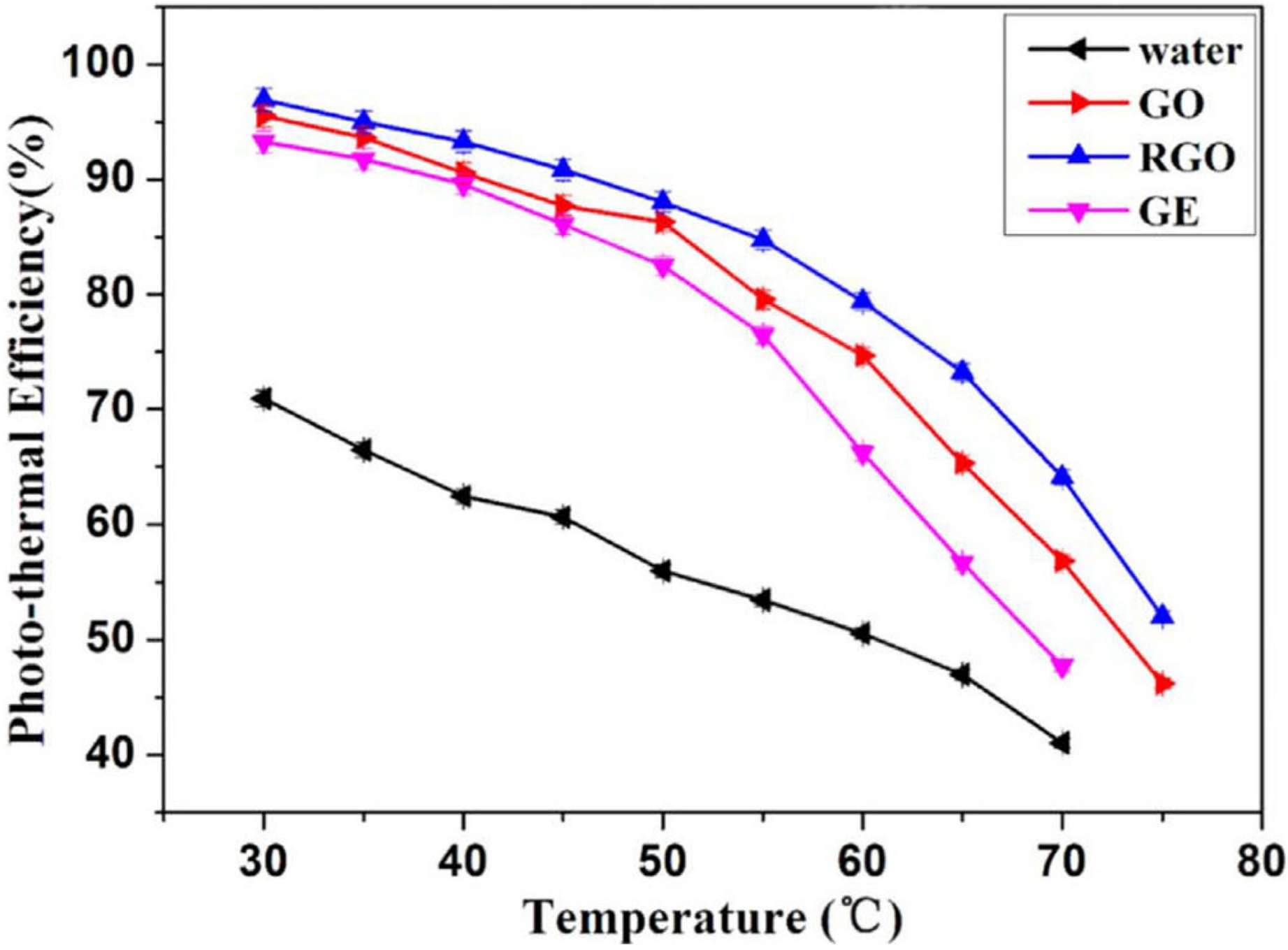
water
GO
RGO
GE
Photo-thermal Efficiency(%)
100
90
80
70
60
50
40
30
40
50
60
70
80
Temperature (℃)

Figure 27

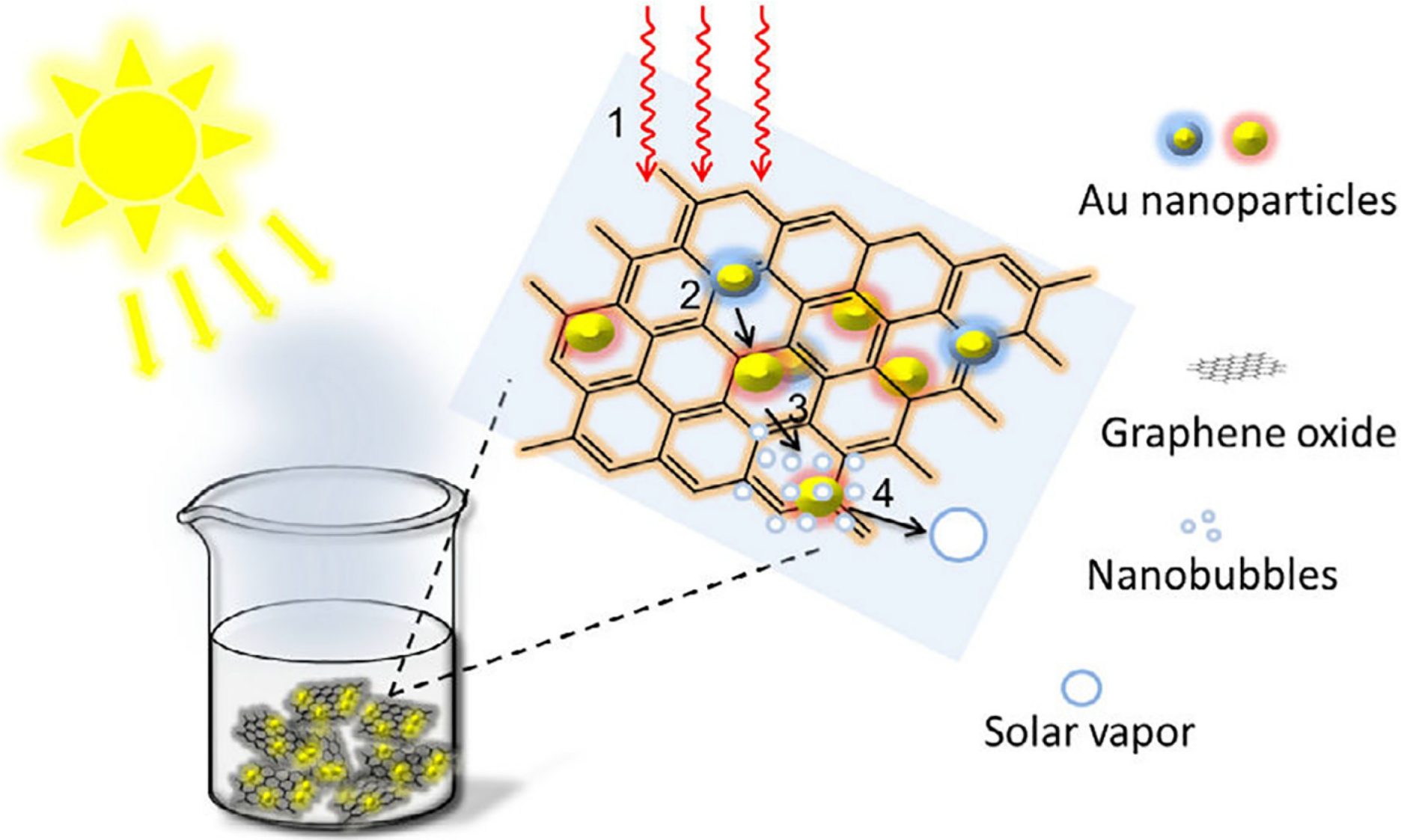
1
2
3
4
Au nanoparticles
Graphene oxide
Nanobubbles
Solar vapor

Figure 28

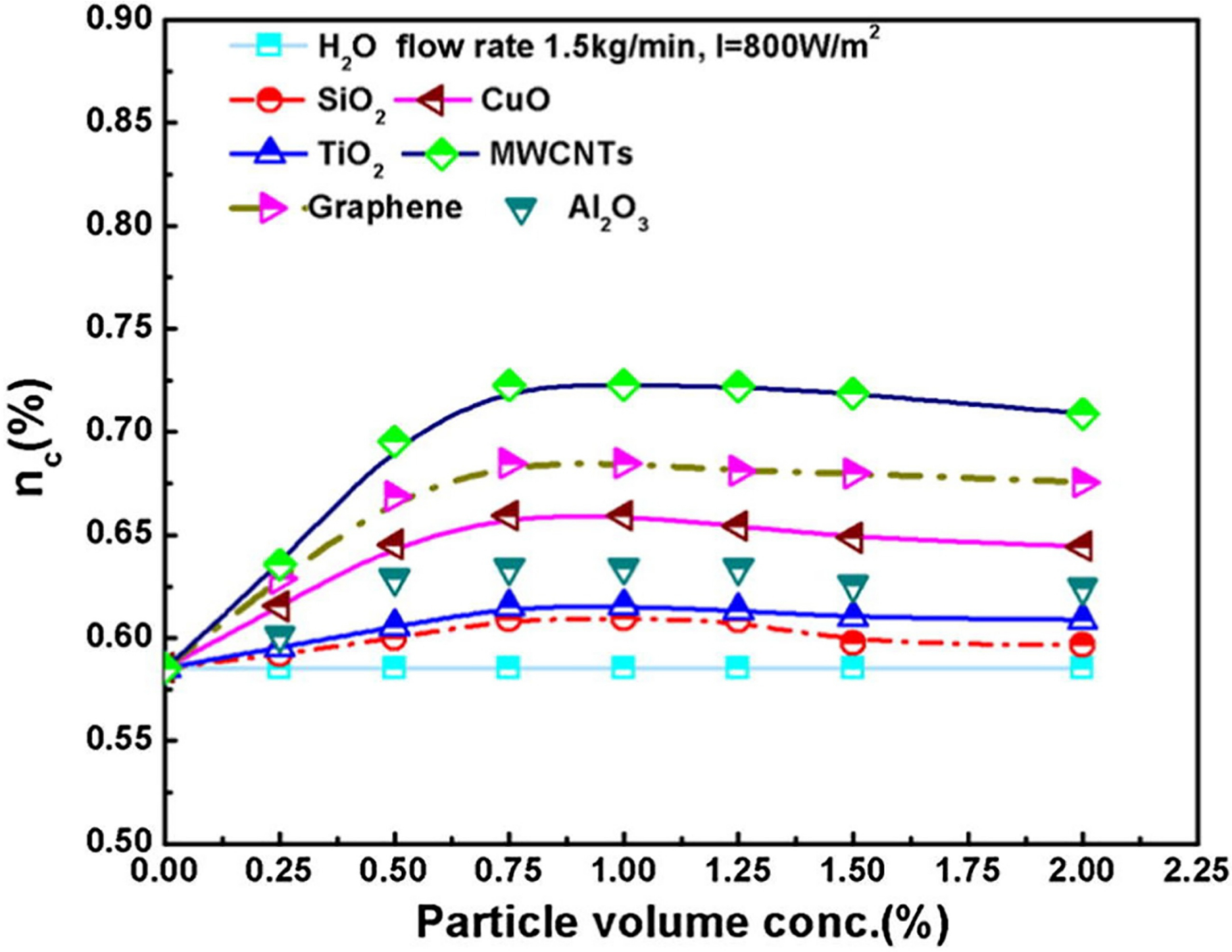
H2O flow rate 1.5kg/min, I=800W/m2
SiO2
CuO
TiO2
MWCNTs
Graphene
Al2O3
nc(%)
0.90
0.85
0.80
0.75
0.70
0.65
0.60
0.55
0.50
0.00
0.25
0.50
0.75
1.00
1.25
1.50
1.75
2.00
2.25
Particle volume conc.(%)

Figure 29